UNIVERSITY OF CALIFORNIA SAN DIEGO

Elastic Composites: Part I - Negative Refraction in Phononic Crystals, Part II - Dissipative Mechanisms in the Evolution of Inhomogeneities

A dissertation submitted in partial satisfaction of the
requirements for the degree of Doctor of Philosophy

in

Engineering Sciences (Applied Mechanics)

by

Shailendra Pal Veer Singh

Committee in charge:

Professor Siavouche Nemat-Nasser, Chair
Professor Prabhakar R. Bandaru
Professor Shengqiang Cai
Professor Boubacar Kanté
Professor Daniel F. Sievenpiper

2018

The Dissertation of Shailendra Pal Veer Singh is approved and is acceptable in quality and form for publication on microfilm and electronically:

Chair

University of California San Diego

2018

DEDICATION

To my parents.

EPIGRAPH

Ask the right questions,
and Nature will open
the doors to her secrets.

C. V. Raman

TABLE OF CONTENTS

LIST OF FIGURES

LIST OF TABLES

ACKNOWLEDGEMENTS

I would like to express my sincere gratitude towards my advisor Prof. Nemat-Nasser for giving me the opportunity to work under him at Center of Excellence for Advanced Materials (CEAM), and for training me to be an independent researcher. I thank him for his patience, motivation and vast knowledge; he has been a great personal and professional mentor for me. Without his astute advice and invaluable guidance, this work would not have been possible. I am also grateful to him for the hands-on help getting my experimental research started and showing me ropes around the lab. My deepest appreciation goes to Lauri Jacobs-Cohantz for her great help during my study at CEAM, and for her support and guidance in overcoming many technical issues during my PhD.

I would like to thank the members of my dissertation committee: Prof. Prabhakar R. Bandaru, Prof. Shengqiang Cai, Prof. Boubacar Kanté and Prof. Daniel F. Sievenpiper. I also thank Prof. Xanthippi Markenscoff for her guidance at the early stage of my PhD study.

My sincere thanks also goes to my colleagues and mentors at CEAM: Prof. Alireza V. Amirkhizi, Dr. Arif Hasan, Dr. Wiroj Nantasetphong, Dr. Zhanzhan Jia, Dr. Aref Tehranian, and Dr. Hossein Sadeghi. I would also like to thank Mr. Jon Isaac, whose experience and insight into experimental methods was a great help for my experimental research. I am especially thankful to him for training me in Split-Hopkinson pressure bar experimental techniques. I also thank Hansong Liu for assisting me to set up, and conduct experiments. An acknowledgement and thanks goes to Don and Bob at the campus research machine shop for helping me fabricate the important parts of my experiments. I would like to thank Zachary Dake, Patrick Mallon, Lydia Ramirez, Linda McKamey, and Joana Halnez from the Mechanical and Aerospace Engineering department. I am thankful to all of my peers and friends for their help and support during my stay at UCSD, with whom I have developed an everlasting bond of friendship.

Of course my deepest gratitude goes to my family: my father Sri Jai Bir, my mother Srimati Vimala and my sister Anuja, I am deeply indebted of their patience, love, support and encouragement from other side of the world.

The work of Chapter 2 and Chapter 3 has been done with Professor S. Nemat-Nasser. The dissertation author was the primary investigator of this research work. The work is being prepared for a publication.

Chapter 4, in part, is reprint of the material as it appears in "Markenscoff, X., and Singh, S. (2015). Dynamic conservation integrals as dissipative mechanisms in the evolution of inhomogeneities. Journal of Mechanics of Materials and Structures, 10(3), 331-353". The dissertation author was the primary investigator of this paper.

The work of Chapter 5, and the mathematical derivations in Appendix, have been done with Professor X. Markenscoff. The dissertation author was the primary investigator of this research work. The work is being prepared for a publication.

VITA

2011	B.Tech. - M.Tech. Dual Degree in Mechanical Engineering, Indian Institute of Technology, Kanpur, India
2011-2018	Graduate Research Assistant and Teaching Assistant, University of California, San Diego, USA.kk
2018	Ph.D. in Engineering Sciences (Applied Mechanics), University of California, San Diego, USA.

PUBLICATIONS

- Markenscoff, X., and Singh, S. (2015). Dynamic conservation integrals as dissipative mechanisms in the evolution of inhomogeneities. Journal of Mechanics of Materials and Structures, 10(3), 331-353.
- Singh, S. (2011). Dynamical Evolution of Rubble-Pile Binaries. Master's thesis. Indian Institute of Technology Kanpur.

FIELDS OF STUDY

Major Field: Applied Mechanics (Mechanical Engineering)

ABSTRACT OF THE DISSERTATION

Elastic Composites: Part I - Negative Refraction in Phononic Crystals, Part II - Dissipative Mechanisms in the Evolution of Inhomogeneities

by

Shailendra Pal Veer Singh

Doctor of Philosophy in Engineering Sciences (Applied Mechanics)

University of California San Diego, 2018

Professor Siavouche Nemat-Nasser, Chair

We experimentally demonstrate the presence of negative refraction on acoustic passbands of two-dimensional phononic crystals for the in-plane and the anti-plane shear waves. We investigate the phenomenon on two geometrically identical *two-phase* crystals of different material properties, i.e., one stiff crystal (Aluminum matrix with PMMA inclusions), and another a soft crystal (PMMA matrix with Aluminum inclusions). We demonstrate that in the case of in-plane shear wave, the soft crystal does not show negative refraction in the first passband, however, the stiff crystal does show negative refraction for the first mode. In the case of the anti-plane shear wave tests, both crystals show only positive refraction in the first passband.

However, in the soft crystal, negative refraction is present in the second passband. We also investigate and show that for the longitudinal mode (second acoustic passband), both stiff and soft crystals, exhibit negative refraction. The experimental results confirm the prediction of our theoretical model, which allows us to predict the behaviors of phononic crystals as we change the properties of their constituents.

In the second part of this dissertation, by the application of Noether's theorem, conservation laws in linear elastodynamics are derived by invariance of the Lagrangean functional under a class of infinitesimal transformations. The work of Gupta and Markesncoff (2012), which provides a physical meaning to the dynamic J-integral as the variation of the Hamiltonian of the system due to an infinitesimal translation of the inhomogeneity if linear momentum is conserved in the domain, is extended here to the dynamic M- and L- integrals in terms of the 'if' conditions. We show that the variation of the Lagrangean is equal to the negative of the variation of the Hamiltonian under the above transformations for inhomogeneities, and hence provide a physical meaning to the dynamic J-, L- and M-integrals as dissipative mechanisms in elastodynamics. We prove that if linear momentum is conserved in the domain, the total energy loss of the system per unit scaling under the infinitesimal scaling transformation of the inhomogeneity is equal to the dynamic M-integral. Moreover, if linear and angular momenta are conserved, the total energy loss of the system per unit rotation under the infinitesimal rotational transformation is equal to the dynamic L-integral.

Chapter 1

Introduction

This dissertation consists of two parts. The first part serves to design the elastic phononic crystals and the experimental demonstration of negative refractions in them. In the second part we study dissipative mechanisms in the evolution of inhomogeneities in elastic solids.

1.1 Phononic Crystals

Phononic crystals are composite materials consisting of periodically distributed inclusions in a matrix with high contrast of mass densities and/or elastic moduli, which can exhibit specific characteristics such as acoustic band structures and negative refraction (Nemat-Nasser, 1972b; Kushwaha et al., 1993; Liu et al., 2000; Nemat-Nasser et al., 2011; Srivastava, 2015; Sadeghi, 2016). These materials have natural applications in the research areas of clocking, elastic wave focusing, and noise and vibration control.

The first acoustic composite, *'sonic crystals'* (Liu et al., 2000), used rubber-coated lead spheres to create locally resonant and deeply subwavelength structures. Subsequently, Li and Chan (2004) theoretically showed the double-negative *'acoustic metamaterials'* in which both the effective density and bulk modulus are simultaneously negative, and later this result was experimentally demonstrated by Lee et al. (2010). Several other researchers have done experiments showing negative refraction of longitudinal waves (Croënne et al., 2011; García-Chocano et al., 2014; Zhu et al., 2014). Most of the *pressure waves* experiments have been done in

fluid media. Morvan et al. (2010) experimentally demonstrated negative refraction of transverse elastic waves in a two-dimensional phononic crystal made of a square lattice of cylindrical air cavities in an aluminum matrix. Soon after, Lee et al. (2011) conducted negative refraction experiments with guided SH waves in a thin phononic crystal plate. Both of them demonstrated experimental verification of negative refraction for shear waves, only for higher modes. The objective of the first part of this dissertation is to design and fabricate the phononic crystals to study in-plane and anti-plane shear wave, and longitudinal wave propagation. Furthermore, with the guidance of theoretical calculations, we experimentally demonstrate the presence of negative refraction on the acoustic-branch passbands (lowest two modes).

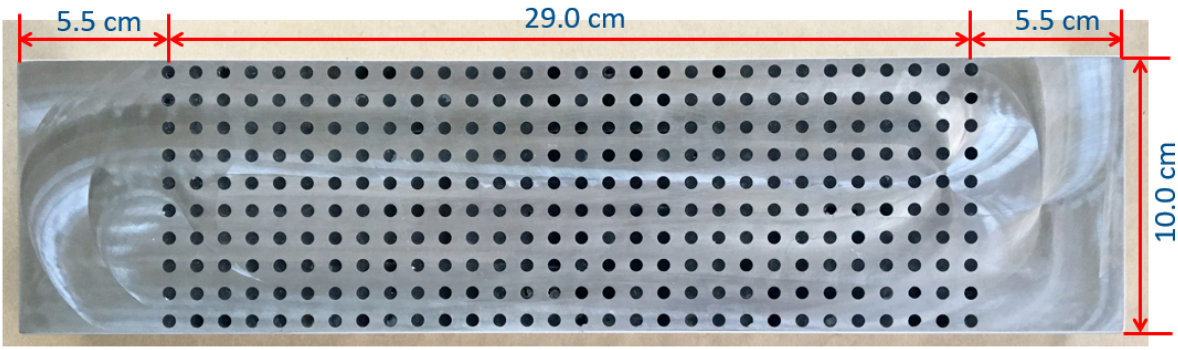

Figure 1.1. An aluminum matrix contains 10 mm spaced, 4.76 mm diameter circular PMMA inclusions (Sample 1).

We have prepared two doubly periodic phononic crystals with a thickness of 1.5 *inches*. One crystal is made of Aluminum matrix with periodically inserted circular PMMA pins of 4.76 *mm* diameter. The spacing between the pins in both x and y directions is 10 *mm*, and we call this *'Sample 1'*. The material properties are following:

$$E_1^M = E_2^M = 68\,GPa, \quad \nu^M = 0.33, \quad \rho^M = 2700\,kg/m^3;$$
$$E_1^I = E_2^I = 3\,GPa, \quad \nu^I = 0.40, \quad \rho^I = 1200\,kg/m^3,$$

where E_1 and E_2 are the elastic moduli, and ν, ρ are the Poisson's ratio and the mass density,

respectively. The superscripts M and I denote the matrix and the inclusion, respectively.

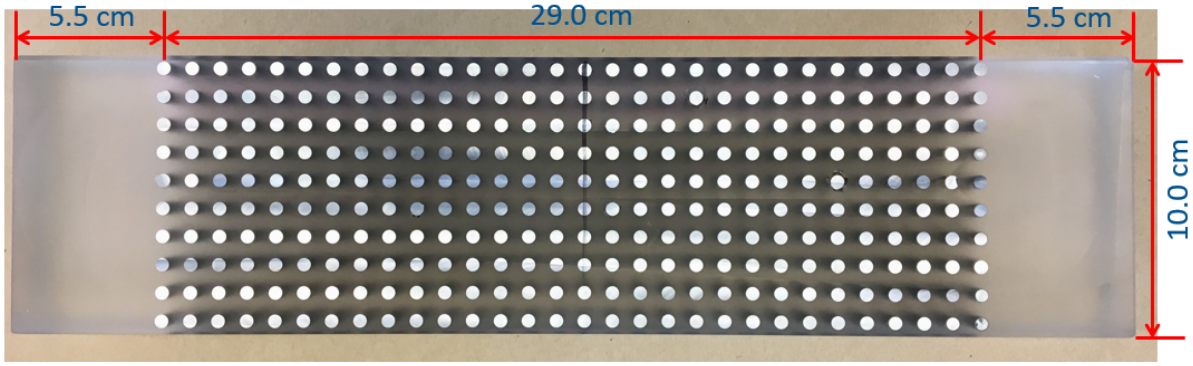

Figure 1.2. A PMMA matrix contains10 mm spaced, 4.76 mm diameter circular Aluminum inclusions (Sample 2).

The second crystal is made of PMMA matrix with periodically inserted circular Aluminum pins of 4.76 *mm* diameter. The spacing between pins in both x and y directions is 10 *mm*, and we call this *'Sample 2'*. The material properties are following:

$$E_1^M = E_2^M = 3\,GPa, \quad \nu^M = 0.40, \quad \rho^M = 1200\,kg/m^3$$
$$E_1^I = E_2^I = 68\,GPa, \quad \nu^I = 0.33, \quad \rho^I = 2700\,kg/m^3.$$

Band Structure for 2D Phononic Crystals

In anti-plane shear case, acoustic and optical branch only has one passband in it, whereas in-plane case has two pass passbands in each branch. In each branch, the lower passband is in-plane shear wave mode, and the second passband is the longitudinal wave mode (Figure 1.3).

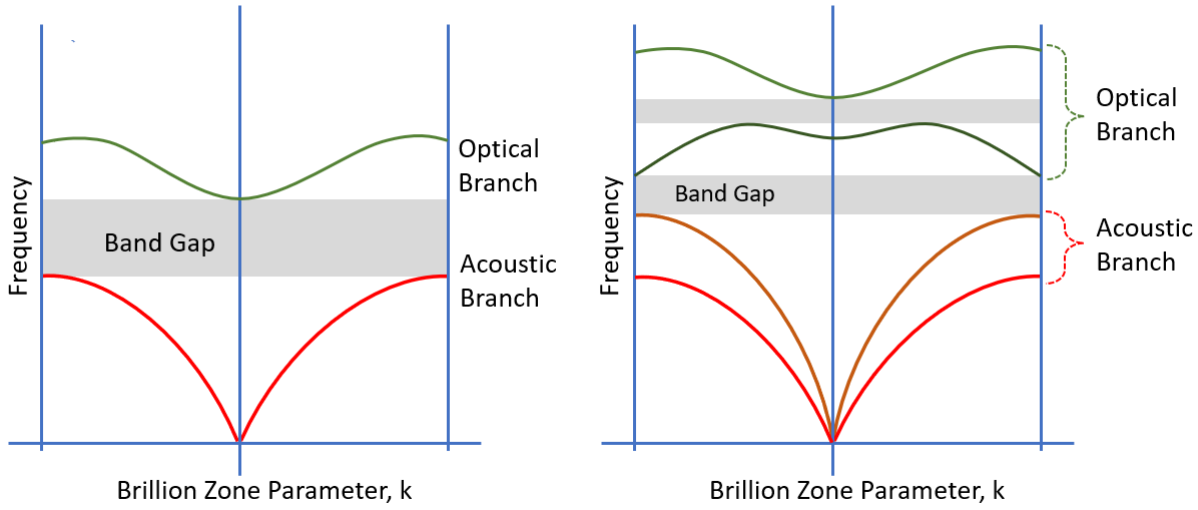

Figure 1.3. Typical band structures for 2D phononic crystals. (Left) Anti-plane shear case, and (Right): in-plane case.

1.1.1 Positive and Negative Refraction

Phononic crystals consisting of periodic arrangement of elastic inclusions in an elastic matrix material exhibit band structure, negative refraction, and effective material properties, which are frequency dependent. This means that at the same incident angle at one frequency, the phononic crystal would display positive refraction, and at another certain frequency, it might display a negative refraction. We also show in later chapters that at the same frequency, but at different components of the wave vector, the phononic crystal can exhibit positive and/or negative refraction. In this dissertation we focus on demonstrating lowest passband negative refraction in phononic crystals. With the help of negative refraction in a phononic crystal, it is possible to design flat lens for elastic wave focusing (Yang et al., 2004; Zhu et al., 2014), or acoustic beam shifters (Wei et al., 2015).

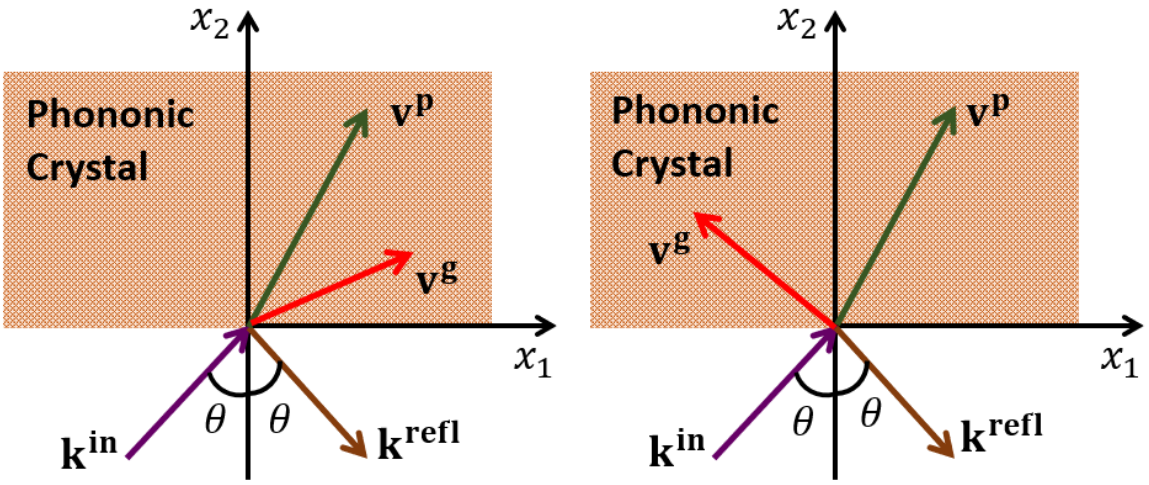

Figure 1.4. A plane wave is incident from a homogeneous half-space $x_2 < 0$ towards the interface $x = 0$ at an incidence angle θ. $\mathbf{k}^{\mathbf{in}}$ and $\mathbf{k}^{\mathbf{refl}}$ are incident and reflected wave vectors, respectively. $\mathbf{v}^{\mathbf{p}}$ and $\mathbf{v}^{\mathbf{g}}$ show the direction of phase and group velocity in the phononic crystal, respectively. (Left): A typical positive refraction, and (Right): a typical negative refraction.

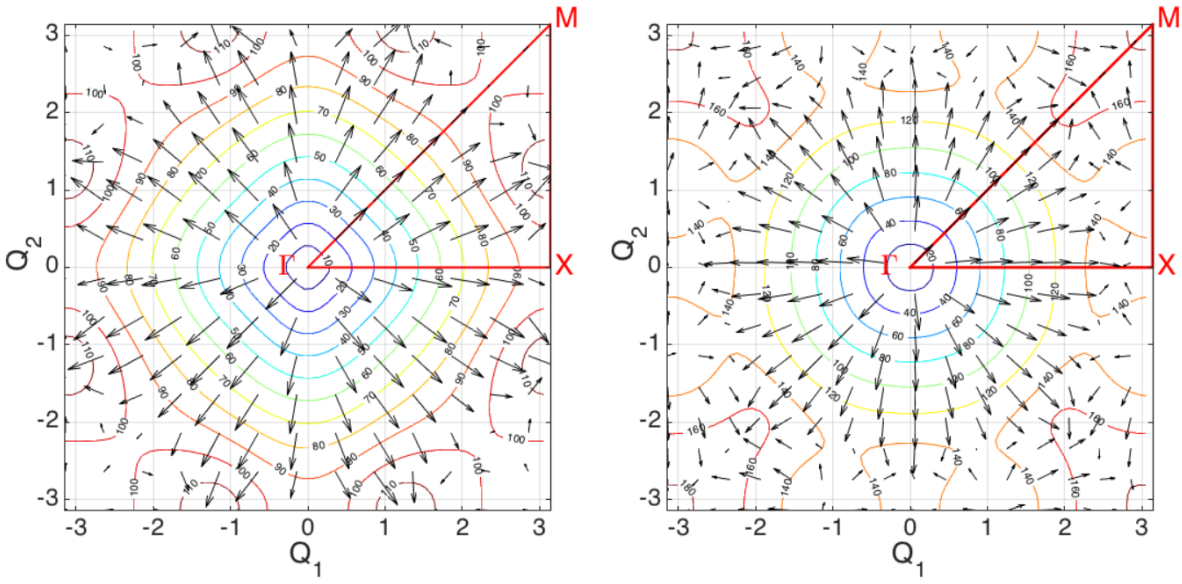

Figure 1.5. Sample 1 acoustic-branch equi-frequency contours and energy flux vectors of: (Left): shear mode, and (Right): longitudinal mode; $Q_1 = k_1 a$ and $Q_2 = k_2 a$ are the normalized x_1 and x_2 components of the wave vector.

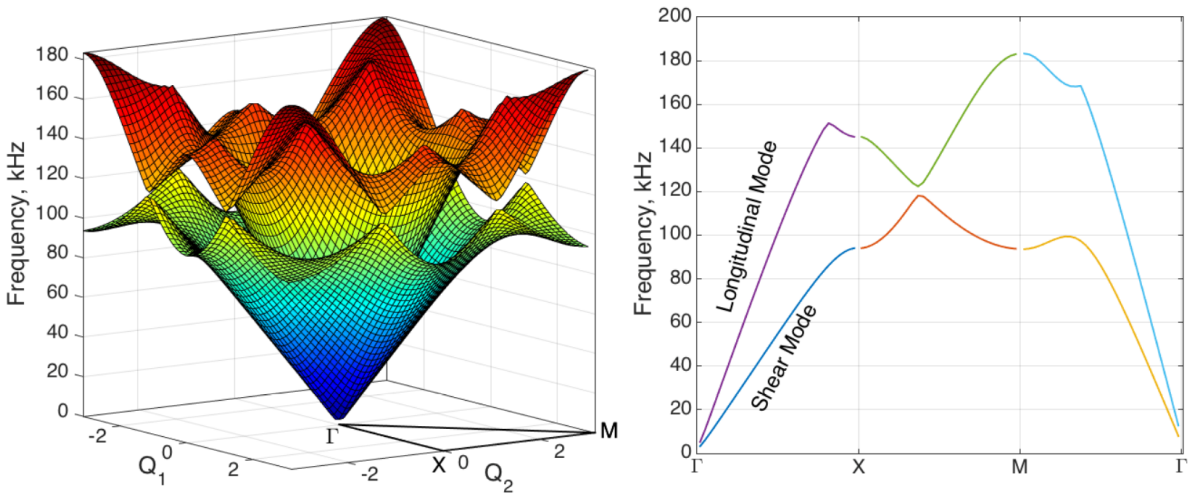

Figure 1.6. (Left): Sample 1 acoustic-branch frequency surfaces for shear (lowest) mode, and longitudinal mode; $Q_1 = k_1 a$ and $Q_2 = k_2 a$ are the normalized x_1 and x_2 components of the wave vector. (Right): Frequency variation along the Γ, X, M, Γ lines for shear and longitudinal modes.

The lower modes in the band structure have a higher energy associated with them. That is why our goal is to investigate and design a phononic crystal, which exhibits negative refraction in the first passband (acoustic branch). The presence of negative and positive refractions on the acoustic-branch passband enables focusing and filtering elastic waves at very low frequency. As the material properties given above for Sample 1, using *'new quotient'* method (Nemat-Nasser, 1972a,b; Nemat-Nasser et al., 1975) we evaluate the acoustic-branch (Figures 1.5, and 1.6). In Figure 1.5, we give the equi-frequency contours with the energy flux vectors, as we see the directions of the energy flux vectors, we notice that both shear and longitudinal modes for Sample 1 display positive and negative refractions. We also show the frequency surfaces for the shear and the longitudinal modes (Figure 1.6), and the variation of the shear and longitudinal mode frequency along the Γ, X, M, Γ lines. Figure 1.6 makes it very clear that there is no mode mixing between first two passbands in Sample 1.

1.1.2 λ_N: New Quotient (Mixed-variational Formulation) for Waves in Elastic Phononic Crystals

Consider a two-dimensional elastic phononic crystal with arbitrarily oriented elliptical inclusions, with a representative unit cell shown in Figure 1.7. Two edges of the unit cell are defined by the two vectors $\mathbf{l}^\beta$, $\beta = 1,2$. Let us denote the region occupied by this unit cell by Ω, having boundary $\partial\Omega$, and let Σ be the collection of all interior surfaces which separate different material constituents within the unit cell (Nemat-Nasser et al., 1975; Srivastava and Nemat-Nasser, 2014).

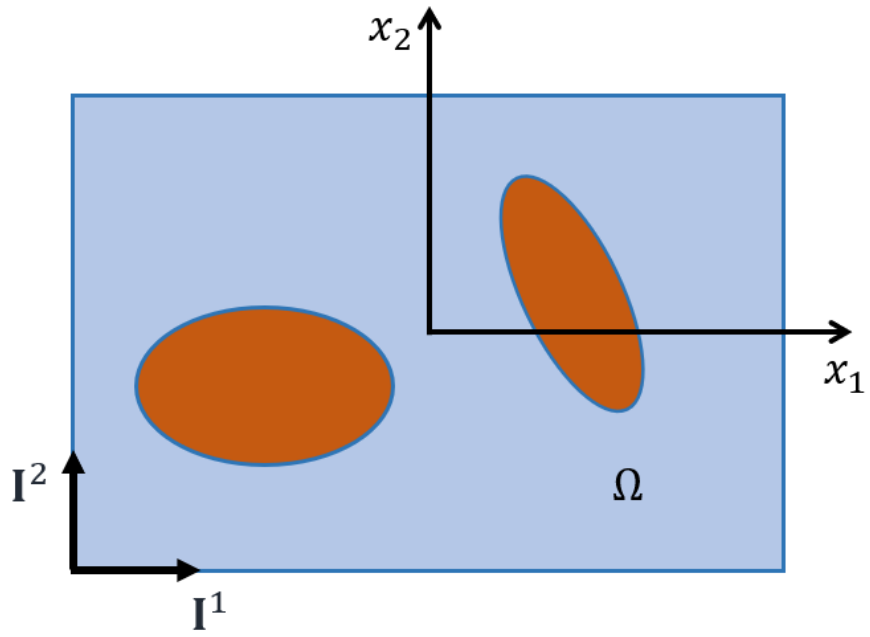

Figure 1.7. A typical representative unit cell of a two-dimensional elastic phononic crystal.

The mass density $\rho(\mathbf{x})$ and the elasticity tensor with rectangular Cartesian components $C_{jkmn}(\mathbf{x})$ are continuous and continuously differentiable functions in the subregions occupied by each constituent, but in general have a finite discontinuities across Σ, where $\mathbf{x}$ is the position vector with components x_j, $j = 1,2$. The periodicity condition implies:

$$\rho(\mathbf{x}) = \rho(\mathbf{x} + m'\mathbf{l}^\beta); \quad C_{jkmn}(\mathbf{x}) = C_{jkmn}(\mathbf{x} + m'\mathbf{l}^\beta), \tag{1.1}$$

where m' is an integer. For harmonic waves with frequency ω, all the field quantities are proportional to $e^{\pm \mathrm{i}\omega t}$, where $\mathrm{i} = \sqrt{-1}$. Thus the elastodynamics equations of motion, kinematic relation and constitutive relation at any point $\mathbf{x}$ in Ω are given by

$$\sigma_{jk,k} = -\lambda \rho u_j; \quad \varepsilon_{jk} = \frac{1}{2}(u_{j,k} + u_{k,j}) \quad \text{and} \quad \sigma_{jk} = C_{jkmn} u_{m,n}, \tag{1.2}$$

where $\lambda = \omega^2$. For harmonic waves with wave vector $\mathbf{q}$, the boundary condition takes on the following quasi-periodic form (Bloch boundary conditions),

$$u_j(\mathbf{x} + \mathbf{l}^\beta) = u_j(\mathbf{x}) e^{\mathrm{i}q\mathbf{l}^\beta}; \quad t_j(\mathbf{x} + \mathbf{l}^\beta) = t_j(\mathbf{x}) e^{\mathrm{i}q\mathbf{l}^\beta}, \quad \mathbf{x} \in \partial\Omega, \tag{1.3}$$

where $t_j = \sigma_{jk} n_k$ is the traction vector, which must remain continuous across any interior surface, in particularly

$$\left[\sigma_{jk}(\mathbf{x}^+) - \sigma_{jk}(\mathbf{x}^-)\right] n_k = 0, \quad \mathbf{x} \in \Sigma, \tag{1.4}$$

where n_k is a unit outward normal vector on a surface.

Nemat-Nasser et al. (1975); Minagawa and Nemat-Nasser (1976) have shown that the solution to the above problem renders the following function (new quotient) stationary:

$$\lambda_N = \frac{\langle \sigma_{jk}, u_{j,k} \rangle + \langle u_{j,k}, \sigma_{jk} \rangle + \langle D_{jkmn} \sigma_{jk}, \sigma_{mn} \rangle}{\langle \rho u_j, u_j \rangle}, \tag{1.5}$$

where D_{jkmn} is the elastic compliance tensor and inner product is given by

$$\langle u, v \rangle = \int_\Omega u\, v^* \mathrm{d}\Omega, \tag{1.6}$$

where v^* is the complex conjugate of v. Now we approximate the stress and displacement field

as:

$$\bar{u}_j = \sum_{\alpha,\beta=-M}^{M} U_j{}^{(\alpha,\beta)} f^{(\alpha,\beta)}(\mathbf{x}), \quad \bar{\sigma}_{jk} = \sum_{\alpha,\beta=-M}^{M} S_{jk}{}^{(\alpha,\beta)} f^{(\alpha,\beta)}(\mathbf{x}), \tag{1.7}$$

where an orthogonal sequence of functions, $f^{(\alpha,\beta)}(\mathbf{x})$, $\alpha,\beta = -M,\ldots,M$ are continuous and continuously differentiable, and which satisfy the Bloch boundary conditions (1.3). Substituting from (1.7) to (1.5) and setting the derivative of λ_N with respect to the unknown coefficients, $U_j{}^{(\alpha,\beta)}$ and $S_{jk}{}^{(\alpha,\beta)}$, equal to zero, we arrive at the following set of $9(2M+1)^2$ linear homogeneous equations:

$$\langle \bar{\sigma}_{jk,k} + \lambda_N \rho \bar{u}_j, f^{(\alpha,\beta)} \rangle = 0 \tag{1.8a}$$

$$\langle D_{jkmn}\bar{\sigma}_{mn} - \bar{u}_{j,k}, f^{(\alpha,\beta)} \rangle = 0, \quad j,k,m,n = 1,2. \tag{1.8b}$$

Equations (1.8b), which are $6(2M+1)^2$ in number, can be solved for $S_{jk}{}^{(\alpha,\beta)}$ in terms of $U_j{}^{(\alpha,\beta)}$, and the result substituted into equation (1.8a). This leads to a system of $3(2M+1)^2$ linear equations for two-dimensional case. The roots of the determinant of these equations give the approximate values of the first $3(2M+1)^2$ eigenfrequencies. The corresponding eigenvectors are $U_j{}^{(\alpha,\beta)}$ from which the displacement field within the unit cell is reconstituted. The stress variation in the unit cell is then obtained from equation (1.8b).

The above method using new quotient, λ_N, is extremely efficient for composites in which the elasticity tensor admits large discontinuities, whereas the traditional Rayleigh quotient, $\lambda_R = \langle C_{jkmn} u_{m,n}, u_{j,k} \rangle / \langle \rho u_j, u_j \rangle$ method is not as efficient (Nemat-Nasser et al., 1975).

In Chapter 2, we numerically investigate, and experimentally demonstrate the negative refraction on acoustic passbands of two-dimensional phononic crystals for in-plane and anti-plane shear waves.

In Chapter 3, we numerically investigate, and experimentally demonstrate the negative refraction on acoustic passbands of two-dimensional phononic crystals for longitudinal waves.

1.2 Dissipative Mechanisms and Conservation Laws

Conservation laws can be expressed as dissipative mechanisms related to the variation of energy of the system due to infinitesimal configurational variations in inhomogeneities. Eshelby (1951) used the energy momentum tensor to define the *force on an elastic singularity* as a variation of the total energy of the body due to the infinitesimal displacement of the defect. Furthermore, he provided additional insights by extending this idea in a series of papers (Eshelby, 1956, 1970, 1975) through his ingenious cutting and rewelding thought experiment. Rice (1968) independently discovered the two-dimensional path independent J-integral for a crack. Günther (1962) and Knowles and Sternberg (1972) derived two additional nontrivial conservation laws (M- and L-integrals) by applying Noether's theorem (Noether, 1918) in linear elastostatics. Rice and Drucker (1967) calculated the energy changes during the growth of voids and cracks. Budiansky and Rice (1973) interpreted these new laws as energy release rates associated with the expansion, and the rotation rates of a cavity, or a crack. Rice (1985) provided further applications of these integrals to the defects.

Fletcher (1976) extended the application of Noether's theorem to derive the conservation laws in linear elastodynamics, and established the completeness of the corresponding conservation laws under a certain group of infinitesimal transformations. Herrmann (1981, 1982) presented a unified formulation to recover the conservation laws by employing different vector calculus operations on the Lagrangean density. Eischen and Herrmann (1987) extended this formulation to account for material inhomogeneity temperature gradients, anisotropy, and body forces. Herrmann and Kienzler (1999) represented these balance laws of continuum mechanics by 4×4 matrices.

In Chapter 4, we impose the scaling transformation to derive the M- integral, and for infinitesimal rotational transformation, we derive the dynamic L-integral. Furthermore, we also relate the variation of the Lagrangean to the variation of the Hamiltonian for scaling and rotation of the inhomogeneity.

In Chapter 5, we calculate the M-integral for cavities, inclusions, and inhomogeneities under tensile loading, or loading of transformation strains, and we also relate the total M-integral to the total energy release rate of the system as the defect expands self-similarly.

Chapter 2

Experimental Demonstration of Negative Refraction for In-plane and Anti-plane Shear Waves in 2D Phononic Crystals: Soft Crystal versus Stiff Crystal

We experimentally demonstrate the presence of negative refraction on acoustic passbands of two-dimensional phononic crystals for in-plane and anti-plane shear waves. We investigate the phenomenon on two geometrically identical *two-phase* crystals with inverse material properties: one stiff crystal (Sample 1: Aluminum matrix with PMMA inclusions), and another a soft crystal (Sample 2: PMMA matrix with Aluminum inclusions). We show that in the case of the in-plane shear wave, the soft crystal does not show negative refraction in the first passband; however, the stiff crystal does show negative refraction for the first mode. In the case of the anti-plane shear wave tests, both crystals show only positive refraction in the first passband. But, in the soft crystal, negative refraction is present in the second passband (optical branch). The experimental results confirm the prediction of our theoretical model, which allows us to predict the behaviors of phononic crystals as we change the properties of their constituents.

2.1 Introduction

Recent surge of research in the field of phononic crystals and acoustic metamaterials has guided the researchers towards the experimental validation of various intriguing phenomena

such as the negative refraction and the acoustic imaging. Morvan et al. (2010) experimentally demonstrated negative refraction of transverse elastic waves in a two-dimensional phononic crystal made of a square lattice of cylindrical air cavities in an aluminum matrix. Soon after, Lee et al. (2011) conducted negative refraction experiments with guided SH waves in a thin phononic crystal plate. Both of them demonstrated experimental verification of negative refraction for shear waves only for higher modes. Nemat-Nasser (2017b) has recently developed a unified approach to show the negative refraction with positive phase velocity refraction over the first or any desired passband of simple photonic and phononic crystals. Nemat-Nasser (2017a) shows the existence of negative refraction on the two lowest acoustic-branch passbands (shear and longitudinal modes) using a simple two-dimensional phononic crystal.

In this chapter, we examine the dynamic response of *two-phase* phononic crystal in detail with a focus on shear wave refraction through the crystals. We investigate the refraction of in-plane shear and anti-plane shear wave at a plane interface between a homogeneous elastic wedge and the elastic composite crystal. The theoretical model is based on the *new quotient* method by Nemat-Nasser (1972a,b). In this approach, both the displacement and stress fields, in the phononic crystals are varied independently. The theoretical work (Nemat-Nasser, 1972a, 2017b) provides the range of frequency, and the direction of incident wave vector, where the negative or the positive refraction can be detected by small variations in the incident phase angle or in the incident frequency. These calculations provide us the suitable guidance to design the phononic crystals. The focus of this chapter is on the experimental verification of the negative refraction in the first passband (for in-plane shear case), and in the second passband (for anti-plane shear case).

Metamaterials offer an advantage over the natural materials, as they allow the material to be based on the desired properties. For example, metamaterials can possess various phononic band structures and energy-flux patterns depending on their material properties and microstructures. These outcomes are quite sensitive to the micro-architectures of the crystals. Furthermore, the equi-frequency contours together with the energy flux vectors provide us with deep information

and understanding about the phononic crystals. Selecting proper materials, we can design various crystals exhibiting different overall properties including positive and negative refractions for a range of frequencies. The presence of negative and positive refractions on the acoustic-branch passbands provides useful capabilities of acoustic wave manipulation, such as focusing (Yang et al., 2004; Zhang et al., 2009), scattering (Kaina et al., 2015), filtering and acoustic beam steering. In case of the ultrasonic acoustics, one of the most important applications could be in the field of medical imaging.

2.2 Experimental Setup and Results

As described in the previous chapter, we use two phononic crystals, Sample 1 and Sample 2, in order to experimentally demonstrate the presence of negative refraction in the lowest longitudinal mode. Sample 1 is made of Aluminum matrix with periodically inserted circular PMMA pins of 4.76 *mm* diameter. The spacing between the pins in both x and y directions is 10 *mm*, the material properties are following:

$$E_1^M = E_2^M = 68\,GPa, \quad \nu^M = 0.33, \quad \rho^M = 2700\,kg/m^3;$$
$$E_1^I = E_2^I = 3\,GPa, \quad \nu^I = 0.40, \quad \rho^I = 1200\,kg/m^3,$$

where E_1 and E_2 are the elastic moduli, and ν, ρ are the Poisson's ratio and the mass density, respectively. The superscripts M and I denote the matrix and the inclusion, respectively. Both matrix and inclusions are made of isotropic materials.

Sample 2 is made of PMMA matrix with periodically inserted circular Aluminum pins of 4.76 *mm* diameter. The spacing between pins in both x and y directions is 10 *mm*, the material

properties are following:

$$E_1^M = E_2^M = 3\,GPa, \quad \nu^M = 0.40, \quad \rho^M = 1200\,kg/m^3;$$
$$E_1^I = E_2^I = 68\,GPa, \quad \nu^I = 0.33, \quad \rho^I = 2700\,kg/m^3.$$

The theoretical model presented by Nemat-Nasser (1972a, 2017b) provides the band gaps in the phononic crystals by giving the working frequency range, and also the appropriate incident angle of the incidence wave for the crystal. To achieve that, we have machined various triangular '*incidence wedges*' each of thickness 1.5 *inches*. We have machined the wedges of different materials to achieve different wave speeds of the incident shear wave. The reason that we have made the triangular shaped wedges is to obtain the desired incident angles. We use the normal incidence shear wave transducers (Olympus Panametrics NDT Transducers: V151, V153), the input transducer is mounted on a plane-smooth surface, and the wave propagates perpendicular to that surface. The direction of the polarization of shear wave is nominally in the line with the right angle connector (Olympus, 2016).

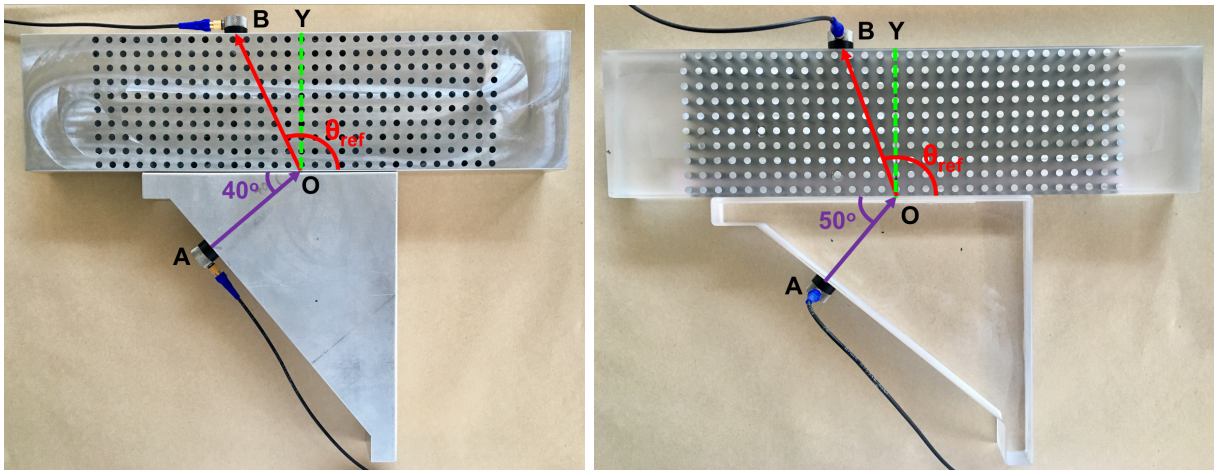

Figure 2.1. Transducer A is a transmitter, and transducer B is working as a receiver. (Left): Sample 1 with a 40° homogeneous Aluminum wedge for in-plane test. (Right): Sample 2 with a 50° homogeneous PMMA wedge for anti plane shear test. Notice the orientation of the transducers.

In the experiment, we send the incident signal by transducer A through one of the

homogeneous wedge of appropriate incident angle. The signal falls on the interface of the wedge and the sample at point O. A part of the signal refracts into the sample, we record the refracted signal with transducer B on the other side of the Sample (Figure 2.1). The refraction angle is manually measured as the angle of OB from the interface in the counter clockwise direction from the positive x_1 direction. We further study the recorded signals on the Oscilloscope in time domain as well as in the frequency domain (FFT).

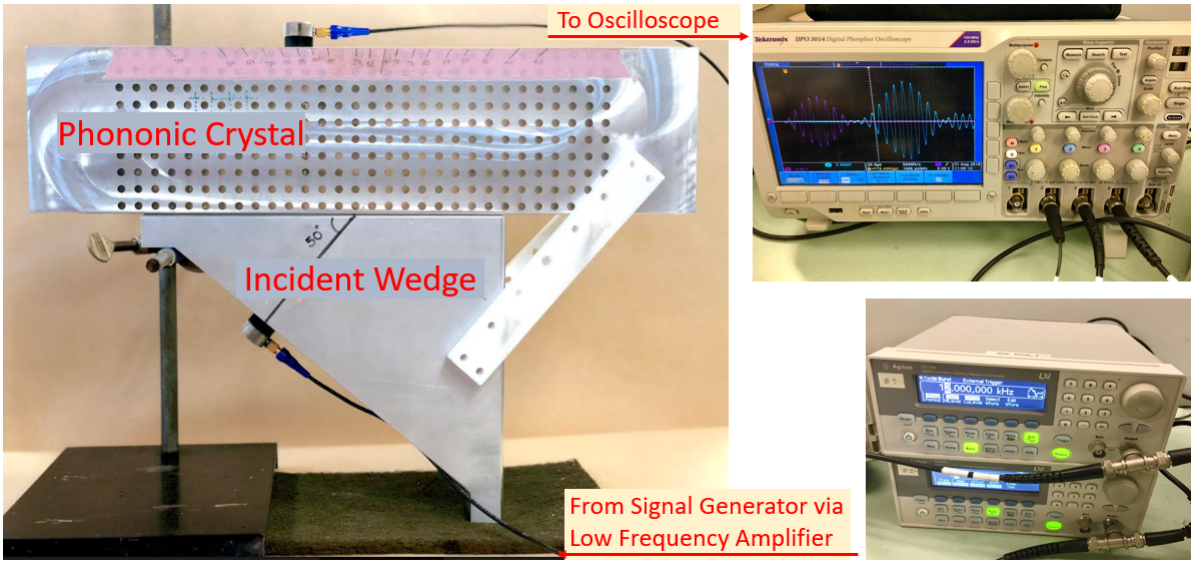

Figure 2.2. Experimental Setup

Figure 2.2 is an actual image of the experimental setup, with the help of a laboratory stand we rest one of incident wedge such that it's top surface is horizontal. We apply an appropriate couplant on the top surface of the wedge and on one of the surface of the phononic crystal. Next we mount the crystal on the incident wedge with the help of Teflon clamps to secure the setup.

If the incident angle at the interface of the wedge and the sample is θ_0, the x_1 component of the wave vector in the homogeneous wedge is given by $k_1 = \frac{\omega \cos\theta_0}{c_2}$, where ω is the angular frequency of the signal and c_2 is the shear wave speed in the homogeneous wedge. Note that the x_1 component of the wave vector must be continuous at the interface, hence the x_1 component of the wave vector in the sample equals to that in the wedge. This fact along with the dispersion

relation in the sample from the theoretical model provides us the information about the both components of the wave vector for the refracted signal at each frequency of the desired range. Using this technique (Table 2.1) the group-velocity and energy-flux directions can be computed in the desired frequency range, and that result is being compared to the experiment in following sections (2.2.1) and (2.2.2) .

Table 2.1. Selection Algorithm: Calculating theoretical refraction angle, θ_{ref}, in J^{th} mode at frequency $\bar{\omega}$ for an incident wedge with angle θ_0, and wave speed c. $\mathbf{v^p}$ and $\mathbf{v^g}$ show the direction of phase and group velocity in the phononic crystal, respectively.

Step 1:	Continuity at the interface $\Rightarrow \text{Q}_1^{\text{ref}} = \text{Q}_1^{\text{in}} = \frac{\bar{\omega}\cos\theta_0}{\text{c}}\text{a}_1$
Step 2:	Evaluate corresponding Q_2^{ref} at the same frequency $\bar{\omega}$, such that $\omega_{\text{J}}(\text{Q}_1^{\text{ref}}, \text{Q}_2^{\text{ref}}) = \bar{\omega}$
Step 3:	Calculate theoretical refraction angle θ_{ref} at $(\text{Q}_1^{\text{ref}}, \text{Q}_2^{\text{ref}})$ in J^{th} mode
Step 4:	Repeat Steps 1-3 for next frequency in J^{th} mode

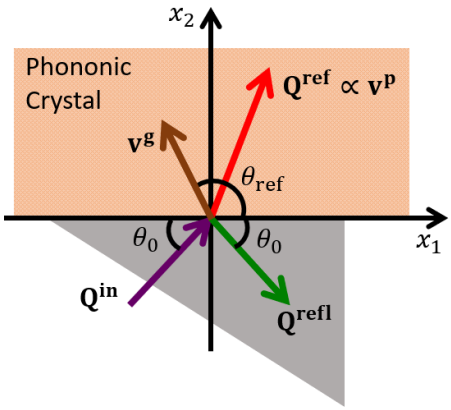

2.2.1 In-plane Shear Tests Results

Aluminum Matrix-PMMA Pins: Sample 1

In this case, we focus on the first passband (shear mode) for the material properties given in the previous section for the Sample 1. We evaluate the equi-frequency contours along with the energy flux vectors to know the direction of the refraction (Figure 2.3). We have also shown the frequency surface of the first passband. As seen from the figure, we notice for Sample 1, the shear mode (first passband) displays positive and negative refraction. Using these calculations and results, we choose two homogeneous wedges of Aluminum, one with incidence angle 40°, and other with the angle of 50°. We choose these two wedges knowing that it can carry the incident wave within the desired frequency range of the shear mode. It is also the case when, for the

same incident angle, the positive and the negative refractions are found as we vary the frequency within it's range. We show the experimental measurements with respect to the theoretical results in Figures 2.4 and 2.5 for the wedge with incident angle 40° and 50°, respectively. We note that the experimental results are in reasonable agreement with the theoretical calculations using the new quotient.

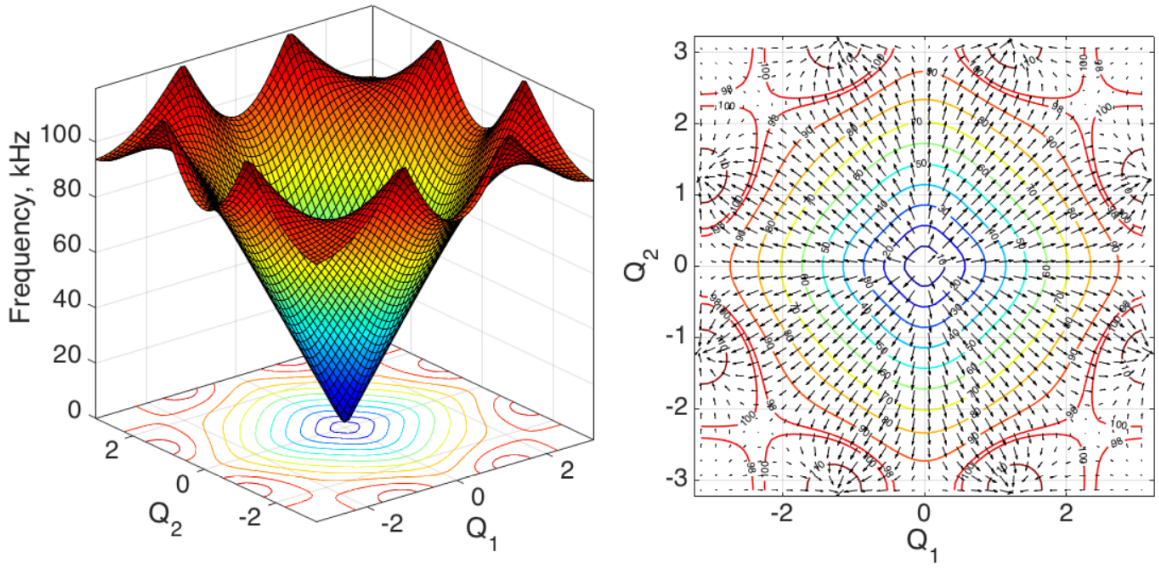

Figure 2.3. Sample 1 acoustic branch in-plane shear passband. (Left): Frequency surface, (Right): equi-frequency contour and energy flux vectors of shear mode for Sample 1. We do observe negative refraction in this case.

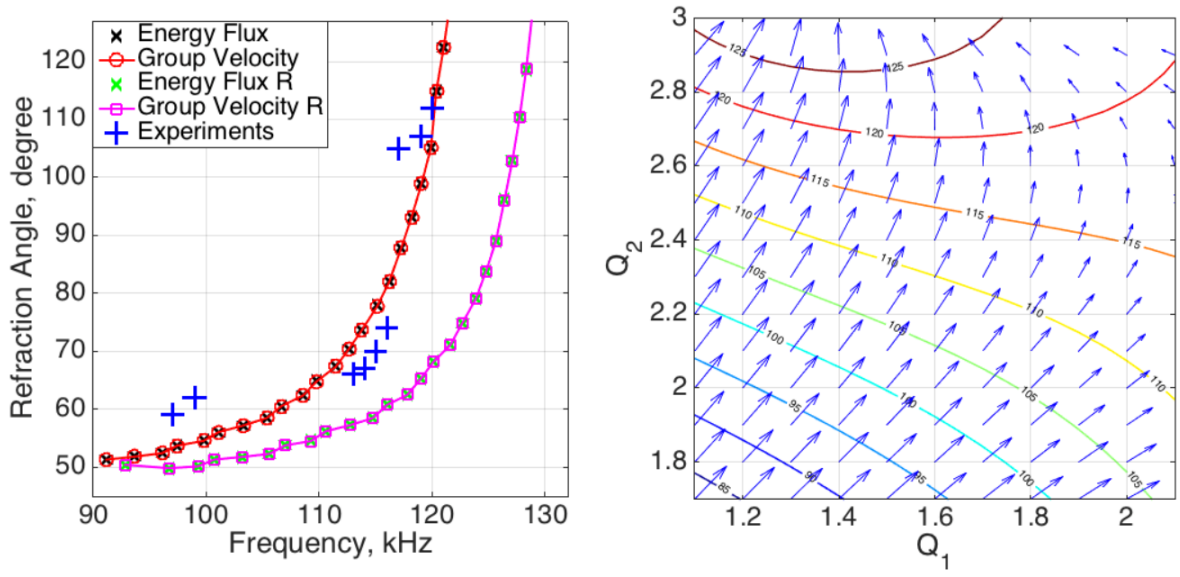

Figure 2.4. In-plane shear wave test of Sample 1. (Left): Group velocity and energy-flux directions and experimental results using an aluminum wedge with incident angle 40°, R denotes the calculations done using Rayleigh quotient. (Right): The plot of equi-frequency contours and the energy flux vectors of the first (shear mode) passband.

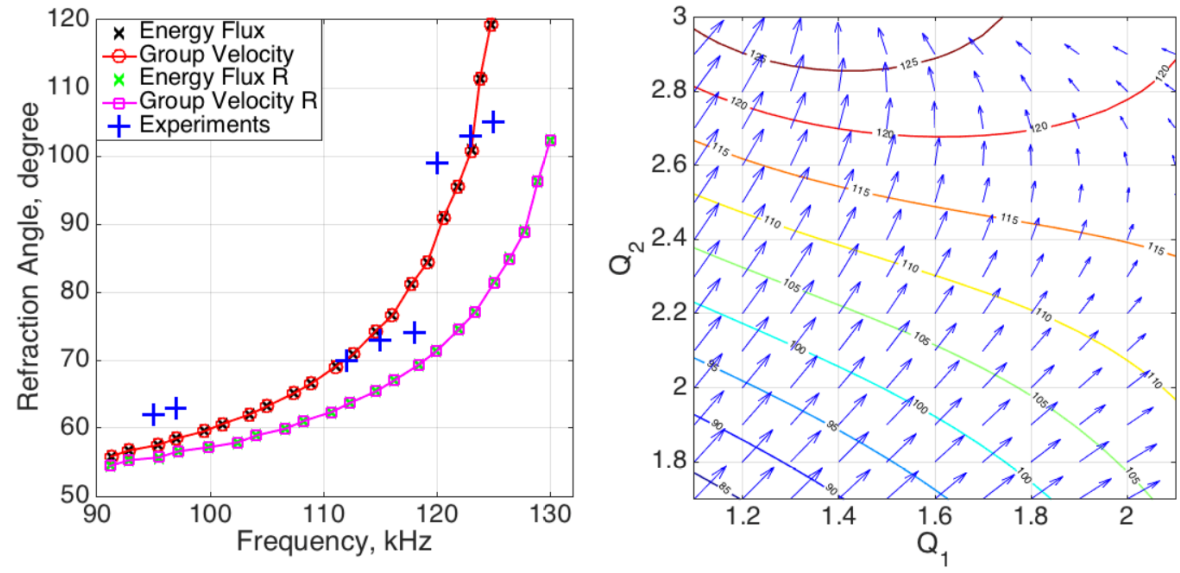

Figure 2.5. In-plane shear wave test of Sample 1. (Left): Group velocity and energy-flux directions and experimental results using an aluminum wedge with incident angle 50°, R denotes the calculations done using Rayleigh quotient. (Right): The plot of equi-frequency contours and the energy flux vectors of the first (shear mode) passband.

PMMA Matrix-Aluminum Pins: Sample 2

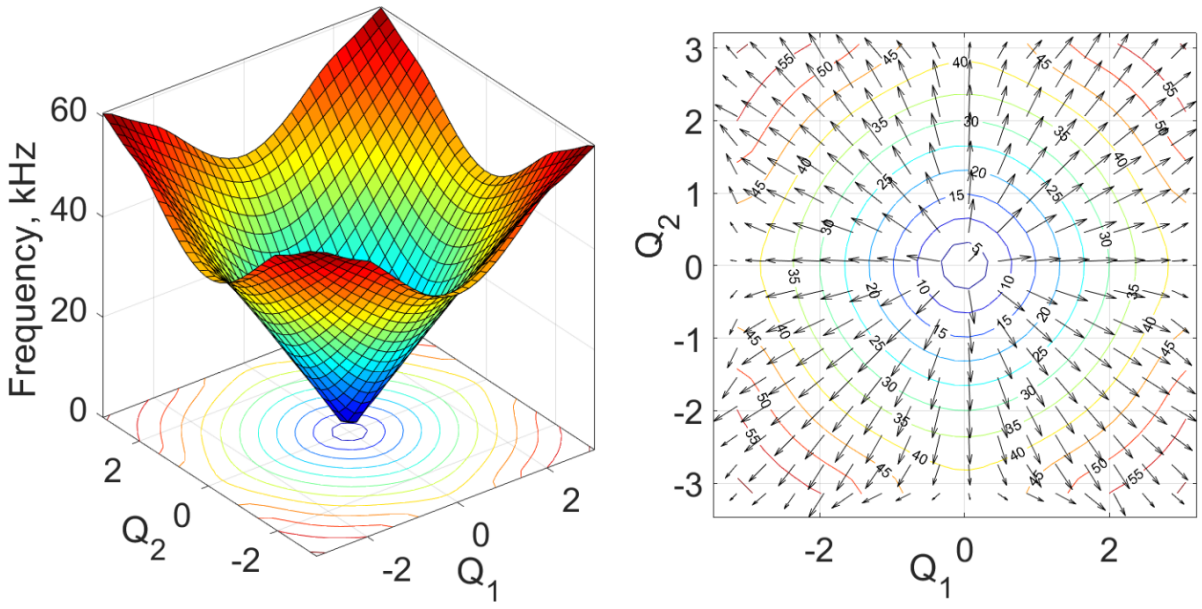

Figure 2.6. Sample 2 acoustic branch in-plane shear passband. (Left): Frequency surface, (Right): equi-frequency contour and energy flux vectors of shear mode for Sample 2. Note that there is no negative refraction in this case.

In this case we focus on the first passband (shear mode), for the material properties given above for the Sample 2, we evaluate the equi-frequency contours along with the energy flux vectors to know the direction of the refraction (Figure 2.6). We have also shown the frequency surface of the first passband. As seen from the Figure we notice for Sample 2 the shear mode (first passband) only displays positive refraction.

Mode Mixing Investigation

We make sure that we measure truly a shear wave in first mode negative refraction tests in Sample 1. Using the shear and longitudinal transducers, we record shear and longitudinal signals at the same location, and notice that the small longitudinal wave does not affect the shape and magnitude of the transmitted in-plane shear wave signal (Figure 2.7). Our numerical calculations (Figure 1.6) also show very clearly that the shear and the longitudinal passbands do not cross

each other.

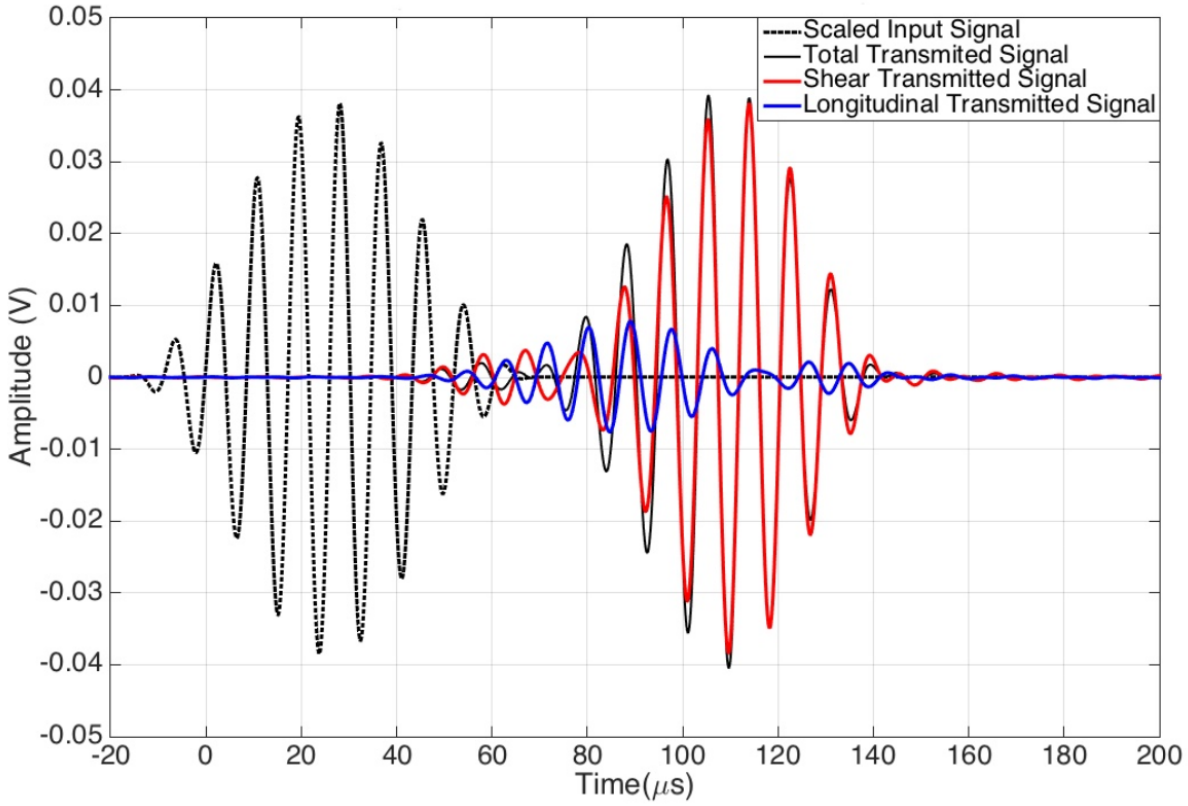

Figure 2.7. A typical negative refraction in-plane shear wave signal is plotted for a Sample 1 test. The plotted shear signal (in red) is the difference between total transmitted signal and the recorded longitudinal signal at the same location. We note that the small longitudinal recorded signal has no effect on the net shear wave signal.

2.2.2 Anti-plane Shear Tests Results

For the case of anti-plane shear, each acoustic, and optical branch has only one passband. Neither of the two samples exhibits negative refraction in the first mode (*acoustic branch passband*). Therefore, for experiments we focus on mode 2 (*optical branch passband*) to demonstrate the negative refraction.

PMMA Matrix-Aluminium Pins: Sample 2

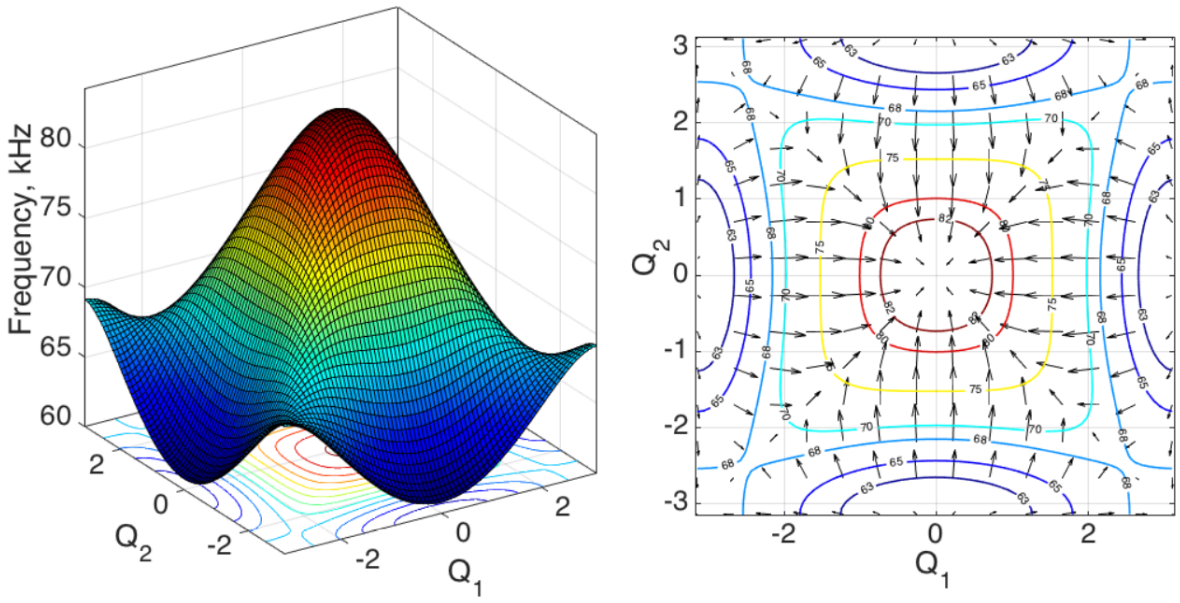

Figure 2.8. Sample 2 anti-plane shear mode 2 (optical branch passband). (Left): Frequency surface, (Right): equi-frequency contour and energy flux vector of anti-plane shear mode 2 (optical branch passband) for Sample 2. We do observe negative refraction in this case.

In this case we focus on the second passband (anti-shear mode), for the material properties given above for the Sample 2, we evaluate the equi-frequency contours along with the energy flux vectors to know the direction of the refraction (Figure 2.8). We have also shown the frequency surface of the second mode. As seen from the figure, we notice for Sample 2, the second mode displays positive and negative refractions. Using these calculations and results, we select a homogeneous wedge of PMMA with the angle of 50°. We choose this wedge knowing that it can carry the incident wave within the desired frequency range of the second mode. It is also the case when, for the same incident angle, the positive and the negative refractions are found as the frequency varies within its range. We show the experimental measurements with respect to the theoretical results in Figure 2.9. We have also shown the group velocity trend following the Rayleigh quotient, which is supposed to provide an upper limit, and rightly, so the experimental points are in between these two curves.

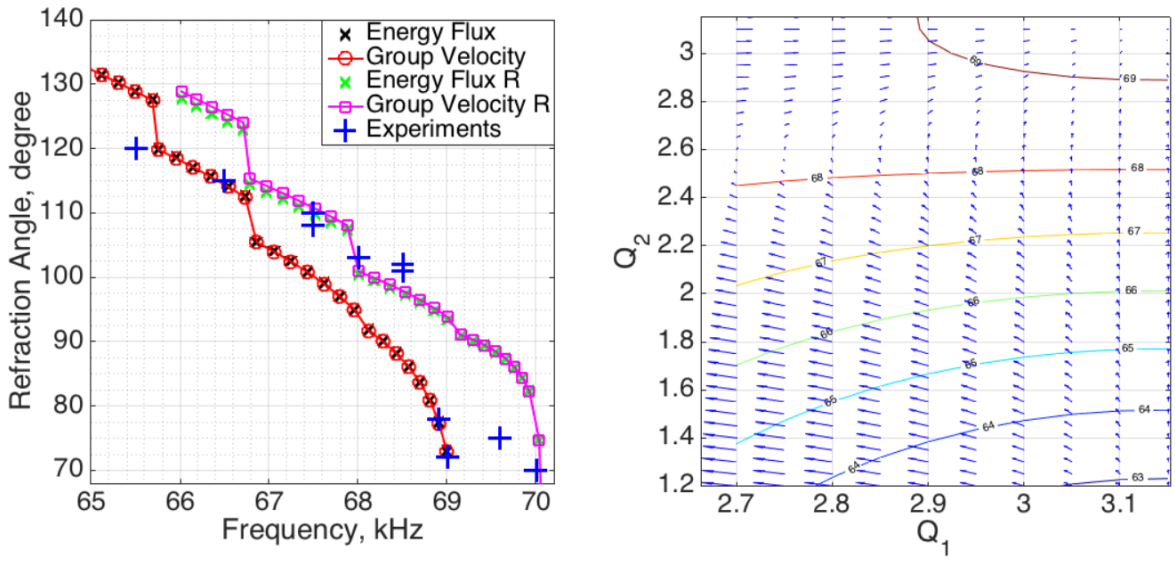

Figure 2.9. Optical branch passband anti-plane shear wave test of Sample 2. (Left): Group velocity and energy-flux directions and experimental results using a PMMA wedge with incident angle 50°, R denotes the calculations done using Rayleigh quotient. (Right): Equi-frequency contours and the energy flux vectors.

It is worth to mention that the theoretical results and trends provide us a tool to design the experiment in terms of choosing the appropriate incidence wedge as well as selecting the desired frequency range. Without the guideline of the robust theoretical framework, it would be almost impossible to carry out such experiments and interpret them in the correct way.

Aluminum Matrix-PMMA Pins: Sample 1

For the anti-plane shear wave calculations with material properties of Sample 1, we notice that there is some negative refraction for the case of second mode, as seen from frequency surface and also equi-frequency contours (Figure 2.10), but it's very weak. It is very hard to detect negative refraction in experiments (Figure 2.11) due to possible dissipation of the energy; the theoretical calculation does not take account of the dissipation in the material.

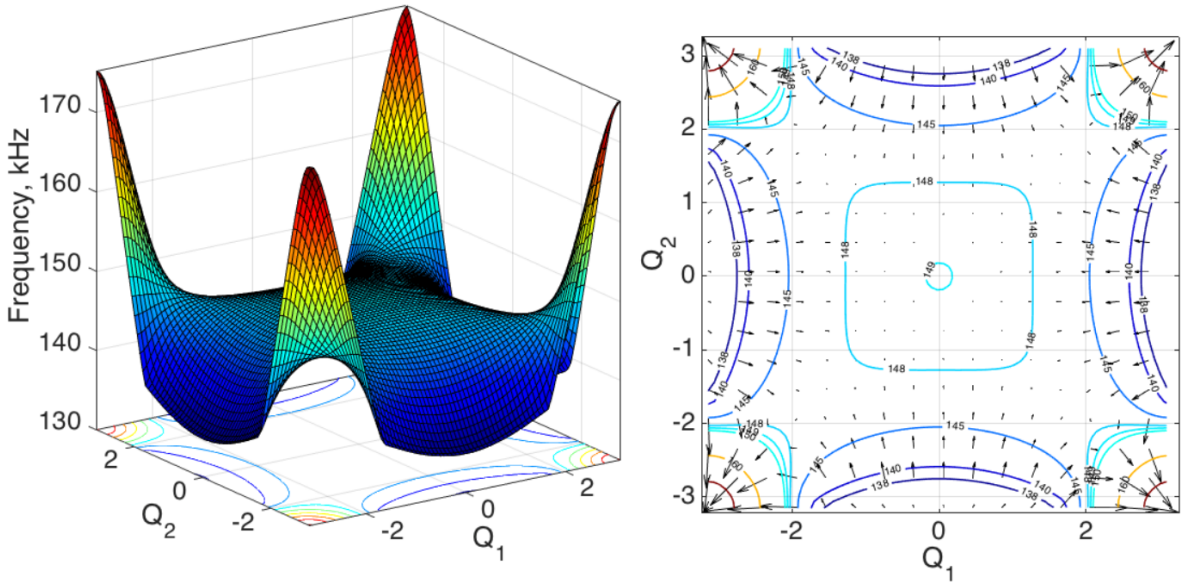

Figure 2.10. Sample 1 anti-plane shear mode 2 (optical branch passband). (Left): Frequency surface, (Right): equi-frequency contour and energy flux vector of anti-plane shear mode 2 (optical branch passband) for Sample 1. Note that the negative refraction in this case is very weak.

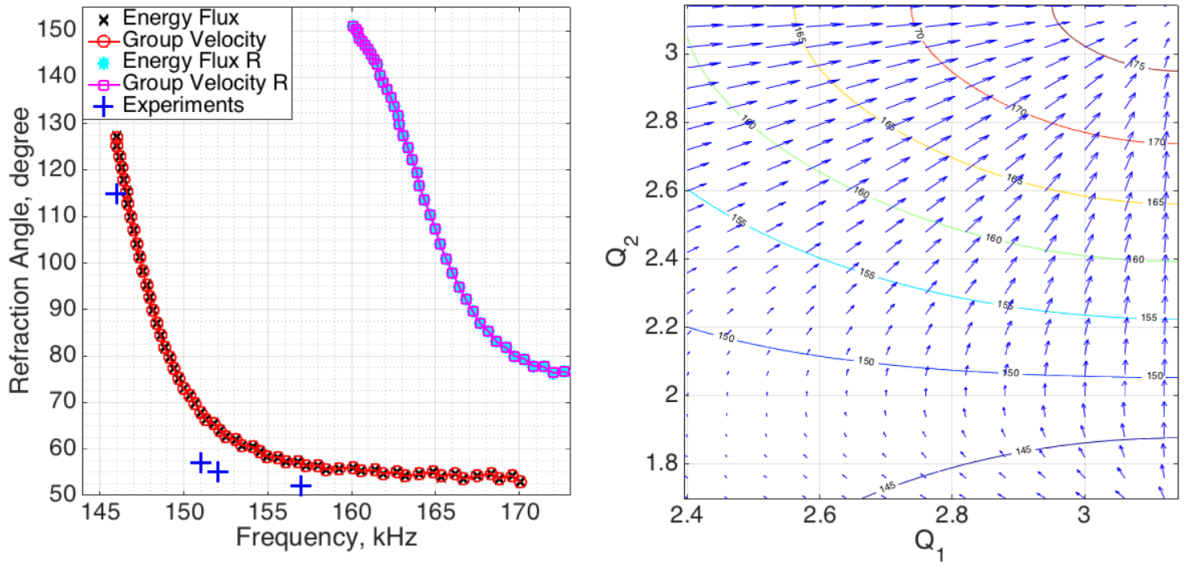

Figure 2.11. Optical branch passband anti-plane shear wave test of Sample 1. (Left): Group velocity and energy-flux directions and experimental results using an aluminum wedge with incident angle 30°, R denotes the calculations done using Rayleigh quotient. (Right): Equi-frequency contours and the energy flux vectors.

2.3 Theoretical Framework

Theoretical model presented in this section is based on the work done by Nemat-Nasser (1972a); Srivastava and Nemat-Nasser (2014); Nemat-Nasser (2017b). We present the theoretical framework including the governing field equations, and the periodic solution for the generic periodic composite materials or termed as crystals. Consider a two phase doubly periodic elastic composite with a rectangular unit cell of dimensions a_1 and a_2. A typical unit cell, Ω_1 has a concentric inclusion, Ω_2 of a rectangular or an elliptical shape. To simplify, consider the coordinate axes, x_1 and x_2 are parallel to the principal axis of the unit cell, a_1 and a_2, respectively.

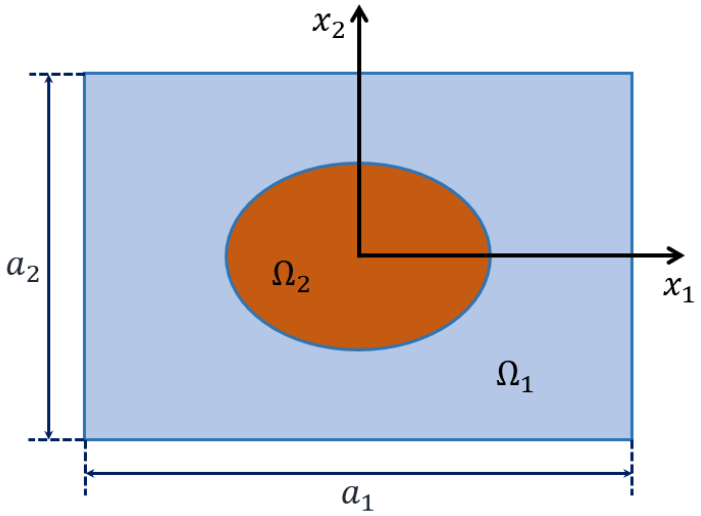

Figure 2.12. A typical unit cell Ω_1 of a two-dimensional periodic elastic composite with elliptical inclusion Ω_2.

2.3.1 Governing Equations and Periodic Solution: In-plane Waves

For Bloch-form time harmonic wave of frequency ω, all the field variables are proportional to $e^{-i\omega t}$. Therefore, the field equations can be written from the first variation of λ_N (1.5) for any arbitrary small variations of displacement and stress field as it's corresponding Euler equation:

$$\sigma_{lj,l} + \omega^2 \rho u_j = 0; \quad \frac{1}{2}(u_{j,l} + u_{l,j}) - D_{ljmn}\sigma_{mn} = 0, \quad j,l,m,n = 1,2 \tag{2.1}$$

where a comma followed by an index denotes the differentiation with respect to the corresponding coordinate variable, ρ is the mass density, $D_{ljmn} = D_{mnlj}$ is the elastic compliance tensor. Now we write the displacement and the stress field as following approximate functions

$$\begin{bmatrix} u_j \\ \sigma_{lj} \end{bmatrix} = \begin{bmatrix} u_j^p(x_1, x_2) \\ \sigma_{lj}^p(x_1, x_2) \end{bmatrix} e^{\mathrm{i}(k_1 x_1 + k_2 x_2)}, \tag{2.2}$$

where the superscript p denotes the periodic part, these functions automatically satisfy Floquet-Bloch boundary conditions. The geometry, mass density, and the elastic compliance are all periodic with the periodicity of the unit cell. For two-dimensional plane strain or the plain stress case, the only non-zero components of the elastic compliance tensor, D, are

$$D_{1111} = D_{11}, \quad D_{1122} = D_{12} = D_{21}, \quad D_{2222} = D_{22}, \quad D_{1212} = D_{2121} = D_{33} \tag{2.3}$$

Furthermore, we can rewrite the above tensor, D as a 3×3 second order tensor as

$$[D] = \frac{1}{\mu} \begin{bmatrix} \frac{\kappa+1}{8} & \frac{\kappa-3}{8} & 0 \\ \frac{\kappa-3}{8} & \frac{\kappa+1}{8} & 0 \\ 0 & 0 & \frac{1}{2} \end{bmatrix}, \qquad \kappa = \begin{cases} 3 - 4\nu & \text{plane strain,} \\ \frac{3-\nu}{1+\nu} & \text{plane stress} \end{cases}, \tag{2.4}$$

where ν is the Poisson's ratio and μ is the shear modulus.

We further express the periodic part of the field variables as:

$$\begin{bmatrix} u_j^p \\ \sigma_{lj}^p \end{bmatrix} = \sum_{n_1, n_2 = -M}^{+M} \begin{bmatrix} U_j^{n_1, n_2} \\ S_{lj}^{n_1, n_2} \end{bmatrix} e^{\mathrm{i}2\pi\left(\frac{n_1 x_1}{a_1} + \frac{n_2 x_2}{a_2}\right)}. \tag{2.5}$$

Now substitute these expressions into equation (2.2), utilize equation (2.1), and multiply each

side of the equations by $e^{-\mathrm{i}2\pi\left(\frac{m_1 x_1}{a_1}+\frac{m_2 x_2}{a_2}\right)}$ to obtain, after the integration over the typical unit cell:

$$\begin{aligned} &H_1 S_{11} + H_2 S_{12} + \Lambda_\rho \omega^2 U_1 = 0 \\ &H_1 S_{21} + H_2 S_{22} + \Lambda_\rho \omega^2 U_2 = 0 \end{aligned} \quad , \quad \begin{bmatrix} H_1 U_1 \\ H_2 U_2 \\ H_1 U_2 + H_2 U_1 \end{bmatrix} = \begin{bmatrix} \Lambda_{D_{11}} S_{11} + \Lambda_{D_{12}} S_{22} \\ \Lambda_{D_{22}} S_{22} + \Lambda_{D_{21}} S_{11} \\ \Lambda_D S_{12} \end{bmatrix} \tag{2.6}$$

where $S_{jl} = [S_{jl}^{n_1,n_2}]$ and $U_j = [U_j^{n_1,n_2}]$ are each $(2M+1)^2 \times (2M+1)^2$ matrix. H_1, H_2 are $(2M+1)^2 \times (2M+1)^2$ diagonal matrices with the diagonal components $\mathrm{i}(k_1 + 2\pi n_1/a_1)\delta_{n_1 m_1}$ and $\mathrm{i}(k_2 + 2\pi n_2/a_2)\delta_{n_2 m_2}$, respectively, where, m_1, m_2 varies similar to n_1, n_2, i.e., $m_1, m_2 = -M, -M+1, \cdots, +M-1, +M$. For any material property f, the components of Λ_f are defines as

$$\Lambda_f^{(n_1,n_2,m_1,m_2)} = \int_\Omega f(\mathbf{x}) e^{\mathrm{i}2\pi\left[\frac{(n_1-m_1)x_1}{a_1}+\frac{(n_2-m_2)x_2}{a_2}\right]} dx_1\, dx_2, \tag{2.7}$$

and $\Lambda_D = \Lambda_{D_{11}} + \Lambda_{D_{22}} - 2\Lambda_{D_{12}}$. We may further manipulate the above expressions to write

$$\begin{bmatrix} \Lambda & -H \\ H & \Psi \end{bmatrix} \begin{bmatrix} S \\ U \end{bmatrix} = 0, \quad \Lambda = \begin{bmatrix} \Lambda_{D_{11}} & \Lambda_{D_{12}} \\ \Lambda_{D_{21}} & \Lambda_{D_{22}} \end{bmatrix}, \quad H = \begin{bmatrix} H_1 & 0 \\ 0 & H_2 \end{bmatrix}, \tag{2.8}$$

and

$$\Psi = \begin{bmatrix} H_2 \Lambda_D^{-1} H_2 + \omega^2 \Lambda_\rho & H_2 \Lambda_D^{-1} H_1 \\ H_1 \Lambda_D^{-1} H_2 & H_1 \Lambda_D^{-1} H_1 + \omega^2 \Lambda_\rho \end{bmatrix}, \quad S = \begin{bmatrix} S_{11} \\ S_{22} \end{bmatrix}, \quad U = \begin{bmatrix} U_1 \\ U_2 \end{bmatrix}. \tag{2.9}$$

Next, we eliminate the stress, S, in order to write the characteristic equation as

$$[H\Lambda^{-1}H + \hat{\Psi} + \omega^2 \Lambda_\rho I]U = 0, \qquad \det|H\Lambda^{-1}H + \hat{\Psi} + \omega^2 \Lambda_\rho I| = 0, \tag{2.10}$$

where $\hat{\Psi} = \Psi - \omega^2 \Lambda_\rho I$, and I is the identity matrix. The determinant in the above equation depends parametrically on the wave vector components, $Q_1 \equiv k_1 a_1$ and $Q_2 \equiv k_2 a_2$, where a_1 and

a_2 are the unit cell dimensions, therefore, equation (2.10) provides the frequency bands, ω, as a function of Q_1 and Q_2. Furthermore, for each eigenfrequency, the corresponding displacements, U, can be obtained using equation (2.8), and then the stress components are

$$S = \Lambda^{-1} HU, \qquad S_{12} = S_{21} = \Lambda_D^{-1}(H_1 U_2 + H_2 U_1). \tag{2.11}$$

Group Velocity and Energy Flux

Since the eigenfrequencies, ω, are the functions of Q_1 and Q_2, they form surfaces in the (Q_1, Q_2, ω)-space, referred to as the Brillouin zones. The fundamental zone corresponds to $-\pi \le Q_1, Q_2 \le \pi$. We focus on the fundamental zone and examine the dynamic properties of the doubly periodic elastic composites over the first few frequency bands. On each frequency bands, the phase and group velocities are given by

$$v^p_{Jj} = \frac{\omega_J k_j}{k_1^2 + k_2^2}, \qquad v^g_{Jj} = \frac{\partial \omega_J}{\partial k_j}, \qquad j = 1, 2, \tag{2.12}$$

here and below, $J = 1, 2, \ldots$ denotes the frequency band. The refraction angle, say α_J, is computed from

$$\alpha_J = \tan^{-1}\left(\frac{v^g_{J2}}{v^g_{J1}}\right). \tag{2.13}$$

It is known (Brillouin, 1948) that the direction, α_J, is essentially the same as the direction of the energy-flux for non-dissipative media. Next, we outline the energy-flux calculation.

The x_1- and x_2- components of the energy-flux, averaged over a unit cell, are

$$\begin{aligned}\overline{E}_{Jk} &= \frac{\omega_J}{2\pi} \int_0^{2\pi/\omega_j} < Re(\sigma_{kjJ}) Re(\dot{u}_{jJ})^* > dt = -\frac{1}{2} < \sigma^p_{kjJ} \dot{u}^{p*}_{jJ} > \\ &= \frac{1}{2} \mathrm{i}\omega_J \sum_{n_1, n_2 = -N}^{+N} S^{n_1,n_2}_{kjJ} U^{n_1,n_2}_{jJ}, \qquad j, k = 1, 2. \end{aligned} \tag{2.14}$$

The direction of the energy-flux vector, say β_J, can be written as

$$\beta_J = \tan^{-1}\left(\frac{\overline{E}_{J2}}{\overline{E}_{J1}}\right). \tag{2.15}$$

It turns out that $\alpha_J = \beta_J$ for the class of problems considered in the present work, which has also been shown in sections (2.2.1) and (2.2.2). Even the energy-flux velocity can be computed as dividing the energy-flux by the corresponding average elastic strain energy as

$$\overline{V}_{Jk} = \frac{\overline{E}_{Jk}}{\frac{1}{2} < \sigma^{p}_{ljJ}\epsilon^{p*}_{ljJ} >}, \qquad l, j, k = 1, 2. \tag{2.16}$$

We have verified that the calculated group velocity and the energy-flux velocities are essentially come out to be same (Figure 2.13). Willis (2016) has also proved that the energy travels with the group velocity for general plane Floquet-Bloch waves in the periodic elastic composites.

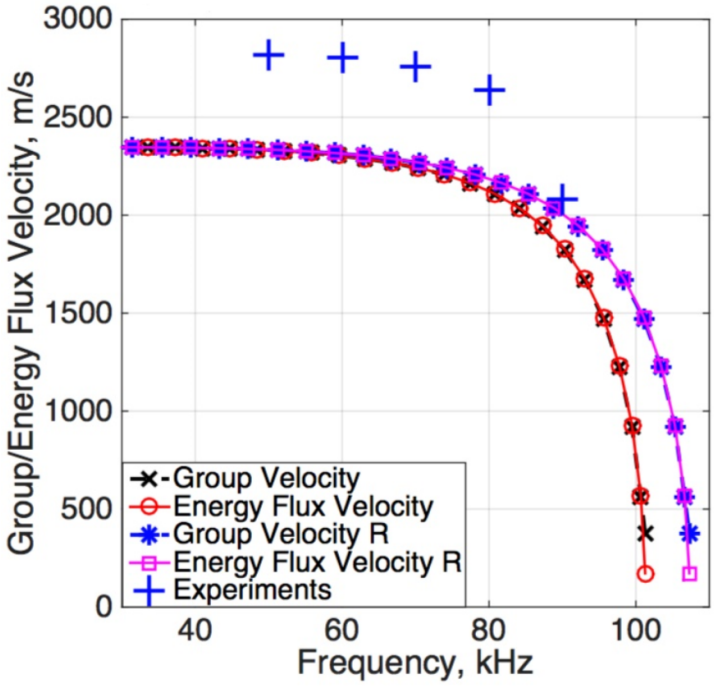

Figure 2.13. In-plane shear wave test of Sample 1. Acoustic-branch shear mode energy-flux and group velocities as a function of frequency for $Q_1 = 0$, we also have plotted the experimental values. R denotes the calculations done using Rayleigh quotient.

Validation of Theoretical Model with COMSOL Multiphysics

In this section we show the validation of theoretical model and it's implementation by comparing the band structure calculations with COMSOL Multiphysics results. Figure 1.6 shows acoustic branch passbands for Sample 1 using new quotient, λ_N calculations. We performed COMSOL Multiphysics simulations to obtain the same band structure, and we get very comparable results (Figure 2.14). The frequency range is higher ($\sim 8\%$) in COMSOL Multiphysics calculations, but the trend is identical. This is excepted because the new quotient gives a lower bound on eigenfrequencies. Figure 2.14 also shows that there is no mode mixing between first two passbands of Sample 1.

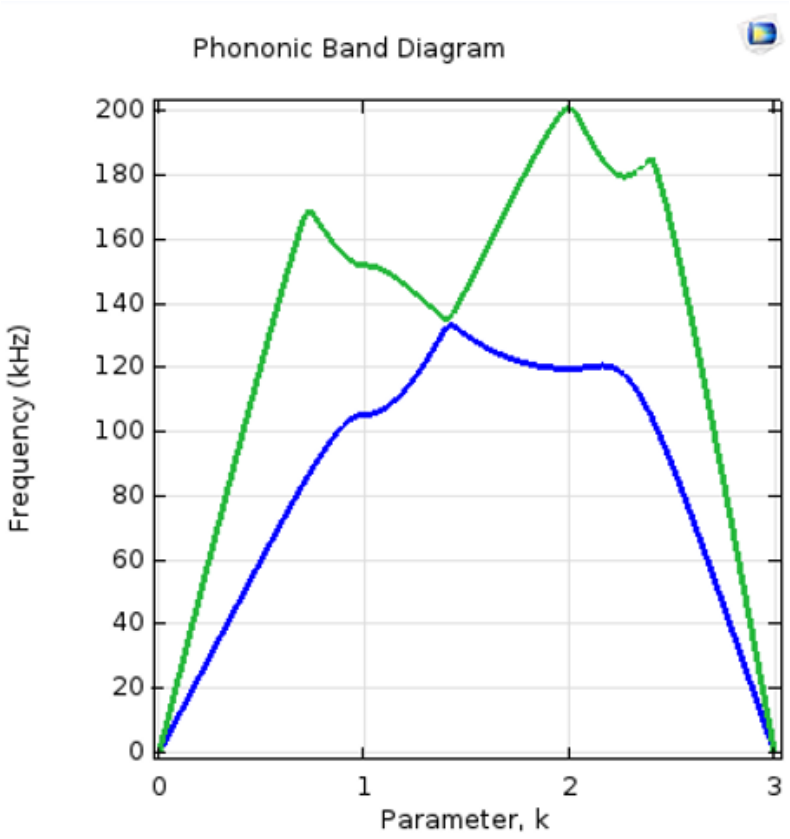

Figure 2.14. COMSOL Multiphysics band structure calculations for Sample 1. Frequency variation for the first two passbands along the Γ, X, M, Γ lines is plotted. Γ, X, M, Γ points are denoted by parametric values of k as 0,1,2,3, respectively.

2.3.2 Governing Equations and Periodic Solution: Anti-plane Waves

The Bloch-form SH waves of frequency ω involve two shear stress components, $\tau_j(x_1, x_2)$, where $j = 1, 2$, and a out of plane displacement, $w(x_1, x_2)$. The stress and the displacement field satisfy the following field equations:

$$\begin{aligned} \tau_{j,j} + \omega^2 \rho w = 0, \quad \gamma_j = w_{,j}, \\ \tau_j = \mu_{jk}\gamma_k, \quad \gamma_j = D_{jk}\tau_k, \quad j,k = 1,2, \end{aligned} \tag{2.17}$$

where ρ is the mass density, γ_j are shear strain components and $\mu_{jk} = \mu_{kj}$ and $D_{jk} = D_{kj}$ are the components of the shear and the compliance moduli, respectively. The repeated indices are summed, and a comma followed by an index denotes the differentiation with respect to the corresponding coordinate variable. Since the principal axes of the elasticity tensor, therefore, μ_{jk}, are in the x_1, x_2-directions, $\mu_{12} = \mu_{21} = 0$. Also,

$$\begin{bmatrix} w \\ \tau_j \end{bmatrix} = \begin{bmatrix} w^p(x_1, x_2) \\ \tau_j^p(x_1, x_2) \end{bmatrix} e^{\mathrm{i}(k_1 x_1 + k_2 x_2)}, \tag{2.18}$$

where superscript p denotes the periodic part. The geometry, mass density, and the elastic compliance are all periodic with the periodicity of the unit cell. We further express the periodic part of the field variables as:

$$\begin{bmatrix} w^p \\ \tau_j^p \end{bmatrix} = \sum_{n_1, n_2 = -M}^{+M} \begin{bmatrix} W^{n_1, n_2} \\ T_j^{n_1, n_2} \end{bmatrix} e^{\mathrm{i}2\pi\left(\frac{n_1 x_1}{a_1} + \frac{n_2 x_2}{a_2}\right)}. \tag{2.19}$$

Next we substitute the above expression into equation (2.18), utilize equation (2.17), multiply each side of the equations by $e^{-\mathrm{i}2\pi\left(\frac{m_1 x_1}{a_1} + \frac{m_2 x_2}{a_2}\right)}$ and integrate over the unit cell to obtain (Nemat-Nasser,

2015)

$$\begin{bmatrix} H_1 & H_2 & \omega^2\Lambda_\rho \\ \Lambda_{D_{11}} & 0 & -H_1 \\ 0 & \Lambda_{D_{22}} & -H_2 \end{bmatrix} \begin{bmatrix} T_1 \\ T_2 \\ W \end{bmatrix} = 0 \tag{2.20}$$

which can be further expressed as

$$[\Phi - \omega^2\Lambda_\rho I]W = 0, \qquad \Phi = H_1\Lambda_{D_{11}}^{-1}H_1 + H_2\Lambda_{D_{22}}^{-1}H_2, \tag{2.21}$$

where $D_{11} = 1/\mu_{11}$ and $D_{22} = 1/\mu_{22}$. Therefore for given values of Q_1 and Q_2, the eigenfrequencies can be determined by the characteristic equation

$$\det|\Phi - \omega^2\Lambda_\rho I| = 0. \tag{2.22}$$

For each eigenfrequency the corresponding displacement, W, can be computed using equation (2.21), and the stress components becomes

$$T_1 = \Lambda_{D_{11}}^{-1}H_1W, \qquad T_2 = \Lambda_{D_{22}}^{-1}H_2W. \tag{2.23}$$

Group Velocity and Energy Flux

With similar calculations as we do for in-plane problem, on each frequency bands, the phase and group velocities are given by

$$v_{Jj}^p = \frac{\omega_J k_j}{k_1^2 + k_2^2}, \qquad v_{Jj}^g = \frac{\partial\omega_J}{\partial k_j}, \qquad j = 1, 2, \tag{2.24}$$

here and below, $J = 1, 2, \ldots$ denotes the frequency band. The refraction angle, say α_J, is computed from

$$\alpha_J = \tan^{-1}\left(\frac{v^g_{J2}}{v^g_{J1}}\right). \tag{2.25}$$

For the expression of evergy-flux, we have

$$\begin{aligned}\overline{E}_{Jk} &= \frac{\omega_J}{2\pi}\int_0^{2\pi/\omega_j} < Re(\tau_{kJ})Re(\dot{w}_J)^*) > dt = -\frac{1}{2} < \tau^p_{kJ}\dot{w}^{p*}_J > \\ &= \frac{1}{2}\mathrm{i}\omega_J \sum_{n_1,n_2=-N}^{+N} T^{n_1,n_2}_{kJ} W^{n_1,n_2}_J, \qquad k = 1, 2.\end{aligned} \tag{2.26}$$

The direction of the energy-flux vector, say β_J, can be written as

$$\beta_J = \tan^{-1}\left(\frac{\overline{E}_{J2}}{\overline{E}_{J1}}\right). \tag{2.27}$$

The energy-flux velocity would be

$$\overline{V}_{Jk} = \frac{\overline{E}_{Jk}}{\frac{1}{2} < \tau^p_{jJ} w^{p*}_{J,j} >}, \qquad j, k = 1, 2. \tag{2.28}$$

2.4 Conclusion

We have shown that stiff crystal (Sample 1) and soft crystal (Sample 1) exhibit different behaviors when they are examined for the in-plane or the anti-plane shear waves. For the in-plane shear wave, in the first (shear mode) passband, the soft crystal does not show the negative refraction while the stiff crystal does. Our main discovery comprised of designing a 'stiff crystal' with a hard matrix and soft inclusions to achieve negative refraction on the lowest acoustic passband. However, traditionally, researcher have always designed the phononic crystals with a

soft matrix material and a hard inclusions material.

In the case of anti-plane shear wave tests, both crystals show only positive refraction in the acoustic branch passband, however, both crystals show negative refraction for some range of frequencies in the optical branch passband (mode 2).

The work of Chapter 2 has been done with Professor S. Nemat-Nasser. The dissertation author was the primary investigator of this research work. The work is being prepared for a publication.

Chapter 3

Experimental Demonstration of Negative Refraction for Longitudinal Waves in 2D Phononic Crystals: Soft Crystal versus Stiff Crystal

We experimentally demonstrate the presence of negative refraction on acoustic passbands of two-dimensional phononic crystals for the longitudinal waves (second mode). Similar to the previous chapter, we investigate the phenomenon on two geometrically identical *two-phase* crystals: one stiff crystal (Sample 1: Aluminum matrix with PMMA inclusions), and another a soft crystal (Sample 2: PMMA matrix with Aluminum inclusions). We validate our experiments with the theoretical results of the model outlined in the previous chapter.

3.1 Introduction

Several researchers have done experiments showing negative refraction of longitudinal waves (García-Chocano et al., 2014; Zhu et al., 2014). Most of the *pressure waves* experiments have been done in fluid media; mainly water being the matrix material. Phononic crystals of these types are easier to assemble, however, in that case they can transmit only dilatational waves. Croënne et al. (2011) designed a two-dimensional phononic crystal made of triangular arrangement of steel rods embedded in epoxy. They have shown negative refraction of a higher longitudinal branch for the frequency range of 750 kHz to 860 kHz.

In this chapter we examine and detect the negative refraction on 'lowest' longitudinal mode. As outlined in the previous chapter, theoretical model is based on the *new-quotient* method developed by Nemat-Nasser (Nemat-Nasser, 1972a,b), which is an effective method for composites where the elastic modulus admits large discontinuity between the matrix and its inclusions.

3.2 Experimental Setup and Results

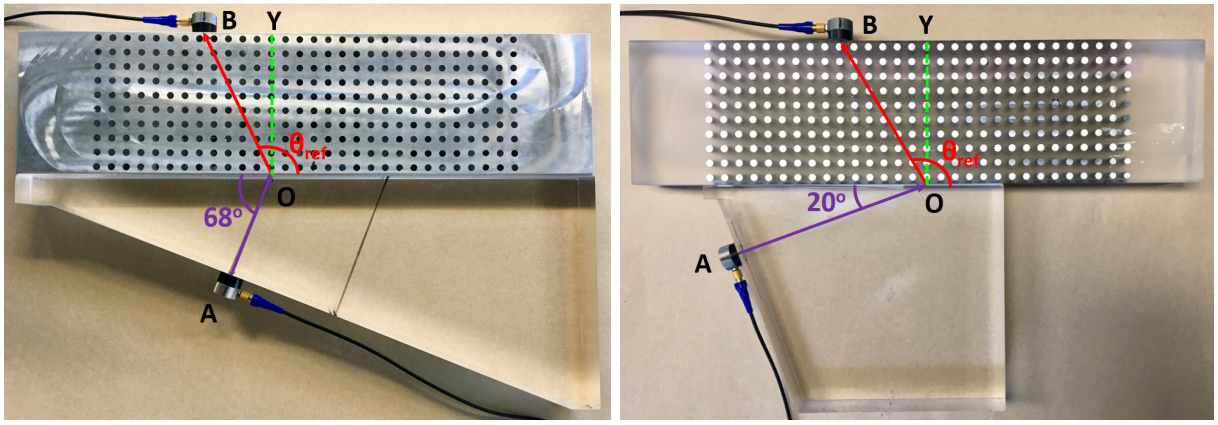

Figure 3.1. Transducer A is a transmitter, and transducer B is working as a receiver, for the longitudinal wave test. (Left): Sample 1 with a 68° homogeneous PMMA wedge. (Right): Sample 2 with a 20° homogeneous PMMA wedge.

As described in the previous chapters, we use two phononic crystals, Sample 1 and Sample 2, to numerically as well as experimentally investigate for the negative refraction in the lowest longitudinal mode (second acoustic branch). Sample 1 is made of Aluminum matrix with periodically inserted circular PMMA pins, and Sample 2 is made of PMMA matrix with periodically inserted circular Aluminum pins. In the experiment, we send the incident signal by a longitudinal wave transducer A through one of the homogeneous wedge of an appropriate incident angle. The signal falls on the interface of the wedge and the sample at point O. A part of the signal refracts into the sample, we record the refracted signal with transducer B on the other side of the sample (Figure 3.1). For both incident and receiving signal, we use standard contact longitudinal wave transducers (Olympus Panametrics NDT Transducer: V103). The

refraction angle is manually measured as the angle of OB from the interface in the counter clockwise direction from the positive x_1 direction. We further study the recorded signals on the Oscilloscope in time domain as well as in the frequency domain (FFT).

If the incident angle at the interface of the wedge and the sample is θ_0, the x_1 component of the wave vector in the homogeneous wedge is given by $k_1 = \frac{\omega \cos\theta_0}{c_1}$, where ω is the angular frequency of the signal, and c_1 is the longitudinal wave speed in the homogeneous wedge. Note that the x_1 component of the wave vector must be continuous at the interface, hence the x_1 component of the wave vector in the sample equals to that in the wedge. This fact along with the dispersion relation in the sample from the theoretical model provides us the information about both components of the wave vector for the refracted signal at each frequency of the desired range (Table 2.1). That is why we have manufactured the triangular wedges of various incident angles. Using this technique the group-velocity and energy-flux directions can be computed in the desired frequency range, and that result is being compared to the experiment in following sections.

3.2.1 Aluminum Matrix-PMMA Pins: Sample 1

In this chapter the focus of our study is on the second passband (longitudinal mode). We evaluate the equi-frequency contours along with the energy flux vectors to know the direction of the refraction for Sample 1 (Figure 3.2). We have also shown the frequency surface of the longitudinal mode. From Figure 3.2, we notice that the longitudinal mode displays positive as well as negative refraction for Sample 1. Using these calculations and results, we choose a homogeneous wedge of PMMA with the incidence angle 68°. We have selected this particular wedge because it can carry the incident wave within the desired frequency range of the longitudinal mode, and we would detect positive and negative refraction as the frequency of incident wave is varied. We show the experimental measurements with respect to the theoretical results in Figure 3.3. We note that in this example, the experimental results are in a better agreement with the theoretical calculations done at an average $Q_1 = k_1 a = 2.2$.

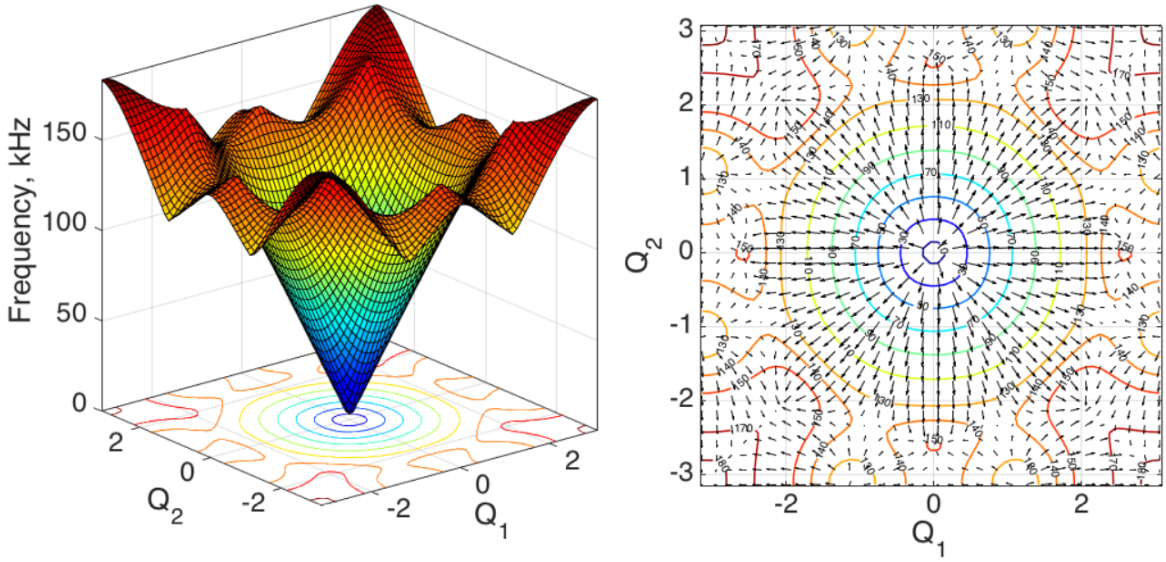

Figure 3.2. Sample 1 acoustic branch longitudinal mode passband. (Left): Frequency surface, (Right): equi-frequency contour and energy flux vectors of longitudinal mode for Sample 1. We do observe negative refraction in this case.

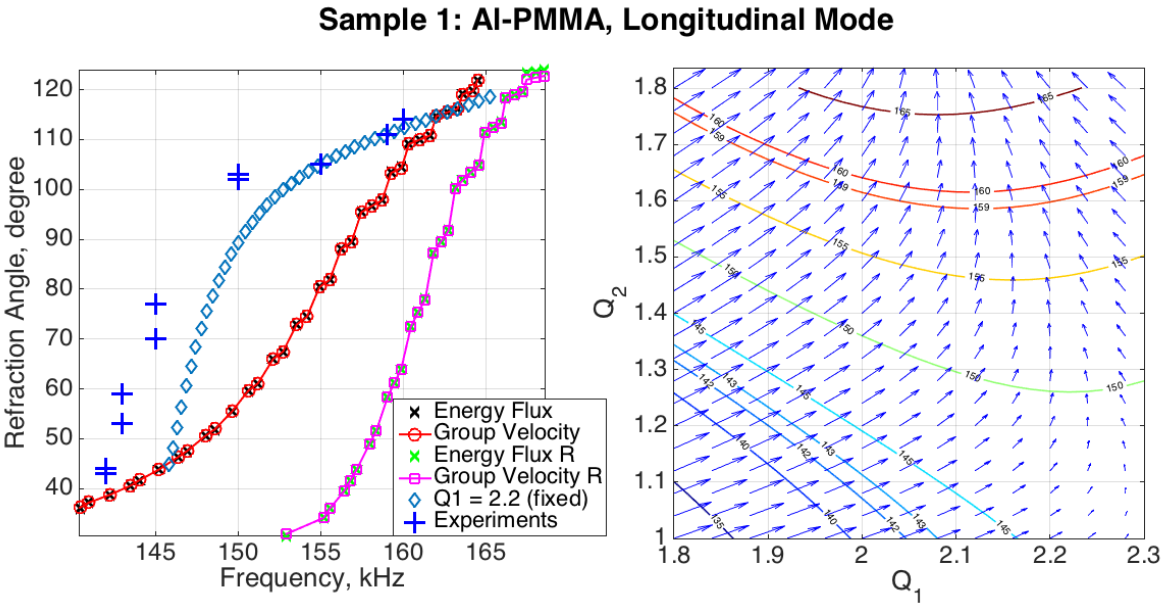

Figure 3.3. Longitudinal wave test of Sample 1. (Left): Group velocity and energy-flux directions and experimental results using a PMMA wedge with incident angle 68°, R denotes the calculations done using Rayleigh quotient. We also plot the theoretical results at a fixed $Q_1 = 2.2$ to show a better agreement with the experiments. (Right): The plot of equi-frequency contours and the energy flux vectors of the second (longitudinal mode) passband.

3.2.2 PMMA Matrix-Aluminum Pins: Sample 2

For the second passband (longitudinal mode) of Sample 2, we evaluate the equi-frequency contours along with the energy flux vectors to know the direction of the refraction for Sample 2 (Figure 3.4). We have also shown the frequency surface of the longitudinal mode. From Figure 3.4 we notice that the longitudinal mode displays positive as well as negative refraction for Sample 2. Using these calculations and results, we choose a homogeneous wedge of PMMA with the incidence angle 20°. We have selected this particular wedge because it can carry the incident wave within the desired frequency range of the longitudinal mode, and we would detect positive and negative refraction as the frequency of incident wave is varied. We have shown the experimental measurements with respect to the theoretical results in Figure 3.5.

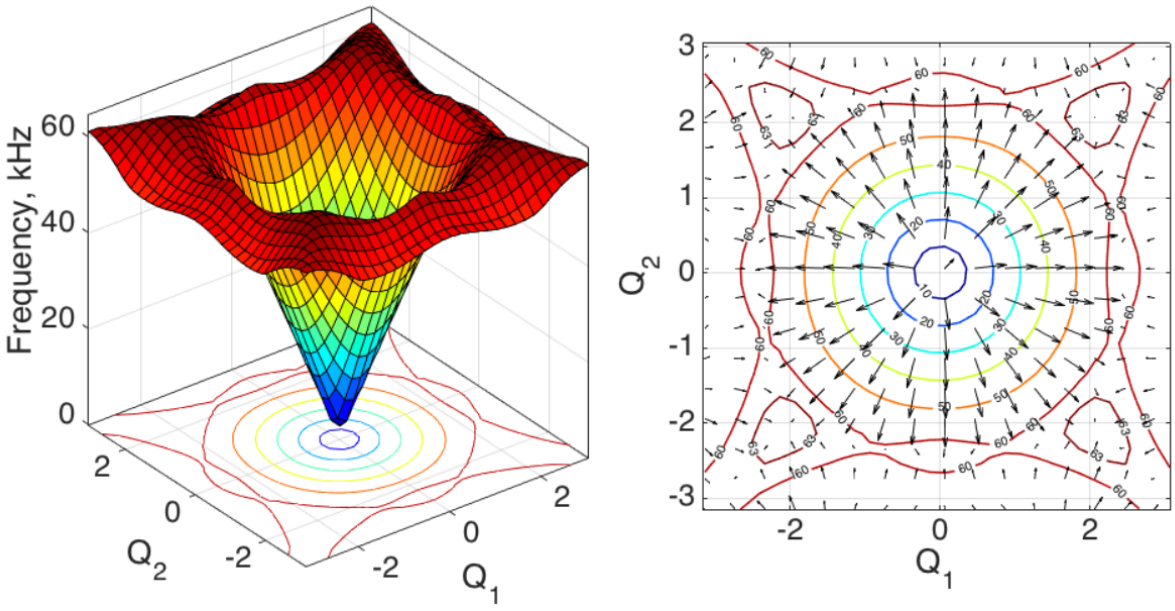

Figure 3.4. Sample 2 acoustic branch longitudinal mode passband. (Left): Frequency surface, (Right): equi-frequency contour and energy flux vectors of longitudinal mode for Sample 2. We do observe negative refraction in this case.

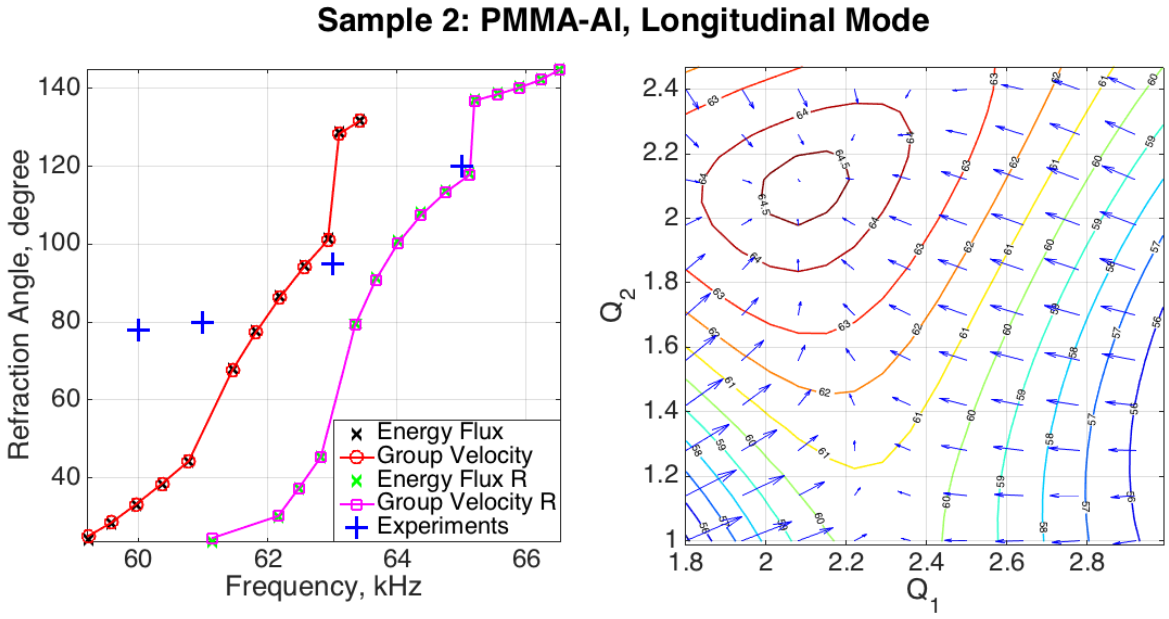

Figure 3.5. Longitudinal wave test of Sample 2. (Left): Group velocity and energy-flux directions and experimental results using a PMMA wedge with incident angle 20°, R denotes the calculations done using Rayleigh quotient. (Right): The plot of equi-frequency contours and the energy flux vectors of the second (longitudinal mode) passband.

3.3 Conclusion

We have shown that both phononic crystals, Sample 1 (stiff crystal) and Sample 2 (soft crystal), exhibit negative refraction on the lowest longitudinal mode (second acoustic passband). Although, as discussed in Chapter 2, only Sample 1 displays negative refraction for the in-plane shear mode (first acoustic passband).

The work of Chapter 3 has been done with Professor S. Nemat-Nasser. The dissertation author was the primary investigator of this research work. The work is being prepared for a publication.

Chapter 4

Dynamic Conservation Integrals as Dissipative Mechanisms in the Evolution of Inhomogeneities

By the application of Noether's theorem, conservation laws in linear elastodynamics are derived by invariance of the Lagrangean functional under a class of infinitesimal transformations. The work of Gupta and Markesncoff (2012), which provides a physical meaning to the dynamic J-integral as the variation of the Hamiltonian of the system due to an infinitesimal translation of the inhomogeneity if linear momentum is conserved in the domain, is extended here to the dynamic M- and L- integrals in terms of the 'if' conditions. We show that the variation of the Lagrangean is equal to the negative of the variation of the Hamiltonian under the above transformations for inhomogeneities, and hence provide a physical meaning to the dynamic J-, L- and M-integrals as dissipative mechanisms in elastodynamics. We prove that if linear momentum is conserved in the domain, the total energy loss of the system per unit scaling under the infinitesimal scaling transformation of the inhomogeneity is equal to the dynamic M-integral. Moreover, if linear and angular momenta are conserved, the total energy loss of the system per unit rotation under the infinitesimal rotational transformation is equal to the dynamic L-integral.

4.1 Introduction

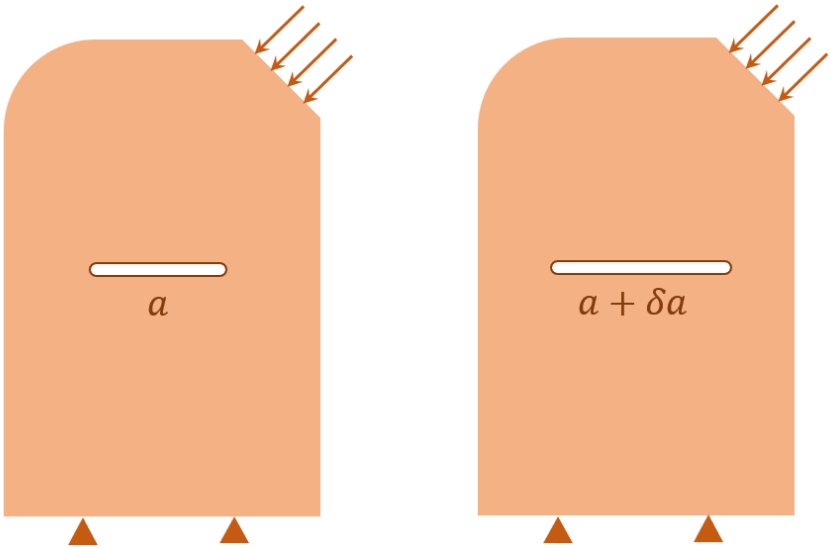

Figure 4.1. A typical growth of a crack from length a to $a+\delta a$.

A defect, for example, cavity, crack, inlcusion, or inhomogeneity, needs some external energy to move from one configuration to another. The change in energy is related to the conservation integrals. In Figure 4.1 there is a crack of length a, and it grows to length $a+\delta a$. There must be some difference in energy between these to configurations. The energy difference is equal to the energy, which is released when the crack grows. This energy released is related to the well-known J-integral. In the case of the translation of the defect, the change in energy is related to the J-integral, for self-similar scaling it is provided by the M-integral, and in case of the rotation of the defect the change in total energy is related by the L-integral.

Markenscoff (2006) expressed the conservation integrals as a variation of the total energy of the system by extending Eshelby's thought experiment (Eshelby, 1951, 1957) to elastodynamics. In elastostatics, Gupta and Markenscoff (2008) showed that the total energy dissipation due to material translation of the inhomogeneity equals the configurational force (J-integral) times the infinitesimal displacement of the inhomogeneity, if and only if equilibrium is preserved in the domain. They extended the proof to elastodynamics (Gupta and Markenscoff, 2012), where the

variation of the Lagrangean or the Hamiltonian is equal to the dynamic J-integral, if and only if linear momentum is conserved in the domain.

In elastodynamics, Fletcher (1976) proved that the Lagrangean functional was invariant under a certain group of infinitesimal transformations; Kienzler and Herrmann (2000, p 66) also have a detailed proof for elastostatics, which we extend to elastodynamics. We impose the scaling transformation to derive the M- integral, and for infinitesimal rotational transformation, we derive the dynamic L-integral. Furthermore, we also relate the variation of the Lagrangean to the variation of the Hamiltonian for scaling and rotation of the inhomogeneity. This allows us to give an energy dissipative meaning to the above 'if' statements and to the dynamic J-, L-, and M-integrals as dissipated energy by mechanisms not considered in elasticity theory (Eshelby, 1951, p 108).

4.2 Mathematical Framework

We briefly present the mathematical framework of the derivation of the conservation integrals from Noether's theorem in linear elastodynamics.

Consider the Lagrangean functional (Gelfand et al., 2000; Fletcher, 1976)

$$\Pi^{\mathcal{L}} = \int_R \mathcal{L}(x_\alpha, u_i, u_{i_{x_\alpha}})\, dx_1 dx_2 dx_3 dx_4 \qquad (i = 1,2,3), \quad (\alpha = 1,2,3,4), \tag{4.1}$$

where R is the region of integration. In elastodynamics, the independent variables are the material coordinates x_1, x_2, x_3 and x_4 is the time variable, and the dependent variable u_i is the displacement field. For the infinitesimal transformations on the independent and the dependent variables,

$$x^*_\alpha = x_\alpha + \epsilon\phi_\alpha(x_\beta, u_i, u_{i,\beta}) + O(\epsilon^2) \qquad (i = 1,2,3), \quad (\alpha,\beta = 1,2,3,4) \tag{4.2a}$$

$$u^*_j = u_j + \epsilon\psi_j(x_\beta, u_i, u_{i,\beta}) + O(\epsilon^2) \qquad (i,j = 1,2,3), \quad (\beta = 1,2,3,4), \tag{4.2b}$$

where ϵ is the infinitesimal transformation parameter. The variation of the functional (4.1) is written as

$$\delta\Pi^{\mathcal{L}} = \int_{R^*} \mathcal{L}(x^*_\alpha, u^*_i, u^*_{i_{x^*_\alpha}})\, dx^*_1 dx^*_2 dx^*_3 dx^*_4 - \int_R \mathcal{L}(x_\alpha, u_i, u_{i_{x_\alpha}})\, dx_1 dx_2 dx_3 dx_4, \tag{4.3}$$

where R^* is a new region of integration. In view of equations (4.2a) and (4.2b), equation (4.3) can be further written as (Gelfand et al., 2000, p 176)

$$\delta\Pi^{\mathcal{L}} = \int_R \left\{ \frac{\partial \mathcal{L}}{\partial u_j} - \frac{\partial}{\partial x_\alpha} \frac{\partial \mathcal{L}}{\partial u_{j,\alpha}} \right\} \overline{\delta u_j}\, dx_1 dx_2 dx_3 dx_4 + \int_R \frac{\partial}{\partial x_\alpha} \left\{ \frac{\partial \mathcal{L}}{\partial u_{j,\alpha}} \overline{\delta u_j} + \mathcal{L}\, \delta x_\alpha \right\} dx_1 dx_2 dx_3 dx_4, \tag{4.4}$$

where (see also, figure 10, page 171 in Gelfand et al. (2000))

$$\begin{aligned} \delta u_j &= u^*_j(x^*_\alpha) - u_j(x_\alpha) = \{u^*_j(x^*_\alpha) - u^*_j(x_\alpha)\} + \{u^*_j(x_\alpha) - u_j(x_\alpha)\} \\ &\approx \frac{\partial u^*_j}{\partial x_\alpha} \delta x_\alpha + \overline{\delta u_j} \approx \frac{\partial u_j}{\partial x_\alpha} \delta x_\alpha + \overline{\delta u_j} \end{aligned} \tag{4.5}$$

or

$$\overline{\delta u_j} = \delta u_j - u_{j,\alpha} \delta x_\alpha. \tag{4.6}$$

Furthermore, in terms of the transformations ϕ_α and ψ_j, equation (4.4) becomes

$$\delta\Pi^{\mathcal{L}} = \epsilon \int_R \left\{ \frac{\partial \mathcal{L}}{\partial u_j} - \frac{\partial}{\partial x_\alpha} \frac{\partial \mathcal{L}}{\partial u_{j,\alpha}} \right\} \overline{\psi}_j\, dx_1 dx_2 dx_3 dx_4 + \epsilon \int_R \frac{\partial}{\partial x_\alpha} \left\{ \frac{\partial \mathcal{L}}{\partial u_{j,\alpha}} \overline{\psi}_j + \mathcal{L}\phi_\alpha \right\} dx_1 dx_2 dx_3 dx_4, \tag{4.7}$$

where, from relation (4.6),

$$\overline{\psi}_j = \psi_j - u_{j,\alpha}\phi_\alpha. \tag{4.8}$$

Note that above, and in the sequel, the partial derivatives with respect to x_i and t, for any $A(x_j, u_j, \dot{u}_j, u_{j,k})$ are defined as

$$\frac{\partial(A)}{\partial x_i} = \left.\frac{\partial(A)}{\partial x_i}\right|_{exp} + \frac{\partial(A)}{\partial u_l}u_{l,i} + \frac{\partial(A)}{\partial \dot{u}_l}\dot{u}_{l,i} + \frac{\partial(A)}{\partial u_{l,m}}u_{l,mi} \tag{4.9a}$$

and

$$\frac{\partial(A)}{\partial t} = \left.\frac{\partial(A)}{\partial t}\right|_{exp} + \frac{\partial(A)}{\partial u_l}\dot{u}_l + \frac{\partial(A)}{\partial \dot{u}_l}\ddot{u}_l + \frac{\partial(A)}{\partial u_{l,m}}\dot{u}_{l,m}. \tag{4.9b}$$

Under the infinitesimal transformations (4.2a) and (4.2b) the functional $\Pi^{\mathcal{L}}$ is said to be invariant at $\boldsymbol{u}$ if

$$\delta\Pi^{\mathcal{L}} = 0. \tag{4.10}$$

Furthermore, if $\boldsymbol{u}$ satisfies the Euler-Lagrange equations (Gelfand et al., 2000)

$$\frac{\partial \mathcal{L}}{\partial u_j} - \frac{\partial}{\partial x_\alpha}\frac{\partial \mathcal{L}}{\partial u_{j,\alpha}} = 0, \tag{4.11}$$

then the first term in equation (4.7) vanishes, and it yields

$$\int_R \frac{\partial}{\partial x_\alpha}\left\{\frac{\partial \mathcal{L}}{\partial u_{j,\alpha}}\overline{\psi}_j + \mathcal{L}\phi_\alpha\right\} dx_1 dx_2 dx_3 dx_4 = 0. \tag{4.12}$$

Let Ω be a region in three-dimensional space occupied by a linearly elastic solid, undergoing small deformations and containing an inhomogeneity which is a surface of discontinuity in the strain and velocity. Let $u_j(x_i, t)$ denote the displacement, ε_{ij} are the small strains, C_{ijkl} the components of the elasticity tensor, ρ the density — which in linear elasticity is assumed

constant, independent of time — and $(\cdot)$ the time derivative, and denote the Cauchy stress by $\sigma_{ij} = C_{ijkl}\varepsilon_{kl}$. The Lagrange density is defined as

$$\mathcal{L} = T - W \tag{4.13}$$

where the strain energy density is

$$W = \frac{1}{2}C_{ijkl}\varepsilon_{ij}\varepsilon_{kl} = \frac{1}{2}C_{ijkl}\,u_{i,j}u_{k,l}, \tag{4.14}$$

and the specific kinetic energy is

$$T = \frac{1}{2}\rho\dot{u}_i\dot{u}_i. \tag{4.15}$$

We write the total Lagrangean functional for $\Omega \subset \mathbb{R}^3$ and $[0,t] \subset \mathbb{R}$, and assume further $\mathcal{L} \in C^\infty$, so that $\mathcal{L}$ posses continuous partial derivatives of all orders with respect to the element of its matrix arguments on its domain of definition:

$$\Pi^{\mathcal{L}}(u_{i,j},\dot{u}_i) = \int_0^t \int_\Omega \mathcal{L}(u_{i,j},\dot{u}_i)\,dV\,dt = \int_0^t \int_\Omega \{T(\dot{u}_i) - W(u_{i,j})\}\,dV\,dt. \tag{4.16}$$

For $\mathcal{L} = T - W$, the Euler-Lagrange equations (4.11) give

$$\frac{\partial\sigma_{ij}}{\partial x_i} - \frac{\partial(\rho\dot{u}_j)}{\partial t} = 0, \tag{4.17}$$

which represents the conservation of the linear momentum. If the Euler-Lagrange equations (4.11) are satisfied then equation (4.12) should be satisfied in order for the Lagrangean functional $\Pi^{\mathcal{L}}$ to be invariant under the transformation (4.2a) and (4.2b). This will give the equations to derive the families ϕ_α and ψ_j of the infinitesimal transformations.

Equation (4.12) is expanded in space and time variables as

$$\int_0^t \int_\Omega \left[\frac{\partial}{\partial x_i} \left\{ \frac{\partial \mathcal{L}}{\partial u_{j,i}} \overline{\psi}_j + \mathcal{L}\phi_i \right\} + \frac{\partial}{\partial t} \left\{ \frac{\partial \mathcal{L}}{\partial \dot{u}_j} \overline{\psi}_j + \mathcal{L}\phi_4 \right\} \right] dV\, dt = 0. \tag{4.18}$$

Using equation (4.13), equation (4.18) is written

$$\int_0^t \int_\Omega \left[\frac{\partial}{\partial x_i} \left\{ -\sigma_{ij} \overline{\psi}_j + \mathcal{L}\phi_i \right\} + \frac{\partial}{\partial t} \left\{ \rho \dot{u}_j \overline{\psi}_j + \mathcal{L}\phi_4 \right\} \right] dV\, dt = 0. \tag{4.19}$$

The above relation applied to infinitesimal transformations given by equations (4.2a) and (4.2b) provides the corresponding conservation laws for translation, scaling and rotation of the inhomogeneities (under which the Lagrangean remains invariant), which are additional field equations and are derived in the following section.

4.3 Family of Infinitesimal Transformations and Dynamic Conservation Laws

In this section we extend the work of Kienzler and Herrmann (2000, p 66) to elastodynamics in order to obtain the family of infinite transformations under which the Lagrangean remains invariant. In this section, for the sake of notational simplicity we define and use

$$\frac{d}{dx_i} \equiv \frac{\partial}{\partial x_i} \tag{4.20a}$$

$$\frac{d}{dt} \equiv \frac{\partial}{\partial t}, \tag{4.20b}$$

where the partial derivative with respect to x_i and t are taken as in equations (4.9a) and (4.9b), respectively.

Equation (4.19) is true for any arbitrary volume Ω and any arbitrary time interval, so we

can write

$$\frac{d}{dx_i}\left\{-\sigma_{ij}\overline{\psi}_j + \mathcal{L}\phi_i\right\} + \frac{d}{dt}\left\{\rho\dot{u}_j\overline{\psi}_j + \mathcal{L}\phi_4\right\} = 0. \tag{4.21}$$

Next, using $\overline{\psi}_j$ from equation (4.8), expanded in space and time variables $\overline{\psi}_j = \psi_j - u_{j,l}\phi_l - \dot{u}_j\phi_4$ we rewrite equation (4.21) as

$$\frac{d}{dx_i}\left\{-\sigma_{ij}(\psi_j - u_{j,l}\phi_l - \dot{u}_j\phi_4) + \mathcal{L}\phi_i\right\} + \frac{d}{dt}\left\{\rho\dot{u}_j(\psi_j - u_{j,l}\phi_l - \dot{u}_j\phi_4) + \mathcal{L}\phi_4\right\} = 0, \tag{4.22}$$

and we employ linear momentum balance to obtain

$$-\sigma_{ij}\frac{d}{dx_i}(\psi_j - u_{j,l}\phi_l - \dot{u}_j\phi_4) + \frac{d}{dx_i}(\mathcal{L}\phi_l)\,\delta_{il} + \rho\dot{u}_j\frac{d}{dt}(\psi_j - u_{j,l}\phi_l - \dot{u}_j\phi_4) + \frac{d}{dt}(\mathcal{L}\phi_4) = 0. \tag{4.23}$$

Differentiating explicitly the terms on the left-hand side of equation (4.23) with the derivatives

$$\frac{d\mathcal{L}}{dx_i} = \frac{\partial\mathcal{L}}{\partial x_i} + \frac{\partial\mathcal{L}}{\partial u_{k,j}}\frac{\partial u_{k,j}}{\partial x_i} + \frac{\partial\mathcal{L}}{\partial\dot{u}_k}\frac{\partial\dot{u}_k}{\partial x_i} = -\sigma_{jk}u_{k,ji} + \rho\dot{u}_k\dot{u}_{k,i}, \tag{4.24a}$$

$$\frac{d\mathcal{L}}{dt} = \frac{\partial\mathcal{L}}{\partial t} + \frac{\partial\mathcal{L}}{\partial u_{k,j}}\frac{\partial u_{k,j}}{\partial t} + \frac{\partial\mathcal{L}}{\partial\dot{u}_k}\frac{\partial\dot{u}_k}{\partial t} = -\sigma_{jk}\dot{u}_{k,j} + \rho\dot{u}_k\ddot{u}_k, \tag{4.24b}$$

$$\frac{d\phi_j}{dx_i} = \frac{\partial\phi_j}{\partial x_i} + \frac{\partial\phi_j}{\partial u_k}u_{k,i}, \quad \frac{d\phi_4}{dx_i} = \frac{\partial\phi_4}{\partial x_i} + \frac{\partial\phi_4}{\partial u_k}u_{k,i}, \tag{4.24c}$$

$$\frac{d\phi_j}{dt} = \frac{\partial\phi_j}{\partial t} + \frac{\partial\phi_j}{\partial u_k}\dot{u}_k, \quad \frac{d\phi_4}{dt} = \frac{\partial\phi_4}{\partial t} + \frac{\partial\phi_4}{\partial u_k}\dot{u}_k, \tag{4.24d}$$

$$\frac{d\psi_j}{dx_i} = \frac{\partial\psi_j}{\partial x_i} + \frac{\partial\psi_j}{\partial u_k}u_{k,i}, \quad \frac{d\psi_j}{dt} = \frac{\partial\psi_j}{\partial t} + \frac{\partial\psi_j}{\partial u_k}\dot{u}_k. \tag{4.24e}$$

Therefore, equation (4.23) becomes

$$
\begin{aligned}
&-\sigma_{ij}\left(\frac{\partial\psi_j}{\partial x_i}+\frac{\partial\psi_j}{\partial u_k}u_{k,i}\right)+\sigma_{ij}u_{j,l}\left(\frac{\partial\phi_l}{\partial x_i}+\frac{\partial\phi_l}{\partial u_k}u_{k,i}\right)+\phi_l\sigma_{ij}u_{j,li}+\sigma_{ij}\dot{u}_j\left(\frac{\partial\phi_4}{\partial x_i}+\frac{\partial\phi_4}{\partial u_k}u_{k,i}\right)\\
&\quad+\phi_4\sigma_{ij}\dot{u}_{j,i}+\mathcal{L}\left(\frac{\partial\phi_l}{\partial x_i}+\frac{\partial\phi_l}{\partial u_k}u_{k,i}\right)\delta_{il}+\phi_l\delta_{il}(-\sigma_{jk}u_{k,ji}+\rho\dot{u}_k\dot{u}_{k,i})+\rho\dot{u}_j\left(\frac{\partial\psi_j}{\partial t}+\frac{\partial\psi_j}{\partial u_k}\dot{u}_k\right)\\
&\quad-\rho\dot{u}_ju_{j,l}\left(\frac{\partial\phi_l}{\partial t}+\frac{\partial\phi_l}{\partial u_k}\dot{u}_k\right)-\phi_l\rho\dot{u}_j\dot{u}_{j,l}-\rho\dot{u}_j\dot{u}_j\left(\frac{\partial\phi_4}{\partial t}+\frac{\partial\phi_4}{\partial u_k}\dot{u}_k\right)-\phi_4\rho\dot{u}_j\ddot{u}_j\\
&\quad+\mathcal{L}\left(\frac{\partial\phi_4}{\partial t}+\frac{\partial\phi_4}{\partial u_k}\dot{u}_k\right)+\phi_4(-\sigma_{jk}\dot{u}_{k,j}+\rho\dot{u}_k\ddot{u}_k)=0. \qquad (4.25)
\end{aligned}
$$

Rearranging this equation as in Kienzler and Herrmann (2000, p 64) leads to

$$
\begin{aligned}
0=&\frac{\partial\phi_l}{\partial u_k}[\sigma_{ij}u_{j,l}u_{k,l}-Wu_{k,i}\delta_{il}] && \left[\sim u_{i,l}^3\right] && (4.26a)\\
&+\frac{\partial\phi_l}{\partial u_k}[Tu_{k,i}\delta_{il}-\rho\dot{u}_j\dot{u}_ku_{j,l}] && \left[\sim u_{j,l}\dot{u}_k^2\right] && (4.26b)\\
&+\frac{\partial\phi_4}{\partial u_k}[\sigma_{ij}\dot{u}_ju_{k,l}-W\dot{u}_k] && \left[\sim u_{i,j}^2\dot{u}_k\right] && (4.26c)\\
&+\frac{\partial\phi_4}{\partial u_k}[T\dot{u}_k-\rho\dot{u}_j\dot{u}_j\dot{u}_k] && \left[\sim \dot{u}_k^3\right] && (4.26d)\\
&+\frac{\partial\psi_j}{\partial u_k}[-u_{k,i}\sigma_{ij}]+\frac{\partial\phi_l}{\partial x_i}[\sigma_{ij}u_{j,l}-W\delta_{il}]+\frac{\partial\phi_4}{\partial t}[-W] && \left[\sim u_{j,k}^2\right] && (4.26e)\\
&+\frac{\partial\psi_j}{\partial u_k}[\rho\dot{u}_j\dot{u}_k]+\frac{\partial\phi_l}{\partial x_i}[T\delta_{il}]+\frac{\partial\phi_4}{\partial t}[-\rho\dot{u}_j\dot{u}_j+T] && \left[\sim \dot{u}_k^2\right] && (4.26f)\\
&+\frac{\partial\phi_l}{\partial t}[-\rho\dot{u}_ju_{j,l}]+\frac{\partial\phi_4}{\partial x_i}[\sigma_{ij}\dot{u}_j] && \left[\sim u_{j,l}\dot{u}_j\right] && (4.26g)\\
&+\frac{\partial\psi_j}{\partial x_i}[\sigma_{ij}] && \left[\sim u_{i,j}\right] && (4.26h)\\
&+\frac{\partial\psi_j}{\partial t}[-\rho\dot{u}_j]. && \left[\sim \dot{u}_j\right] && (4.26i)
\end{aligned}
$$

Setting all the coefficients equal to zero leads to the requirement that the functions ϕ_l, ϕ_4 and ψ_j satisfy an over-determined system of linear differential equations.

From (4.26a) it follows that ϕ_l must not be a function of u_j. Thus,

$$\phi_l=\phi_l(x_k,t), \qquad (4.27)$$

with this, part (4.26b) is also satisfied. From (4.26c) it follows that ϕ_4 must not be a function of u_k. Thus,

$$\phi_4 = \phi_4(x_k, t), \tag{4.28}$$

with this, part (4.26d) is also satisfied. From (4.26i) it follows that ψ_j must not be a function of t. Thus,

$$\psi_j = \psi_j(x_k, u_l). \tag{4.29}$$

Using relations (4.27)–(4.29), from (4.26e) or (4.26f) it follows

$$\partial\psi_j/\partial u_k = h_{jk}(x_l), \tag{4.30}$$

that is,

$$\psi_j = h_{jk}(x_l)u_k + g_j(x_l). \tag{4.31}$$

From (4.26h) it follows that the functions $h_{jk}(x_l)$ are actually constants, and due to the symmetry of the stress tensor, the terms $\partial g_j/\partial x_i$ form a skew symmetric constant matrix. Thus,

$$\psi_j = \alpha_{jk}u_k + \Omega_k\varepsilon_{kil}x_i + r_j. \tag{4.32}$$

Because $\partial\psi_j/\partial u_k$ is matrix of constant coefficients, from (4.26e) or (4.26f), we further conclude that ϕ_l must not be a function of t as well, thus,

$$\phi_l = \phi_l(x_k), \tag{4.33}$$

furthermore, ϕ_4 must not be a function of x_i as well, thus,

$$\phi_4 = \phi_4(t). \tag{4.34}$$

With this, (4.26g) is also satisfied. Therefore, we can write

$$\psi_j = \alpha_{jk} u_k + \Omega_k \varepsilon_{kil} x_i + r_j, \tag{4.35a}$$

$$\phi_j = \beta_{jk} x_k + a_j, \tag{4.35b}$$

$$\phi_4 = l_0 t + t_0. \tag{4.35c}$$

Now we split the constant matrices α_{ij} and β_{ij} into symmetric and antisymmetric parts and, further, the symmetric parts into spherical and deviatoric parts as follows

$$\beta_{ji} = l\,\delta_{ij} + \beta'_{ji} + m_n \varepsilon_{nij}, \tag{4.36a}$$

$$\alpha_{jk} = l\,\gamma\,\delta_{kj} + \alpha'_{jk} + \omega_n \varepsilon_{nkj} \tag{4.36b}$$

with $l, \gamma, m_n, \omega_n, \beta'_{ji}, \alpha'_{jk}$ being constant parameters or matrices of constant coefficients, satisfying

$$\beta'_{ji} = \beta'_{ij} \quad \alpha'_{jk} = \alpha'_{kj} \quad \beta'_{jj} = \alpha'_{jj} = 0.$$

With this, using (4.26e) and (4.26f) we obtain

$$(l\,\gamma\,\delta_{kj} + \alpha'_{jk} + \omega_n \varepsilon_{nkj})[-u_{k,i}\sigma_{ij} + \rho \dot{u}_j \dot{u}_k] + \tag{4.37}$$

$$(l\,\delta_{il} + \beta'_{li} + m_n\,\varepsilon_{nil})[\sigma_{ij} u_{j,l} + \mathcal{L}\delta_{il}] + l_0[-\rho \dot{u}_j \dot{u}_j + \mathcal{L}] = 0 \tag{4.38}$$

after rearranging, we can write

$$l(-\gamma\,\delta_{kj}u_{k,i}\sigma_{ij} + \gamma\,\delta_{kj}\rho\dot{u}_j\dot{u}_k + \delta_{il}\sigma_{ij}u_{j,l} + \delta_{il}\mathcal{L}\delta_{il}) + l_0(-2T + \mathcal{L}) + \tag{4.39a}$$

$$\omega_n\varepsilon_{nkj}(-u_{k,i}\sigma_{ij} + \rho\dot{u}_j\dot{u}_k) + m_n\varepsilon_{nil}(\sigma_{ij}u_{j,l} + \mathcal{L}\delta_{il}) + \tag{4.39b}$$

$$\alpha'_{jk}(-u_{k,i}\sigma_{ij} + \rho\dot{u}_j\dot{u}_k) + \beta'_{il}(\sigma_{ij}u_{j,l} + \mathcal{L}\delta_{il}) = 0, \tag{4.39c}$$

and we further simplify to write

$$l[-\gamma\,2W + \gamma\,2T + 2W + n(T - W)] + l_0(-2T + \mathcal{L}) + \tag{4.40a}$$

$$\varepsilon_{npq}\sigma_{ip}(\omega_n u_{q,i} + m_n u_{i,q}) + \tag{4.40b}$$

$$(\beta'_{il}\sigma_{ij}u_{j,l} - \alpha'_{jk}u_{k,i}\sigma_{ij}) + \alpha'_{jk}\rho\dot{u}_j\dot{u}_k = 0, \tag{4.40c}$$

where $n = \delta_{ii}$ is the number of space dimensions. If $l_0 = l$ then for the first term (4.40a) to vanish we have

$$-2\gamma W + 2\gamma T + 2W + n(T - W) - 2T + T - W = 0 \implies \gamma = \frac{1-n}{2}, \tag{4.41}$$

and the second term (4.40b) vanishes if

$$m_n = \omega_n, \tag{4.42}$$

provided that the material is isotropic, i.e., $\varepsilon_{npq}\sigma_{ip}[u_{q,i} + u_{i,q}] = 0$ (Eshelby, 1975). The third term (4.40c) vanishes only if $\alpha'_{jk} = \beta'_{il} = 0$, which means that

$$\beta_{ji} = l\,\delta_{ij} + \omega_n\varepsilon_{nij}, \quad \alpha_{ji} = l\frac{1-n}{2}\delta_{ij} + \omega_n\varepsilon_{nij} \quad \text{and} \quad \phi_4 = l\,t + t_0. \tag{4.43}$$

Hence, we state the suitable infinitesimal transformations

$$\phi_j = \omega_n \varepsilon_{nij} x_i + l\, x_j + a_j \tag{4.44a}$$

$$\phi_4 = l\, t + t_0 \tag{4.44b}$$

$$\psi_j = \omega_n \varepsilon_{nij} u_i + l\, \frac{1-n}{2} u_j + \Omega_n \varepsilon_{nij} x_i + r_j \tag{4.44c}$$

or

$$x_j^* = x_j + \epsilon \left(\omega_n \varepsilon_{nij} x_i + l\, x_j + a_j\right) \tag{4.45a}$$

$$t^* = t + \epsilon (l\, t + t_0) \tag{4.45b}$$

$$u_j^* = u_j + \epsilon \left(\omega_n \varepsilon_{nij} u_i + l\, \frac{1-n}{2} u_j + \Omega_n \varepsilon_{nij} x_i + r_j\right), \tag{4.45c}$$

where l, t_0 are constant parameters and $\omega_n, a_j, \Omega_n, r_j$ are vectors with constant components. The vectors r_j and Ω_n describe a rigid body translation and rotation, respectively, while a_j and ω_n describe material translation (coordinate translation) and material rotation (coordinate rotation), respectively, and the parameter l represents the scaling. The above family of transformations agrees with Fletcher (1976) in three dimensions ($n = 3$). Applying the transformations indicated by equations (4.45a), (4.45b) and (4.45c) for the material translation, scaling and rotation separately to equation (4.19), the conservation laws for elastodynamics are derived in the following subsections.

4.3.1 Invariance of the Lagrangean under Translation

For the infinitesimal translation of the material, we utilize the transformation (Fletcher, 1976) such that the new coordinates are $x_i^* = x_i + \epsilon a_i$ and the new time and displacement field remain invariant ($t^* = t$, $u_i^* = u_i$), where ϵa_i is the infinitesimal translation. After comparing the

transformation with equations (4.45) and (4.44), we have

$$\phi_i = a_i, \quad \phi_4 = 0, \qquad \text{and} \qquad \psi_j = 0, \tag{4.46}$$

therefore, from equation (4.8)

$$\overline{\psi}_j = -u_{j,k} a_k . \tag{4.47}$$

Inserting the above transformation in equation (4.19) to obtain the conservation law for translation, we obtain

$$\int_0^t \int_\Omega \left[\frac{\partial}{\partial x_i} \left\{ (\mathcal{L}\delta_{ik} + \sigma_{ij} u_{j,k}) a_k \right\} - \frac{\partial}{\partial t} \left\{ \rho \dot{u}_j u_{j,k} a_k \right\} \right] dV\, dt = 0. \tag{4.48}$$

The relation is true for any a_k; therefore, we get

$$\int_0^t \int_\Omega \left[\frac{\partial}{\partial x_i} \left\{ \mathcal{L}\delta_{ik} + \sigma_{ij} u_{j,k} \right\} - \frac{\partial}{\partial t} \left\{ \rho \dot{u}_j u_{j,k} \right\} \right] dV\, dt = 0. \tag{4.49}$$

Equation (4.49) holds true for any arbitrary volume Ω and any arbitrary time interval, so we have

$$\frac{\partial}{\partial x_i} \left\{ \mathcal{L}\delta_{ik} + \sigma_{ij} u_{j,k} \right\} - \frac{\partial}{\partial t} \left\{ \rho \dot{u}_j u_{j,k} \right\} = 0, \tag{4.50}$$

which is in agreement with Fletcher (1976, eq 3.4). Equation (4.50) is an additional field equation valid anywhere in the domain of analyticity. Ni and Markenscoff (2009) have used equation (4.50) as a field equation to obtain the logarithmic singularity of the near field of an accelerating (generally moving) dislocations rather than by singular asymptotics of the full solution (Callias and Markenscoff, 1988).

Analogously to statics, for linear elastodynamics we define the dynamic J-integral as

(Bui, 1977; Maugin, 1993; Markenscoff, 2006)

$$J_k^{\text{dyn}} \equiv -\int_{\Omega} \left[\frac{\partial}{\partial x_i} \left\{ \mathcal{L}\delta_{ik} + \sigma_{ij} u_{j,k} \right\} - \frac{\partial}{\partial t} \left\{ \rho \dot{u}_j u_{j,k} \right\} \right] dV. \tag{4.51}$$

The dynamic J- integral would be zero if the region Ω excludes the inhomogeneity, but it would be non-zero if the volume Ω includes it. The above expression for the dynamic J integral agrees in the static case with Eshelby (1959); Günther (1962); Rice (1968); Knowles and Sternberg (1972).

Relation of J_k^{dyn} with the Energy Release Rate

If Ω is a region of analyticity excluding the inhomogeneity, from equation (4.50) using relation (4.13) we can write

$$\int_{\Omega} \left[\frac{\partial}{\partial x_i} \left\{ (T-W)\delta_{ik} + \sigma_{ij} u_{j,k} \right\} - \frac{\partial}{\partial t} \left\{ \rho \dot{u}_j u_{j,k} \right\} \right] dV = 0, \tag{4.52}$$

which, equivalently is written as

$$\int_{\Omega} \left[\frac{\partial}{\partial x_i} \left\{ (W+T)\delta_{ik} - \sigma_{ij} u_{j,k} \right\} - 2\frac{\partial T}{\partial x_k} + \frac{\partial}{\partial t} \left\{ \rho \dot{u}_j u_{j,k} \right\} \right] dV = 0. \tag{4.53}$$

We may write the above equation in a form similar to the one in Gupta and Markenscoff (2012, eq 10), as

$$\int_{\Omega} \frac{\partial}{\partial x_i} \left\{ (W+T)\delta_{ik} - \sigma_{ij} u_{j,k} \right\} dV + \int_{\Omega} \left[\rho \ddot{u}_j u_{j,k} - \rho \dot{u}_i \dot{u}_{i,k} \right] dV = 0. \tag{4.54}$$

By considering the region of analyticity Ω as $\Omega = \Omega_2 - \Omega_1$, i.e., as the difference between two regions, Ω_2 and Ω_1 (with $\Omega_1 \subset \Omega_1$) that include the inhomogeneity then, and by using the

divergence theorem to convert the first volume integral into a surface integral we have

$$\int_{S_1+S_2} \left\{(W+T)n_k - \sigma_{ij}u_{j,k}n_i\right\} dS + \int_{\Omega_2-\Omega_1} \left[\rho\ddot{u}_j u_{j,k} - \rho\dot{u}_i\dot{u}_{i,k}\right] dV = 0, \tag{4.55}$$

where n_i is the outward unit normal vector to the surface $S_1 + S_2$. It follows that

$$\begin{aligned}\int_{S_1} \left\{(W+T)n_k - \sigma_{ij}u_{j,k}n_i\right\} dS + \int_{\Omega_1} \left[\rho\ddot{u}_j u_{j,k} - \rho\dot{u}_i\dot{u}_{i,k}\right] dV = \\ \int_{S_2} \left\{(W+T)n_k - \sigma_{ij}u_{j,k}n_i\right\} dS + \int_{\Omega_2} \left[\rho\ddot{u}_j u_{j,k} - \rho\dot{u}_i\dot{u}_{i,k}\right] dV = J_k^{\text{dyn}}.\end{aligned} \tag{4.56}$$

We now consider the volume Ω_1 to shrink to zero as the contour S_1 shrinks onto the moving inhomogeneity and moves with it. As the volume Ω_1 shrinks to zero, in view of the fact that "the elastic field in the immediate vicinity of the moving inhomogeneity at any instant is indistinguishable from the local field of an appropriate steady state moving inhomogeneity, for which $\partial/\partial t = -v\,\partial/\partial x$ (Freund, 1972)", the volume integral in the region Ω_1 vanishes, so that equation (4.56) yields the expression for J_k^{dyn} as

$$J_k^{\text{dyn}} = \lim_{S_1\to 0} \int_{S_1} \left\{(W+T)n_k - \sigma_{ij}u_{j,k}n_i\right\} dS, \tag{4.57}$$

where S_1 is an arbitrary surface surrounding the inhomogeneity, moving with it and shrinking upon it. The above relation of J_k^{dyn} agrees with Freund (1990, p 269) and Markenscoff (2006, eq 14). This expression will relate J_k^{dyn} to the energy release rate for the moving inhomogeneity, as treated in Section 4.5.1 (see equation (4.116)).

4.3.2 Invariance of the Lagrangean under Scaling

For the self-similar expansion of the material, consider the smooth scaling such that the new coordinates and time are $x_i^* = x_i + \epsilon l x_i$ and $t^* = t + \epsilon l t$, respectively, and the new displacement

field is $u_i^* = u_i + (1-n)\epsilon l u_i/2$, where l is the scaling parameter and n is the number of space dimensions. After comparing the transformation with equations (4.45) and (4.44), we have

$$\phi_i = l x_i, \quad \phi_4 = lt, \qquad \text{and} \qquad \psi_j = \frac{1-n}{2} l u_j, \tag{4.58}$$

therefore, from equation (4.8)

$$\overline{\psi}_j = l\left(\frac{1-n}{2}u_j - u_{j,k}x_k - t\dot{u}_j\right). \tag{4.59}$$

Substituting the above transformation in equation (4.19) to obtain the conservation law for scaling, we write

$$\begin{aligned}\int_0^t \int_\Omega \Bigg[&\frac{\partial}{\partial x_i}\left\{-\sigma_{ij}\, l\left(\frac{1-n}{2}u_j - u_{j,k}x_k - t\dot{u}_j\right) + \mathcal{L}\, l\, x_i\right\} \\ &+ \frac{\partial}{\partial t}\left\{\rho\dot{u}_j\, l\left(\frac{1-n}{2}u_j - u_{j,k}x_k - t\dot{u}_j\right) + \mathcal{L}\, l\, t\right\}\Bigg] dV\, dt = 0.\end{aligned} \tag{4.60}$$

The relation is true for any scaling parameter l, therefore, we get

$$\begin{aligned}\int_0^t \int_\Omega \Bigg[&\frac{\partial}{\partial x_i}\left\{\mathcal{L}x_i + \sigma_{ij}\left(\frac{n-1}{2}u_j + u_{j,k}x_k + t\dot{u}_j\right)\right\} \\ &+ \frac{\partial}{\partial t}\left\{t\mathcal{L} - \rho\dot{u}_j\left(\frac{n-1}{2}u_j + u_{j,k}x_k + t\dot{u}_j\right)\right\}\Bigg] dV\, dt = 0.\end{aligned} \tag{4.61}$$

Equation (4.61) holds true for any arbitrary volume Ω and any arbitrary time interval, so we have

$$\frac{\partial}{\partial x_i}\left\{\mathcal{L}x_i + \sigma_{ij}\left(\frac{n-1}{2}u_j + u_{j,k}x_k + t\dot{u}_j\right)\right\} + \frac{\partial}{\partial t}\left\{t\mathcal{L} - \rho\dot{u}_j\left(\frac{n-1}{2}u_j + u_{j,k}x_k + t\dot{u}_j\right)\right\} = 0. \tag{4.62}$$

Equation (4.62) is compared to Fletcher (1976, eq 3.5) for a three dimensional case ($n = 3$) and it is an additional field equation valid anywhere in the domain of analyticity.

Analogously to statics, for linear elastodynamics we define the dynamic M-integral as

$$M^{\text{dyn}} \equiv -\int_{\Omega} \left[\frac{\partial}{\partial x_i} \left\{ \mathcal{L} x_i + \sigma_{ij} \left(\frac{n-1}{2} u_j + u_{j,k} x_k + t \dot{u}_j \right) \right\} + \frac{\partial}{\partial t} \left\{ t\mathcal{L} - \rho \dot{u}_j \left(\frac{n-1}{2} u_j + u_{j,k} x_k + t \dot{u}_j \right) \right\} \right] dV. \tag{4.63}$$

The dynamic M- integral would be zero if the region Ω excludes the inhomogeneity, but it would be nonzero if the volume Ω includes the inhomogeneity. The above expression for the dynamic M- integral agrees in the static case with Günther (1962); Knowles and Sternberg (1972). After further rearrangements, we may write the dynamic M-integral as

$$M^{\text{dyn}} = -\int_{\Omega} x_\alpha \left[\frac{\partial}{\partial x_i} \left\{ \mathcal{L} \delta_{i\alpha} + \sigma_{ij} u_{j,\alpha} \right\} - \frac{\partial}{\partial t} \left\{ \rho \dot{u}_j u_{j,\alpha} \right\} \right] dV, \tag{4.64}$$

where x_i are the material coordinates for $i = 1, 2, 3$, and $x_4 = t$(time variable).

4.3.3 Invariance of the Lagrangean under Rotation

From the family of transformations we have two types of rotation: one is rigid-body rotation (Ω_n) and other is material rotation (ω_n). By choosing nonzero physical rotation in equations (4.45) and (4.44) we obtain the angular momentum balance law, and by choosing nonzero material rotation we obtain the expression for the dynamic L-integral.

Rigid-Body Rotation $\Omega_n \neq 0$, $\omega_n = 0$

In the case of a rigid-body rotation of the material, consider the smooth transformation in x_i and u_i such that coordinates and time variable remain unchanged ($x_i^* = x_i$, $t^* = t$), and the new displacement field is $u_i^* = u_i + \varepsilon_{ilm} \epsilon \Omega_m x_l$, where $\epsilon \Omega_m$ is the infinitesimal physical rotation. After comparing the transformation with equations (4.45) and (4.44), we have

$$\phi_i = 0, \quad \phi_4 = 0, \qquad \text{and} \qquad \psi_j = \varepsilon_{jlm} \Omega_m x_l, \tag{4.65}$$

therefore, from equation (4.8)

$$\overline{\psi}_j = \Omega_m \varepsilon_{jlm} x_l. \tag{4.66}$$

Inserting the above transformation in equation (4.19) to obtain the conservation law for rotation, we obtain

$$\int_0^t \int_\Omega \left[\frac{\partial}{\partial t} \left\{ \rho \dot{u}_j \Omega_m \varepsilon_{jlm} x_l \right\} + \frac{\partial}{\partial x_i} \left\{ -\sigma_{ij} \Omega_m \varepsilon_{jlm} x_l \right\} \right] dV\, dt = 0. \tag{4.67}$$

The relation is true for any Ω_m; therefore, the expression for the conservation of the angular momentum is

$$\varepsilon_{jlm} \int_0^t \int_\Omega \left[\frac{\partial}{\partial t} (\rho \dot{u}_j x_l) - \frac{\partial}{\partial x_i} (\sigma_{ij} x_l) \right] dV\, dt = 0. \tag{4.68}$$

The above equation holds true for any arbitrary volume Ω and arbitrary time interval, so we have

$$\frac{\partial}{\partial t} (\varepsilon_{jlm} \rho \dot{u}_j x_l) - \frac{\partial}{\partial x_i} (\varepsilon_{jlm} \sigma_{ij} x_l) = 0, \tag{4.69}$$

which is the field equation for the angular momentum balance.

Material or Coordinate Rotation $\Omega_n = 0$, $\omega_n \neq 0$

In case of the material or coordinate rotation of an *isotropic* material, consider the smooth transformation in x_i and u_i such that the new coordinates are $x_i^* = x_i + \varepsilon_{ilm} \epsilon\, \omega_m x_l$, new time remains unchanged ($t^* = t$), and the new displacement field is $u_i^* = u_i + \varepsilon_{ilm} \epsilon\, \omega_m u_l$, where $\epsilon\, \omega_m$ is the infinitesimal material rotation. After comparing the transformation with equations (4.45) and (4.44), we have

$$\phi_i = \varepsilon_{ilm} \omega_m x_l, \quad \phi_4 = 0, \qquad \text{and} \qquad \psi_j = \varepsilon_{jlm} \omega_m u_l, \tag{4.70}$$

therefore, from equation (4.8)

$$\overline{\psi}_j = \omega_m(\varepsilon_{jlm}u_l - \varepsilon_{klm}u_{j,k}x_l). \tag{4.71}$$

Inserting the above transformation in equation (4.19) to obtain the conservation law for rotation, we obtain

$$\int_0^t \int_\Omega \left[\frac{\partial}{\partial t}\left\{\rho\dot{u}_j\omega_m(\varepsilon_{jlm}u_l - \varepsilon_{klm}u_{j,k}x_l)\right\} \right.$$
$$\left. + \frac{\partial}{\partial x_i}\left\{-\sigma_{ij}\omega_m(\varepsilon_{jlm}u_l - \varepsilon_{klm}u_{j,k}x_l) + \mathcal{L}\varepsilon_{ilm}\omega_m x_l\right\}\right] dV\,dt = 0. \tag{4.72}$$

The relation is true for any ω_m; therefore, we get

$$\int_0^t \int_\Omega \left[\frac{\partial}{\partial x_i}(\varepsilon_{mlj}u_l\sigma_{ij} + \varepsilon_{mkl}x_l u_{j,k}\sigma_{ij} - \varepsilon_{mli}x_l\mathcal{L}) + \frac{\partial}{\partial t}(\rho\,\varepsilon_{mjl}u_l\dot{u}_j + \rho\,\varepsilon_{mlk}x_l\dot{u}_j u_{j,k})\right] dV\,dt = 0. \tag{4.73}$$

Equation (4.73) holds true for any arbitrary volume Ω and any arbitrary time interval, so we have

$$\frac{\partial}{\partial x_i}(\varepsilon_{mlj}u_l\sigma_{ij} + \varepsilon_{mkl}x_l u_{j,k}\sigma_{ij} - \varepsilon_{mli}x_l\mathcal{L}) + \frac{\partial}{\partial t}(\rho\,\varepsilon_{mjl}u_l\dot{u}_j + \rho\,\varepsilon_{mlk}x_l\dot{u}_j u_{j,k}) = 0. \tag{4.74}$$

Equation (4.74) is compared to Fletcher (1976, eq 3.6); however Fletcher's expression has a negative sign in front of the second term of the first integrand on the left-hand side. In addition to equations (4.50) and (4.62), (4.74) is an additional field equation of elastodynamics valid anywhere in the domain of analyticity.

Analogously to statics, for linear elastodynamics we define the dynamic L- integral as

$$L_m^{\text{dyn}} \equiv -\int_\Omega \left[\frac{\partial}{\partial x_i}(\varepsilon_{mlj} u_l \sigma_{ij} + \varepsilon_{mkl} x_l u_{j,k} \sigma_{ij} - \varepsilon_{mli} x_l \mathcal{L}) + \frac{\partial}{\partial t}(\rho\, \varepsilon_{mjl} u_l \dot{u}_j + \rho\, \varepsilon_{mlk} x_l \dot{u}_j u_{j,k}) \right] dV. \tag{4.75}$$

The dynamic L-integral would be zero if the region Ω excludes the inhomogeneity, but it would be nonzero if the volume Ω includes the inhomogeneity. The above expression for the dynamic L-integral agrees in the static case with Günther (1962); Knowles and Sternberg (1972). After further rearrangements, for an isotropic material, we may write the dynamic L-integral as

$$L_m^{\text{dyn}} = -\int_\Omega \varepsilon_{mkl} x_l \left[\frac{\partial}{\partial x_i} \left\{ \mathcal{L}\delta_{ik} + \sigma_{ij} u_{j,k} \right\} - \frac{\partial}{\partial t} \left\{ \rho \dot{u}_j u_{j,k} \right\} \right] dV. \tag{4.76}$$

In the next section, we present these conservation laws as dissipative mechanisms for the corresponding infinitesimal transformations of translation, scaling and rotation of the inhomogeneities.

4.4 Conservation Integrals as Dissipative Mechanisms

With the objective of relating the conservation integrals J, M and L to the corresponding energy loss of the system, in this section we express the variation of the Lagrangean in terms of balance laws of linear and angular momenta and the "conserved" integrals. Subsequently, the variation of the Lagrangean will be related to the variation of the Hamiltonian, which, in term, will be related to the total energy loss of the system.

Equation (4.7) is written after expanding in space and time variables

$$\delta\Pi^{\mathcal{L}} = \epsilon \int_0^t \int_\Omega \left\{ \frac{\partial \mathcal{L}}{\partial u_j} - \frac{\partial}{\partial x_i}\frac{\partial \mathcal{L}}{\partial u_{j,i}} - \frac{\partial}{\partial t}\frac{\partial \mathcal{L}}{\partial \dot{u}_j} \right\} \overline{\psi}_j \, dV \, dt + \epsilon \int_0^t \int_\Omega \left[\frac{\partial}{\partial x_i} \left\{ \frac{\partial \mathcal{L}}{\partial u_{j,i}} \overline{\psi}_j + \mathcal{L}\phi_i \right\} + \frac{\partial}{\partial t} \left\{ \frac{\partial \mathcal{L}}{\partial \dot{u}_j} \overline{\psi}_j + \mathcal{L}\phi_4 \right\} \right] dV \, dt, \tag{4.77}$$

In view of equations (4.13)–(4.15) the term $\partial \mathcal{L}/\partial u_j$ vanishes, $\partial \mathcal{L}/\partial u_{j,i} = -\sigma_{ij}$, and $\partial \mathcal{L}/\partial \dot{u}_j = \rho \dot{u}_j$; therefore, equation (4.77) can be written as

$$\delta\Pi^{\mathcal{L}} = \epsilon \int_0^t \int_\Omega \left\{ \frac{\partial \sigma_{ij}}{\partial x_i} - \frac{\partial (\rho \dot{u}_j)}{\partial t} \right\} \overline{\psi}_j \, dV \, dt + \epsilon \int_0^t \int_\Omega \left[\frac{\partial}{\partial x_i} \left\{ -\sigma_{ij} \overline{\psi}_j + \mathcal{L}\phi_i \right\} + \frac{\partial}{\partial t} \left\{ \rho \dot{u}_j \overline{\psi}_j + \mathcal{L}\phi_4 \right\} \right] dV \, dt. \tag{4.78}$$

Next, equation (4.78) is applied to the infinitesimal transformations $\boldsymbol{\phi}$ and $\boldsymbol{\psi}$ corresponding to translation, scaling and rotation of the inhomogeneities.

4.4.1 Translation of the Inhomogeneity

For translation of the inhomogeneity, we utilize the transformation (Fletcher, 1976) such that the new coordinates are $x_i^* = x_i + \epsilon a_i$ and the new time and displacement field remain invariant ($u_i^* = u_i$), where ϵa_i is the infinitesimal translation of the inhomogeneity. After comparing the transformation with equations (4.45) and (4.44), we have

$$\phi_i = a_i, \quad \phi_4 = 0, \qquad \text{and} \qquad \psi_j = 0, \tag{4.79}$$

therefore, from equation (4.8)

$$\overline{\psi}_j = \psi_j - u_{j,\alpha}\phi_\alpha = -u_{j,k}a_k. \tag{4.80}$$

Substituting the above transformation in equation (4.78) gives (Gupta and Markenscoff, 2012)

$$\delta\Pi^{\mathcal{L}} = \epsilon \int_0^t \int_\Omega \left\{ \frac{\partial \sigma_{ij}}{\partial x_i} - \frac{\partial(\rho \dot{u}_j)}{\partial t} \right\} (-u_{j,k} a_k)\, dV\, dt + \epsilon \int_0^t \int_\Omega \left[\frac{\partial}{\partial x_i} \left\{ (\mathcal{L}\delta_{ik} + \sigma_{ij} u_{j,k}) a_k \right\} + \frac{\partial}{\partial t} \left\{ -\rho \dot{u}_j u_{j,k} a_k \right\} \right] dV\, dt. \tag{4.81}$$

Taking the translation vector a_k out of the second integral of the right hand side, we write

$$\delta\Pi^{\mathcal{L}} = -\epsilon \int_0^t \int_\Omega \left\{ \frac{\partial \sigma_{ij}}{\partial x_i} - \frac{\partial(\rho \dot{u}_j)}{\partial t} \right\} u_{j,k} a_k\, dV\, dt + \epsilon a_k \int_0^t \int_\Omega \left[\frac{\partial}{\partial x_i} \left\{ \mathcal{L}\delta_{ik} + \sigma_{ij} u_{j,k} \right\} - \frac{\partial}{\partial t} \left\{ \rho \dot{u}_j u_{j,k} \right\} \right] dV\, dt. \tag{4.82}$$

Taking the time derivative of the above equation, we obtain

$$\delta\dot{\Pi}^{\mathcal{L}} = -\epsilon \int_\Omega \left\{ \frac{\partial \sigma_{ij}}{\partial x_i} - \frac{\partial(\rho \dot{u}_j)}{\partial t} \right\} u_{j,k} a_k\, dV + \epsilon a_k \int_\Omega \left[\frac{\partial}{\partial x_i} \left\{ \mathcal{L}\delta_{ik} + \sigma_{ij} u_{j,k} \right\} - \frac{\partial}{\partial t} \left\{ \rho \dot{u}_j u_{j,k} \right\} \right] dV. \tag{4.83}$$

From equation (4.51), the integral in the second term of the right-hand side of (4.83) is $-J_k^{\text{dyn}}$, so we can rewrite equation (4.83) as

$$\delta\dot{\Pi}^{\mathcal{L}} = -\int_\Omega \left\{ \frac{\partial \sigma_{ij}}{\partial x_i} - \frac{\partial(\rho \dot{u}_j)}{\partial t} \right\} u_{j,k} a_k\, dV - \epsilon a_k\, J_k^{\text{dyn}}. \tag{4.84}$$

In equation (4.84), the term in the curly brackets in the integrand is the linear momentum balance expression (equation (4.17)) which vanishes by the Euler-Lagrange equations applied to the Lagrangean.

4.4.2 Scaling of the Inhomogeneity

For the self-similar expansion, consider the smooth scaling such that the new coordinates and time are $x_i^* = x_i + \epsilon l x_i$ and $t^* = t + \epsilon l t$, respectively, and the new displacement field is $u_i^* = u_i + (1-n)\epsilon l u_i/2$, where l is the scaling parameter and n is the number of space dimensions. After comparing the transformation with equations (4.45) and (4.44), we have

$$\phi_i = l x_i, \quad \phi_4 = lt, \qquad \text{and} \qquad \psi_j = \frac{1-n}{2} l u_j, \tag{4.85}$$

therefore, from equation (4.8), we have

$$\overline{\psi}_j = \psi_j - u_{j,\alpha}\phi_\alpha = l\left(\frac{1-n}{2}u_j - u_{j,k}x_k - t\dot{u}_j\right). \tag{4.86}$$

Substituting the above transformation in equation (4.78) to obtain the variation of the Lagrangean for scaling of the inhomogeneity, we write

$$\begin{aligned}\delta\Pi^{\mathcal{L}} = \epsilon\int_0^t\int_\Omega \left\{\frac{\partial\sigma_{ij}}{\partial x_i} - \frac{\partial(\rho\dot{u}_j)}{\partial t}\right\}\overline{\psi}_j\, dV\, dt + \epsilon\int_0^t\int_\Omega \left[\frac{\partial}{\partial x_i}\left\{-\sigma_{ij}\, l\left(\frac{1-n}{2}u_j - u_{j,k}x_k - t\dot{u}_j\right) + \mathcal{L}\, l\, x_i\right\}\right.\\ \left. + \frac{\partial}{\partial t}\left\{\rho\dot{u}_j\, l\left(\frac{1-n}{2}u_j - u_{j,k}x_k - t\dot{u}_j\right) + \mathcal{L}\, l\, t\right\}\right] dV\, dt.\end{aligned} \tag{4.87}$$

Taking the scaling parameter l out of the second integral on the right-hand side, we write

$$\begin{aligned}\delta\Pi^{\mathcal{L}} = \epsilon\int_0^t\int_\Omega \left\{\frac{\partial\sigma_{ij}}{\partial x_i} - \frac{\partial(\rho\dot{u}_j)}{\partial t}\right\}\overline{\psi}_j\, dV\, dt + \epsilon l\int_0^t\int_\Omega \left[\frac{\partial}{\partial x_i}\left\{\mathcal{L}x_i + \sigma_{ij}\left(\frac{n-1}{2}u_j + u_{j,k}x_k + t\dot{u}_j\right)\right\}\right.\\ \left. + \frac{\partial}{\partial t}\left\{t\mathcal{L} - \rho\dot{u}_j\left(\frac{n-1}{2}u_j + u_{j,k}x_k + t\dot{u}_j\right)\right\}\right] dV\, dt.\end{aligned} \tag{4.88}$$

Taking the time derivative of the above equation, we write

$$\delta\dot{\Pi}^{\mathcal{L}} = \epsilon \int_{\Omega} \left\{ \frac{\partial \sigma_{ij}}{\partial x_i} - \frac{\partial(\rho \dot{u}_j)}{\partial t} \right\} \overline{\psi}_j \, dV + \epsilon l \int_{\Omega} \left[\frac{\partial}{\partial x_i} \left\{ \mathcal{L} x_i + \sigma_{ij} \left(\frac{n-1}{2} u_j + u_{j,k} x_k + t \dot{u}_j \right) \right\} \right.$$
$$\left. + \frac{\partial}{\partial t} \left\{ t\mathcal{L} - \rho \dot{u}_j \left(\frac{n-1}{2} u_j + u_{j,k} x_k + t \dot{u}_j \right) \right\} \right] dV. \tag{4.89}$$

From equation (4.63), the integral in the second term of the right-hand side of (5.3) is $-M^{\text{dyn}}$, so we can rewrite equation (5.3) as

$$\delta\dot{\Pi}^{\mathcal{L}} = \int_{\Omega} \left\{ \frac{\partial \sigma_{ij}}{\partial x_i} - \frac{\partial(\rho \dot{u}_j)}{\partial t} \right\} \overline{\psi}_j \, dV - \epsilon l \, M^{\text{dyn}}. \tag{4.90}$$

In equation (4.90), the term in the curly brackets in the integrand is the linear momentum balance expression (equation (4.17)) which vanishes by the Euler-Lagrange equations applied to the Lagrangean.

4.4.3 Rotation of the Inhomogeneity

Following the *lever arm* $(u_l + x_l)$ described by Eshelby (1956, p 106), and taking $\Omega_n = \omega_n$ in equation (4.45) for the rotation of the inhomogeneity in an *isotropic* material, we consider the smooth transformation in x_i and u_i such that the new coordinates are $x_i^* = x_i + \varepsilon_{ilm} \epsilon \, \omega_m x_l$, new time remains unchanged ($t^* = t$), and the new displacement field is $u_i^* = u_i + \varepsilon_{ilm} \epsilon \, \omega_m (u_l + x_l)$, where ω_m is the rotation vector. After comparing the transformation with equations (4.45) and (4.44), we have

$$\phi_i = \varepsilon_{ilm} \omega_m x_l, \quad \phi_4 = 0, \qquad \text{and} \qquad \psi_j = \varepsilon_{jlm} \omega_m (u_l + x_l), \tag{4.91}$$

therefore, from equation (4.8), we have

$$\overline{\psi}_j = \psi_j - u_{j,k} \phi_k = \omega_m (\varepsilon_{jlm} (u_l + x_l) - \varepsilon_{klm} u_{j,k} x_l). \tag{4.92}$$

Substituting the above transformation into equation (4.78) to obtain the variation of the Lagrangean for rotation of the inhomogeneity, we write

$$\delta\Pi^{\mathcal{L}} = \epsilon \int_0^t \int_\Omega \left\{ \frac{\partial \sigma_{ij}}{dx_i} - \frac{\partial(\rho \dot{u}_j)}{\partial t} \right\} \overline{\psi}_j \, dV \, dt + \epsilon \int_0^t \int_\Omega \left[\frac{\partial}{\partial t} \left\{ \rho \dot{u}_j \omega_m (\varepsilon_{jlm}(u_l + x_l) - \varepsilon_{klm} u_{j,k} x_l) \right\} + \frac{\partial}{\partial x_i} \left\{ -\sigma_{ij} \omega_m (\varepsilon_{jlm}(u_l + x_l) - \varepsilon_{klm} u_{j,k} x_l) + \mathcal{L} \varepsilon_{ilm} \omega_m x_l \right\} \right] dV \, dt. \tag{4.93}$$

Collecting the angular momentum balance terms gives

$$\delta\Pi^{\mathcal{L}} = \epsilon \int_0^t \int_\Omega \left\{ \frac{\partial \sigma_{ij}}{\partial x_i} - \frac{\partial(\rho \dot{u}_j)}{\partial t} \right\} \overline{\psi}_j \, dV \, dt - \epsilon \, \omega_m \int_0^t \int_\Omega \left[\frac{\partial}{\partial x_i} (\varepsilon_{jlm} x_l \sigma_{ij}) - \frac{\partial}{\partial t} (\rho \, \varepsilon_{jlm} x_l \dot{u}_j) \right] dV \, dt$$
$$+ \epsilon \, \omega_m \int_0^t \int_\Omega \left[\frac{\partial}{\partial x_i} (-\varepsilon_{jlm} u_l \sigma_{ij} + \varepsilon_{klm} x_l u_{j,k} \sigma_{ij} + \varepsilon_{ilm} x_l \mathcal{L}) + \frac{\partial}{\partial t} (\rho \, \varepsilon_{jlm} u_l \dot{u}_j - \rho \, \varepsilon_{klm} x_l \dot{u}_j u_{j,k}) \right] dV \, dt, \tag{4.94}$$

after further rearrangements we obtain

$$\delta\Pi^{\mathcal{L}} = \epsilon \int_0^t \int_\Omega \left\{ \frac{\partial \sigma_{ij}}{\partial x_i} - \frac{\partial(\rho \dot{u}_j)}{\partial t} \right\} \overline{\psi}_j \, dV \, dt - \epsilon \, \omega_m \int_0^t \int_\Omega \left[\frac{\partial}{\partial t} (\rho \, \varepsilon_{mlj} x_l \dot{u}_j) - \frac{\partial}{\partial x_i} (\varepsilon_{mlj} x_l \sigma_{ij}) \right] dV \, dt$$
$$+ \epsilon \, \omega_m \int_0^t \int_\Omega \left[\frac{\partial}{\partial x_i} (\varepsilon_{mlj} u_l \sigma_{ij} + \varepsilon_{mkl} x_l u_{j,k} \sigma_{ij} - \varepsilon_{mli} x_l \mathcal{L}) + \frac{\partial}{\partial t} (\rho \, \varepsilon_{mjl} u_l \dot{u}_j + \rho \, \varepsilon_{mlk} x_l \dot{u}_j u_{j,k}) \right] dV \, dt. \tag{4.95}$$

Taking the time derivative of the above equation, we write

$$\delta\dot{\Pi}^{\mathcal{L}} = \epsilon \int_{\Omega} \left\{ \frac{\partial \sigma_{ij}}{\partial x_i} - \frac{\partial(\rho \dot{u}_j)}{\partial t} \right\} \overline{\psi}_j \, dV - \epsilon \, \omega_m \int_{\Omega} \left[\frac{\partial}{\partial t}(\rho \, \varepsilon_{mlj} x_l \dot{u}_j) - \frac{\partial}{\partial x_i}(\varepsilon_{mlj} x_l \sigma_{ij}) \right] dV$$
$$+ \epsilon \, \omega_m \int_{\Omega} \left[\frac{\partial}{\partial x_i}(\varepsilon_{mlj} u_l \sigma_{ij} + \varepsilon_{mkl} x_l u_{j,k} \sigma_{ij} - \varepsilon_{mli} x_l \mathcal{L}) + \frac{\partial}{\partial t}(\rho \, \varepsilon_{mjl} u_l \dot{u}_j + \rho \, \varepsilon_{mlk} x_l \dot{u}_j u_{j,k}) \right] dV. \tag{4.96}$$

From equation (4.75), the integral in the third term of the right-hand side of (4.96) is $-L_m^{\text{dyn}}$, so we can rewrite equation (4.96) as

$$\delta\dot{\Pi}^{\mathcal{L}} = \epsilon \int_{\Omega} \left\{ \frac{\partial \sigma_{ij}}{\partial x_i} - \frac{\partial(\rho \dot{u}_j)}{\partial t} \right\} \overline{\psi}_j \, dV - \epsilon \, \omega_m \int_{\Omega} \left[\frac{\partial}{\partial t}(\rho \, \varepsilon_{mlj} x_l \dot{u}_j) - \frac{\partial}{\partial x_i}(\varepsilon_{mlj} x_l \sigma_{ij}) \right] dV$$
$$- \epsilon \, \omega_m \, L_m^{\text{dyn}}. \tag{4.97}$$

In equation (4.97), the term in the curly brackets in the first integrand is the linear momentum balance expression (equation (4.17)) and the second integrand on the right hand side is the angular momentum expression (equation (4.69)).

It may be noted that we obtain both the expression for the angular moment balance and the dynamic L-integral from the variation of the Lagrangian functional because the rigid-body rotation (equation (4.65)) and the material rotation (equation (4.70)) are both considered. The transformation of rigid-body rotation (section 3.3.1) by itself leads to the expression for the angular momentum balance (Fletcher, 1976, eq 3.3) and the transformation of material rotation (section 3.3.2) leads to the expression for the dynamic L-integral (Fletcher, 1976, eq 3.6). By using both together we are able to obtain the dissipative statement (equation (4.97)) as further discussed in the following sections.

4.5 Relation of the Variations of the Lagrangean and Hamiltonian under the Transformations of Translation, Scaling and Rotation of Inhomogeneities

In the previous sections Noether's theorem was applied to the Lagrangean functional of the system from which the conservation of linear momentum is derived as the Euler-Lagrange equations (4.11). In this section we relate the variation of the Lagrangean to the variation of the Hamiltonian under translation, scaling and rotation of the inhomogeneities so that we can explicitly relate the conservation integrals with energy release rates (Gupta and Markenscoff (2012); and private communication with Gupta).

The Hamiltonian density is defined as

$$\mathcal{H} = T + W, \tag{4.98}$$

where the strain energy density is $W = \frac{1}{2} C_{ijkl} \varepsilon_{ij} \varepsilon_{kl} = \frac{1}{2} C_{ijkl}\, u_{i,j} u_{k,l}$ and the specific kinetic energy is $T = \frac{1}{2} \rho \dot{u}_i \dot{u}_i$. We consider the total Hamiltonian functional for $\Omega \subset \mathbb{R}^3$ and $[0, t] \subset \mathbb{R}$,

$$\Pi^{\mathcal{H}}(u_{i,j}, \dot{u}_i) = \int_0^t \int_\Omega \mathcal{H}(u_{i,j}, \dot{u}_i)\, dV\, dt = \int_0^t \int_\Omega \{T(\dot{u}_i) + W(u_{i,j})\}\, dV\, dt. \tag{4.99}$$

The functional (4.99) represents the total mechanical energy stored in an arbitrary part Ω of the body during the time interval $[0, t]$. Applying equation (4.7) to the Hamiltonian (equation (4.98)) and expanding in space and time variables, we write (similarly to equation (4.77) for the Lagrangean $\mathcal{L} = T - W$) the variation of the Hamiltonian functional (4.99) under the infinitesimal

transformation (4.2a)–(4.2b) as

$$\delta\Pi^{\mathcal{H}} = \epsilon \int_0^t \int_\Omega \left\{ \frac{\partial \mathcal{H}}{\partial u_j} - \frac{\partial}{\partial x_i}\frac{\partial \mathcal{H}}{\partial u_{j,i}} - \frac{\partial}{\partial t}\frac{\partial \mathcal{H}}{\partial \dot{u}_j} \right\} \overline{\psi}_j \, dV \, dt + \epsilon \int_0^t \int_\Omega \frac{\partial}{\partial x_i} \left\{ \frac{\partial \mathcal{H}}{\partial u_{j,i}} \overline{\psi}_j + \mathcal{H}\phi_i \right\} dV \, dt$$
$$+ \epsilon \int_0^t \int_\Omega \frac{\partial}{\partial t} \left\{ \frac{\partial \mathcal{H}}{\partial \dot{u}_j} \overline{\psi}_j + \mathcal{H}\phi_4 \right\} dV \, dt. \tag{4.100}$$

In view of equations (4.98), (4.14) and (4.15) the term $\partial\mathcal{H}/\partial u_j$ vanishes and $\partial\mathcal{H}/\partial u_{j,i} = \sigma_{ij}$, and $\partial\mathcal{H}/\partial \dot{u}_j = \rho \dot{u}_j$; therefore, above equation can be written as

$$\delta\Pi^{\mathcal{H}} = \epsilon \int_0^t \int_\Omega \left\{ -\frac{\partial \sigma_{ij}}{\partial x_i} - \frac{\partial(\rho \dot{u}_j)}{\partial t} \right\} \overline{\psi}_j \, dV \, dt + \epsilon \int_0^t \int_\Omega \frac{\partial}{\partial x_i} \left\{ \sigma_{ij} \overline{\psi}_j + (W+T)\phi_i \right\} dV \, dt$$
$$+ \epsilon \int_0^t \int_\Omega \frac{\partial}{\partial t} \left\{ \rho \dot{u}_j \overline{\psi}_j + (W+T)\phi_4 \right\} dV \, dt. \tag{4.101}$$

Note that the first term on the right hand side of the above equation is not same as the first term of the variation of the Lagrangean (equation (4.78)), which is the linear momentum balance term. Next, we rearrange the terms as to produce the linear momentum balance expression in the first integrand and make a connection to the variation of the Lagrangean

$$\delta\Pi^{\mathcal{H}} = \epsilon \int_0^t \int_\Omega \left\{ -\frac{\partial \sigma_{ij}}{\partial x_i} + \frac{\partial(\rho \dot{u}_j)}{\partial t} \right\} \overline{\psi}_j \, dV \, dt + \epsilon \int_0^t \int_\Omega \frac{\partial}{\partial x_i} \left\{ \sigma_{ij} \overline{\psi}_j + (W+T)\phi_i \right\} dV \, dt$$
$$+ \epsilon \int_0^t \int_\Omega \left\{ -\overline{\psi}_j \frac{\partial}{\partial t}(\rho \dot{u}_j) + \rho \dot{u}_j \frac{\partial}{\partial t} \overline{\psi}_j + \frac{\partial}{\partial t} \left[(W+T)\phi_4 \right] \right\} dV \, dt, \tag{4.102}$$

we further rearrange as to produce terms with $(W-T)$ in the remaining terms on the right hand

side

$$\delta\Pi^{\mathcal{H}} = \epsilon \int_0^t \int_\Omega \left\{ -\frac{\partial \sigma_{ij}}{\partial x_i} + \frac{\partial(\rho \dot{u}_j)}{\partial t} \right\} \overline{\psi}_j \, dV \, dt + \epsilon \int_0^t \int_\Omega \frac{\partial}{\partial x_i} \left\{ \sigma_{ij} \overline{\psi}_j + (W - T)\phi_i \right\} dV \, dt$$
$$+ \epsilon \int_0^t \int_\Omega \left\{ -\overline{\psi}_j \frac{\partial}{\partial t}(\rho \dot{u}_j) - \rho \dot{u}_j \frac{\partial}{\partial t} \overline{\psi}_j + \frac{\partial}{\partial t} \left[(W - T)\phi_4 \right] \right\} dV \, dt$$
$$+ 2\epsilon \int_0^t \int_\Omega \left\{ \frac{\partial}{\partial x_i}(T\phi_i) + \frac{\partial}{\partial t}(T\phi_4) + \rho \dot{u}_j \frac{\partial}{\partial t} \overline{\psi}_j \right\} dV \, dt. \tag{4.103}$$

We further rewrite the expression using equation (4.13), so that the expression in the variation of the Hamiltonian involves the Lagrangean

$$\delta\Pi^{\mathcal{H}} = \epsilon \int_0^t \int_\Omega \left\{ -\frac{\partial \sigma_{ij}}{\partial x_i} + \frac{\partial(\rho \dot{u}_j)}{\partial \partial t} \right\} \overline{\psi}_j \, dV \, dt + \epsilon \int_0^t \int_\Omega \frac{\partial}{\partial x_i} \left\{ \sigma_{ij} \overline{\psi}_j - \mathcal{L}\phi_i \right\} dV \, dt$$
$$+ \epsilon \int_0^t \int_\Omega \frac{d}{dt} \left\{ -\rho \dot{u}_j \overline{\psi}_j - \mathcal{L}\phi_4 \right\} dV \, dt + 2\epsilon \int_0^t \int_\Omega \left\{ \frac{\partial}{\partial x_i}(T\phi_i) + \frac{\partial}{\partial t}(T\phi_4) + \rho \dot{u}_j \frac{\partial}{\partial t} \overline{\psi}_j \right\} dV \, dt. \tag{4.104}$$

Using (4.78) which is the expression for the variation of the Lagrangean we have

$$\delta\Pi^{\mathcal{H}} = -\delta\Pi^{\mathcal{L}} + 2\epsilon \int_0^t \int_\Omega \left\{ \frac{\partial}{\partial x_i}(T\phi_i) + \frac{\partial}{\partial t}(T\phi_4) + \rho \dot{u}_j \frac{\partial}{\partial t} \overline{\psi}_j \right\} dV \, dt, \tag{4.105}$$

which can be written, using equation (4.8), as

$$\delta\Pi^{\mathcal{H}} = -\delta\Pi^{\mathcal{L}} + 2\epsilon \int_0^t \int_\Omega \left\{ \frac{\partial}{\partial x_i}(T\phi_i) + \frac{\partial}{\partial t}(T\phi_4) + \rho \dot{u}_j \frac{\partial}{\partial t}(\psi_j - u_{j,i}\phi_i - \dot{u}_j \phi_4) \right\} dV \, dt. \tag{4.106}$$

Now we employ relation (4.106) of the variations of the Lagrangean and Hamiltonian to the corresponding infinitesimal transformations of translation, rotation, and scaling of the

inhomogeneity.

4.5.1 Translation of the Inhomogeneity

In this case we use the transformation such that $\phi_i = a_i$, $\phi_4 = 0$ and $\psi_j = 0$, i.e., translation of the inhomogeneity. Inserting it in equation (4.106) gives

$$\begin{aligned}
\delta\Pi^{\mathcal{H}} &= -\delta\Pi^{\mathcal{L}} + 2\epsilon \int_0^t \int_\Omega \left\{ \frac{\partial}{\partial x_i}(T a_i) + \rho \dot{u}_j \frac{\partial}{\partial t}(-u_{j,i} a_i) \right\} dV\, dt \\
&= -\delta\Pi^{\mathcal{L}} + 2\epsilon \int_0^t \int_\Omega \left\{ \rho \dot{u}_k \dot{u}_{k,i} a_i - \rho \dot{u}_j \dot{u}_{j,i} a_i \right\} dV\, dt \\
&= -\delta\Pi^{\mathcal{L}},
\end{aligned} \tag{4.107}$$

Thus, under an infinitesimal translation of the inhomogeneity, the variation of the Lagrangean is equal to the negative variation of the Hamiltonian, which was already shown by Gupta and Markenscoff (2012). Taking the time derivative of equation (4.107) we can write

$$\delta\dot{\Pi}^{\mathcal{H}} = -\delta\dot{\Pi}^{\mathcal{L}}, \tag{4.108}$$

which, using equation (4.84) can be written as

$$\delta\dot{\Pi}^{\mathcal{H}} = -\delta\dot{\Pi}^{\mathcal{L}} = \epsilon \int_\Omega \left\{ \frac{\partial \sigma_{ij}}{\partial x_i} - \frac{\partial(\rho \dot{u}_j)}{\partial t} \right\} u_{j,k} a_k\, dV + \epsilon a_k\, J_k^{\text{dyn}}, \tag{4.109}$$

where J_k^{dyn} is defined by equation (4.51). Considering the definition of the Hamiltonian $\Pi^{\mathcal{H}}(u_{i,j}, \dot{u}_i)$ according to equation (4.99), we define $\delta\mathcal{E}^{tot}$ as

$$\delta\mathcal{E}^{tot} \equiv \delta\dot{\Pi}^{\mathcal{H}}, \tag{4.110}$$

where $\delta\mathcal{E}^{tot}$ is the change of the total energy in the volume Ω under the infinitesimal transformations of equation (4.45) evaluated at time t. The external forces are assumed to be absent. Now, from equations (4.110) and (4.109) we can write

$$\delta\mathcal{E}^{tot} = \epsilon \int_{\Omega} \left\{ \frac{\partial \sigma_{ij}}{\partial x_i} - \frac{\partial(\rho \dot{u}_j)}{\partial t} \right\} u_{j,k} a_k \, dV + \epsilon a_k \, J_k^{\text{dyn}}, \tag{4.111}$$

In equation (4.111), the term in the curly brackets in the integrand is the linear momentum balance expression (equation (4.17)), which will vanish due to conservation of linear momentum. So, if linear momentum is conserved in the whole domain then equation (4.111) can be written as

$$\delta\mathcal{E}^{tot} = \epsilon a_k \, J_k^{\text{dyn}}. \tag{4.112}$$

Moreover, as shown in Gupta and Markenscoff (2012), if $\delta\mathcal{E}^{tot} = \epsilon a_k \, J_k^{\text{dyn}}$ then the first term on the right hand side of equation (4.111) will vanish and if $u_{j,k}$ is invertible, then the term in the curly brackets (linear momentum balance expression) will vanish since the integral is valid for any arbitrary volume Ω. Therefore, equation (4.111) can be stated as the proposition that under an infinitesimal translation of the inhomogeneity (transformation (4.79)), the change of the total energy of the system per unit infinitesimal translation of the inhomogeneity is equal to the dynamic J integral *if and only if* linear momentum is conserved in the whole domain (Gupta and Markenscoff, 2012), provided that $u_{j,k}$ is invertible.

If the inhomogeneity is moving with the velocity $\epsilon \dot{a}_k \equiv v_k$, then we can write the rate of the total energy change $\delta\dot{\mathcal{E}}^{tot}$ as

$$\delta\dot{\mathcal{E}}^{tot} = v_k \, J_k^{\text{dyn}}. \tag{4.113}$$

The above equation agrees in the static case with Budiansky and Rice (1973); Lubarda and Markenscoff (2007). With the expression for J_k^{dyn} given in equation (4.57), equation (4.113)

yields

$$\delta\dot{\mathcal{E}}^{tot} = \lim_{S_d \to 0} \int_{S_d} \left\{ (W+T) n_k v_k - \sigma_{ij} u_{j,k} n_i v_k \right\} dS, \tag{4.114}$$

where S_d is an arbitrary surface surrounds the inhomogeneity, moving with it and shrinking on it, and n_k are the components of the unit outward normal $\boldsymbol{n}$ to the surface S_d. Furthermore, near the core of the moving inhomogeneity, leading-order terms of the fields satisfy the relation $\partial/\partial t = -v_k \partial/\partial x_k$ (Freund, 1972), so we can write $u_{j,k} v_k = -\dot{u}_j$ in equation (4.114) to obtain

$$\delta\dot{\mathcal{E}}^{tot} = \lim_{S_d \to 0} \int_{S_d} \left\{ (W+T) v_n + \sigma_{ij} \dot{u}_j n_i \right\} dS, \tag{4.115}$$

where v_n is the component of the velocity of the inhomogeneity in the direction of the outward normal $\boldsymbol{n}$ to the surface S_d. In agreement with the expression for the energy release rate into the core of the moving inhomogeneity as given by Eshelby (1970, eq 78) we define the energy release rate $\mathcal{G}$ by

$$v\mathcal{G} \equiv \delta\dot{\mathcal{E}}^{tot} = \lim_{S_d \to 0} \int_{S_d} \left\{ (W+T) v_n + \sigma_{ij} \dot{u}_j n_i \right\} dS, \tag{4.116}$$

which represents rate of energy loss of the system flowing into the inhomogeneity under translation. Equation (4.116) is in agreement with the energy release for moving crack by Atkinson and Eshelby (1968, eq 9); Freund (1972, eq 13); Freund (1990, p 262), for dislocations (Clifton and Markenscoff, 1981) and moving phase boundaries (Markenscoff and Ni, 2010; Ni and Markenscoff, 2015). As proven in Freund (1972) the above expression is path independent for a crack, and will also be now for an inhomogeneity, since it is a weaker singularity.

4.5.2 Scaling of the Inhomogeneity

In this case we use the transformation such that $\phi_i = l\,x_i$, $\phi_4 = l\,t$ and $\psi_j = (1-n)l\,u_j/2$, i.e., scaling of the inhomogeneity. Inserting it in equation (4.106) gives

$$\begin{aligned}
\delta\Pi^{\mathcal{H}} &= -\delta\Pi^{\mathcal{L}} + 2\epsilon \int_0^t \int_\Omega \left\{ \frac{\partial}{\partial x_i}(Tlx_i) + \frac{\partial}{\partial t}(Tlt) + \rho\dot{u}_j \frac{\partial}{\partial t}\left(\frac{1-n}{2} l\,u_j - u_{j,i} l x_i - \dot{u}_j lt \right) \right\} dV\,dt \\
&= -\delta\Pi^{\mathcal{L}} + 2\epsilon \int_0^t \int_\Omega \left\{ l x_i \rho \dot{u}_k \dot{u}_{k,i} + nlT + lt\rho\dot{u}_k\ddot{u}_k + Tl + \frac{1-n}{2} l\rho\dot{u}_j\dot{u}_j - l x_i \rho \dot{u}_j \dot{u}_{j,i} \right. \\
&\quad \left. - lt\rho\dot{u}_j\ddot{u}_j - l\rho\dot{u}_j\dot{u}_j \right\} dV\,dt \\
&= -\delta\Pi^{\mathcal{L}} + 2\epsilon \int_0^t \int_\Omega \{ nTl + Tl + (1-n)Tl - 2Tl \}\, dV\,dt \\
&= -\delta\Pi^{\mathcal{L}}, \qquad (4.117)
\end{aligned}$$

where n is equal to number of spatial dimensions.

Thus, under an infinitesimal scaling of the inhomogeneity, the variation of the Lagrangean is equal to the negative variation of the Hamiltonian. Taking the time derivative of equation (4.117), we can write

$$\delta\dot{\Pi}^{\mathcal{H}} = -\delta\dot{\Pi}^{\mathcal{L}}, \qquad (4.118)$$

which, using equation (4.90), can be written as

$$\delta\dot{\Pi}^{\mathcal{H}} = -\delta\dot{\Pi}^{\mathcal{L}} = -\epsilon \int_\Omega \left\{ \frac{\partial\sigma_{ij}}{\partial x_i} - \frac{\partial(\rho\dot{u}_j)}{\partial t} \right\} \overline{\psi}_j\, dV + \epsilon l\, M^{\mathrm{dyn}}, \qquad (4.119)$$

where M^{dyn} is defined by (4.63). Now from (4.99) and (4.119), we can define

$$\delta\mathcal{E}^{tot} \equiv \delta\dot{\Pi}^{\mathcal{H}} = -\epsilon \int_{\Omega} \left\{ \frac{\partial \sigma_{ij}}{\partial x_i} - \frac{\partial(\rho \dot{u}_j)}{\partial t} \right\} \overline{\psi}_j \, dV + \epsilon l \, M^{\text{dyn}}, \tag{4.120}$$

where $\delta\mathcal{E}^{tot}$ is the change of the total energy in the volume Ω due to the scaling of the inhomogeneity evaluated at time t. In equation (4.120), the term in the curly brackets in the integrand is the linear momentum balance expression (equation (4.17)). Therefore, equation (4.120) can be stated as the proposition that if linear momentum is conserved in the whole domain, then the change of the total energy of the system per unit infinitesimal scaling ϵl, under the scaling transformation (4.85), is equal to the dynamic M-integral.

4.5.3 Rotation of the Inhomogeneity

In this case we use the transformation such that $\phi_i = \varepsilon_{ilm}\omega_m x_l$, $\phi_4 = 0$ and $\psi_j = \varepsilon_{jlm}\omega_m(u_l + x_l)$, i.e., rotation of the inhomogeneity. Inserting it in equation (4.106) gives

$$\begin{aligned}
\delta\Pi^{\mathcal{H}} &= -\delta\Pi^{\mathcal{L}} + 2\epsilon \int_0^t \int_{\Omega} \left\{ \frac{\partial}{\partial x_i}(T\varepsilon_{ilm}\omega_m x_l) + \rho\dot{u}_j \frac{\partial}{\partial t}(\varepsilon_{jlm}\omega_m(u_l + x_l) - u_{j,i}\varepsilon_{ilm}\omega_m x_l) \right\} dV\, dt \\
&= -\delta\Pi^{\mathcal{L}} + 2\epsilon \int_0^t \int_{\Omega} \left\{ \varepsilon_{ilm}\omega_m x_l \rho\dot{u}_k\dot{u}_{k,i} + T\varepsilon_{ilm}\omega_m\delta_{il} + \rho\dot{u}_j\varepsilon_{jlm}\omega_m\dot{u}_l - \rho\dot{u}_j\dot{u}_{j,i}\varepsilon_{ilm}\omega_m x_l \right\} dV\, dt.
\end{aligned} \tag{4.121}$$

The first term of the integrand on right-hand side cancels with the fourth term, the second term is zero because δ_{il} is symmetric in i and l but ε_{ilm} is skew-symmetric in i and l, and similarly the third term is also zero because $\dot{u}_j\dot{u}_l$ is symmetric in j and l but ε_{jlm} is skew-symmetric in j and l. Hence, we obtain

$$\delta\Pi^{\mathcal{H}} = -\delta\Pi^{\mathcal{L}}. \tag{4.122}$$

Thus, under an infinitesimal rotation of the inhomogeneity, for an isotropic material the variation of the Lagrangean is equal to the negative variation of the Hamiltonian. Taking the time derivative of equation (4.122) we can write

$$\delta\dot{\Pi}^{\mathcal{H}} = -\delta\dot{\Pi}^{\mathcal{L}}, \tag{4.123}$$

which, using equation (4.97), can be written as

$$\begin{aligned}\delta\dot{\Pi}^{\mathcal{H}} = -\delta\dot{\Pi}^{\mathcal{L}} = &-\epsilon\int_{\Omega}\left\{\frac{\partial\sigma_{ij}}{\partial x_i} - \frac{\partial(\rho\dot{u}_j)}{\partial t}\right\}\overline{\psi}_j\, dV + \epsilon\,\omega_m\int_{\Omega}\left[\frac{\partial}{\partial t}(\rho\,\varepsilon_{mlj}x_l\dot{u}_j) - \frac{\partial}{\partial x_i}(\varepsilon_{mlj}x_l\sigma_{ij})\right] dV \\ &+ \epsilon\,\omega_m\, L_m^{\text{dyn}},\end{aligned} \tag{4.124}$$

where L_m^{dyn} is defined by (4.75). Now, from (4.99) and (4.124), we can define

$$\begin{aligned}\delta\mathcal{E}^{tot} \equiv \delta\dot{\Pi}^{\mathcal{H}} = &-\epsilon\int_{\Omega}\left\{\frac{\partial\sigma_{ij}}{\partial x_i} - \frac{\partial(\rho\dot{u}_j)}{\partial t}\right\}\overline{\psi}_j\, dV + \epsilon\,\omega_m\int_{\Omega}\left[\frac{\partial}{\partial t}(\rho\,\varepsilon_{mlj}x_l\dot{u}_j) - \frac{\partial}{\partial x_i}(\varepsilon_{mlj}x_l\sigma_{ij})\right] dV \\ &+ \epsilon\,\omega_m\, L_m^{\text{dyn}},\end{aligned} \tag{4.125}$$

where $\delta\mathcal{E}^{tot}$ is the change of the total energy in the volume Ω due to the rotation of the inhomogeneity evaluated at time t. In the above equation (4.125), the term in the curly brackets in the first integrand is the linear momentum balance expression (equation (4.17)) and the second integrand on the right hand side is the angular momentum expression (equation (4.69)). Therefore, equation (4.125) can be stated as the proposition that for an isotropic material if linear and angular momenta are conserved in the whole domain, then the change of the total energy of the system per unit infinitesimal rotation $\epsilon\,\omega_m$, under the rotation transformation (4.91) with '*lever arm* $x_i + u_i$', is equal to the dynamic L integral.

4.6 Dissipative Propositions

4.6.1 Translation of the Inhomogeneity

From relation (4.111) we state the following proposition:

Proposition 1. *(Gupta and Markenscoff, 2012) Under the translation transformation of equation (4.79) the total energy loss of the system per unit infinitesimal translation is equal to the dynamic J-integral if and only if linear momentum is conserved in the domain provided that $u_{i,j}$ is invertible.*

This proposition extends the earlier proposition for the static J-integral (Gupta and Markenscoff, 2008) to the elastodynamics.

4.6.2 Scaling of the Inhomogeneity

From relation (4.120) we state the following proposition:

Proposition 2. *If linear momentum is conserved in the domain, under the scaling transformation of equation (4.85) the total energy loss of the system per unit infinitesimal scaling parameter is equal to the dynamic M-integral.*

This proposition is immediately extended to elastostatics for the static M-integral. We show this via various calculations in Chapter 5.

4.6.3 Rotation of the Inhomogeneity

From relation (4.125) we state the following proposition:

Proposition 3. *If linear and angular momenta are conserved in the domain, for an isotropic material under the rotation transformation of equation (4.91) the total energy loss of the system per unit infinitesimal rotation is equal to the dynamic L-integral.*

This proposition is immediately extended to elastostatics for the static L-integral.

These propositions express the fact that when analyticity is lost due to the inhomogeneity (inhomogeneities create discontinuities in the stress), the classical energy conservation of elasticity theory is not valid any longer. Extending Eshelby's famous result (force on an elastic singularity) to the other transformations, we may quote here Eshelby, in "*The Force on an Elastic Singularity*" (Eshelby, 1951, p 108) stating "When all sources of internal stress and inhomogeneity within Σ are given a small displacement $\delta\xi_l$, the energy $F_l\delta\xi_l$ is available for conversion into kinetic energy or dissipation by some process not considered in the elastic theory".

4.7 Conclusion

By applying Noether's theorem we derived the group of infinitesimal transformations of translation, scaling and rotation in elastodynamics under which the Lagrangean functional remains invariant and obtained the corresponding conservation laws. For inhomogeneities, we demonstrated that, under these transformations, the variation of the Lagrangean is equal to the negative of the variation of the Hamiltonian, and this provide the relations between the conservation integrals and the total energy loss of the system due to these transformations. This leads to propositions that under scaling of the inhomogeneity, if linear momentum is conserved in the domain, then the total energy loss of the system per unit infinitesimal scaling is equal to the dynamic M integral, and under rotation, if linear and angular momenta are conserved in the domain, then the total energy loss of the system per unit infinitesimal rotation is equal to the dynamic L integral. Thus, the propositions are interpreted physically as dissipative mechanisms for the loss of the Hamiltonian-energy due to translation, scaling or rotation of the inhomogeneity; these propositions extend the static counterparts (Budiansky and Rice, 1973) to elastodynamics.

Chapter 4, in part, is reprint of the material as it appears in "Markenscoff, X., and Singh, S. (2015). Dynamic conservation integrals as dissipative mechanisms in the evolution of inhomogeneities. Journal of Mechanics of Materials and Structures, 10(3), 331-353". The dissertation author was the primary investigator of this paper.

Chapter 5

Calculation of M-integrals for Self Similarly Growing Cavities, Inclusions and Inhomogeneities in Elastostatics

5.1 Introduction

In this chapter, we calculate the M-integral for cavities, inclusions, and inhomogeneities under tensile loading, or under the loading of transformation strains. We further relate the total M-integral to the total energy release rate of the system as the defect expands self-similarly (Markenscoff and Singh, 2015).

Static M-integral (Kienzler and Herrmann, 2000) is written after omitting the dynamic terms from expression (4.63) of the previous chapter, as

$$\begin{aligned} M &= \int_\Omega \frac{\partial}{\partial x_i}\left(x_j E_{ij} + \frac{2-n}{2} u_j \sigma_{ij}\right) dV \\ &= \int_\Omega \frac{\partial}{\partial x_i}\left[x_j (W\delta_{ij} - \sigma_{ik} u_{k,j}) + \frac{2-n}{2} u_j \sigma_{ij}\right] dV \\ &= \int_\Omega \frac{\partial}{\partial x_i}\left[W x_i - x_j \sigma_{ik} u_{k,j} + \frac{2-n}{2} u_j \sigma_{ij}\right] dV, \end{aligned} \tag{5.1}$$

where n is the number of space dimensions. So, in the case of three-dimensions, we can write

$$M = \int_\Omega \frac{\partial}{\partial x_i}\left[W x_i - x_j \sigma_{ik} u_{k,j} - \frac{1}{2} u_j \sigma_{ij}\right] dV. \tag{5.2}$$

In case of the radial loading in the spherical coordinates, the above expression can be written as

$$M(r) = \int_0^{2\pi} \int_0^{\pi} \left(Wr - r\sigma_{rr} \frac{\partial u_r}{\partial r} - \frac{u_r \sigma_{rr}}{2} \right) r^2 \sin\theta \, d\theta \, d\phi, \tag{5.3}$$

where $M(r)$ is the net M-integral on the surface that encloses a spherical region of radius r. Next, we evaluate the M-integral for a cavity in an infinite material under hydrostatic stresses at infinity. Before we start the calculations, we must understand that, in case of cavity, or inclusions; the 'defect' is the boundary. Therefore the net non-zero integral around the defect would be computed a surface surrounding the boundary.

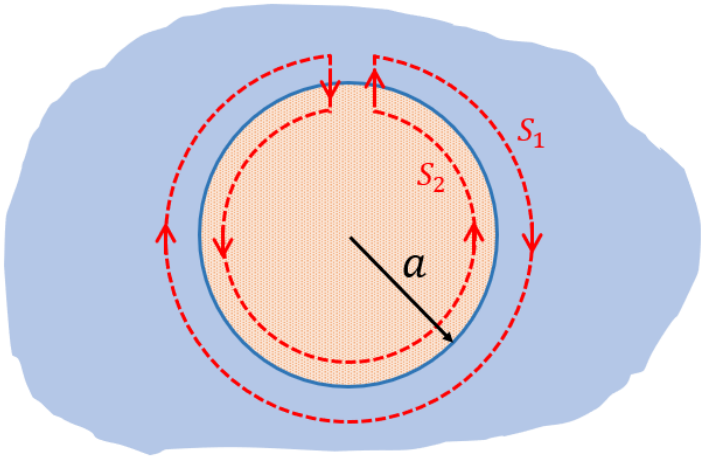

Figure 5.1. Path-independent M-integral surface contour around a *boundary defect*.

Consider a surface contour surrounding the defect boundary of a spherical cavity, or inclusion of radius a, as shown in Figure 5.1. The spherical surfaces S_1 and S_2 are just outside and inside the sphere of radius a. The two vertical surface of this contour on top of the inclusion are infinitesimal distance apart and their outward normal are in opposite direction, so the net surface integral of those two infinitesimal surfaces would be zero. Therefore, total M integral for the above surface contour (Figure 5.1) would be over the surfaces S_1 and S_2, but the outward normal of surface S_2 is pointing inside. In such case we can write $\int_{S_1+S_2} = \int_{S_1} - \int_{S_2}$, and the net M-integral around the spherical boundary defect becomes equal to $\left[M(a^+) - M(a^-)\right]$.

5.2 Growing Cavities

5.2.1 Cavity in an Infinite Matrix under Loading at Infinity

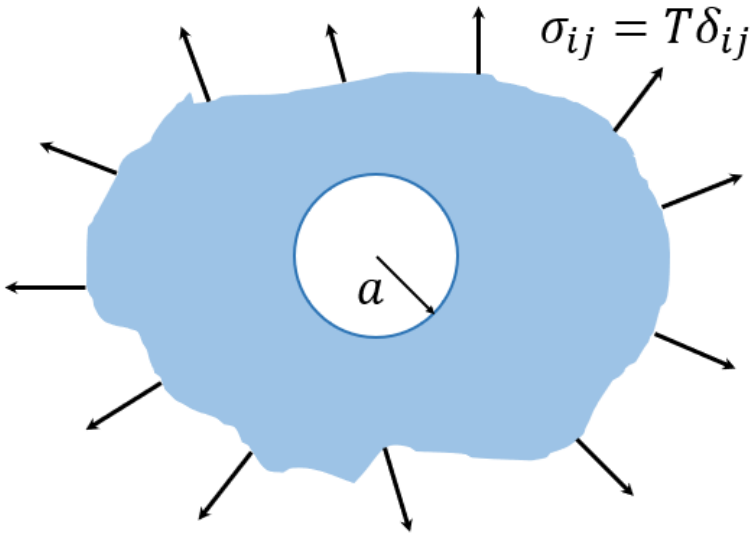

Figure 5.2. A spherical cavity of radius a in an infinite matrix under triaxial-loading T at infinity.

There is a spherical cavity of radius a in an infinite matrix under triaxial-tension T at infinity. Stress field (Lubliner, 2008):

$$\sigma_{rr} = \begin{cases} 0, & \text{if } x \leq a \\ T\left(1 - \frac{a^3}{r^3}\right), & \text{otherwise} \end{cases} \tag{5.4}$$

and

$$\sigma_{\theta\theta} = \sigma_{\phi\phi} = \begin{cases} 0, & \text{if } x \leq a \\ T\left(1 + \frac{a^3}{2r^3}\right), & \text{otherwise} \end{cases} \tag{5.5}$$

Now we can write the strain field for $r > a$ as

$$\begin{aligned}\varepsilon_{rr} &= \frac{1}{E}\left[\sigma_{rr} - 2\nu\sigma_{\theta\theta}\right] = \frac{1}{2\mu(1+\nu)}\left[\sigma_{rr} - 2\nu\sigma_{\theta\theta}\right] \\ &= \frac{T}{2\mu}\left[\frac{1-2\nu}{1+\nu} - \frac{a^3}{r^3}\right],\end{aligned} \tag{5.6}$$

and

$$\begin{aligned}\varepsilon_{\theta\theta} = \varepsilon_{\phi\phi} &= \frac{1}{E}\left[(1-\nu)\sigma_{\theta\theta} - \nu\sigma_{rr}\right] = \frac{1}{2\mu(1+\nu)}\left[(1-\nu)\sigma_{\theta\theta} - \nu\sigma_{rr}\right] \\ &= \frac{T}{4\mu}\left[\frac{2(1-2\nu)}{1+\nu} + \frac{a^3}{r^3}\right].\end{aligned} \tag{5.7}$$

Only nonzero component of displacement is

$$u_r = r\varepsilon_{\theta\theta} = \frac{T}{4\mu}\left[\frac{2(1-2\nu)}{1+\nu}r + \frac{a^3}{r^2}\right]. \tag{5.8}$$

The expression for the strain energy density function is

$$\begin{aligned}W &= \frac{1}{2}\sigma_{ij}\varepsilon_{ij} = \frac{1}{2}(\sigma_{rr}\varepsilon_{rr} + \sigma_{\theta\theta}\varepsilon_{\theta\theta} + \sigma_{\phi\phi}\varepsilon_{\phi\phi}) \\ &= \frac{1}{2E}({\sigma_{rr}}^2 + 2(1-\nu){\sigma_{\theta\theta}}^2 - 4\nu\sigma_{rr}\sigma_{\theta\theta}) \\ &= \frac{3T^2}{4\mu}\left[\frac{1-2\nu}{1+\nu} + \frac{a^6}{2r^6}\right].\end{aligned} \tag{5.9}$$

Now we substitute the expression for strain energy, stress and displacement into equation (5.3) to get the expression for the M-integral outside of the cavity (inside for $r \leq 0$, the M-integral is zero) as

$$M(r) = \frac{9\pi a^3(1-\nu)T^2}{2\mu(1+\nu)}. \tag{5.10}$$

Next, we relate the M-integral to the energy release rate as the cavity expands. The total

energy of the system under external loading $\boldsymbol{F}$ is given by

$$\begin{aligned}
\mathcal{E}^{tot} &= W^{elastic} - \int_S F_i(u_i + u_i^o)dS \\
&= \int_a^R W 4\pi r^2 dr - T u_r 4\pi R^2 \\
&= \int_a^R \frac{3T^2}{4\mu}\left[\frac{1-2\nu}{1+\nu} + \frac{a^6}{2r^6}\right]4\pi r^2 dr - \frac{T}{4\mu}\left[\frac{2(1-2\nu)}{1+\nu}R + \frac{a^3}{R^2}\right]4\pi R^2 \\
&= \frac{3T^2\pi}{\mu}\left[\left(\frac{1-2\nu}{1+\nu}\right)\frac{r^3}{3}\bigg|_a^R - \frac{a^6}{6r^3}\bigg|_a^R\right] - \frac{T\pi}{\mu}\left[\frac{2(1-2\nu)}{1+\nu}R^3 + a^3\right] \\
&= \frac{T^2\pi}{\mu}\left[\left(\frac{1-2\nu}{1+\nu}\right)(R^3 - a^3) - \frac{a^6}{2R^3} + \frac{a^3}{2}\right] - \frac{T\pi}{\mu}\left[\frac{2(1-2\nu)}{1+\nu}R^3 + a^3\right].
\end{aligned} \tag{5.11}$$

Taking the derivative with respect to a to obtain

$$\frac{\partial \mathcal{E}^{tot}}{\partial a} = \frac{3T^2\pi}{\mu}\left[-3a^2\frac{1-2\nu}{1+\nu} - \frac{3a^5}{r^3} + \frac{3a^2}{2}\right] - \frac{T^2\pi}{\mu}3a^2, \tag{5.12}$$

now we take limit R goes to ∞ for the infinite matrix

$$\lim_{R\to\infty}\frac{\partial \mathcal{E}^{tot}}{\partial a} = -\frac{9\pi a^2(1-\nu)T^2}{2\mu(1+\nu)}. \tag{5.13}$$

For an infinitesimal scaling parameter l;

$$\frac{d\mathcal{E}^{tot}}{dl} = \left(\frac{\partial \mathcal{E}^{tot}}{\partial a}\right)\frac{da}{dl} = \left(\frac{\partial \mathcal{E}^{tot}}{\partial a}\right)a = -\frac{9\pi a^3(1-\nu)T^2}{2\mu(1+\nu)}, \tag{5.14}$$

and we obtain

$$\left[M(a^+) - M(a^-)\right] = -d\mathcal{E}^{tot}/dl. \tag{5.15}$$

Therefore, we conclude that the total energy release rate of the system per unit scaling parameter

l is equal to the total M-integral when cavity expands self-similarly (Markenscoff and Singh, 2015).

5.2.2 Spherical Annulus under External Loading

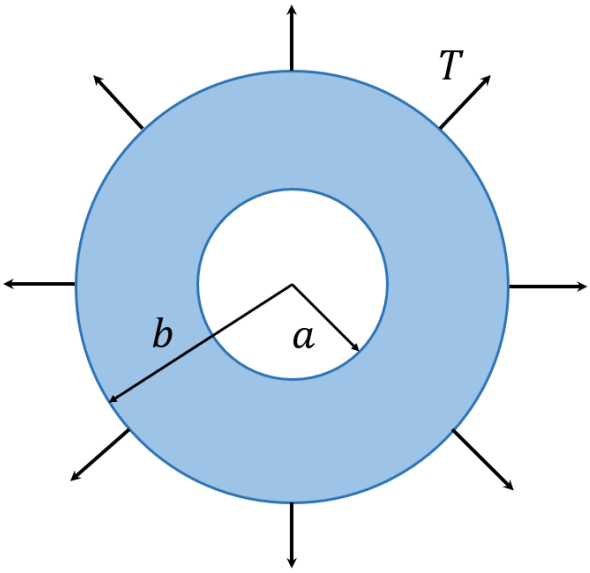

Figure 5.3. A spherical annulus of internal radius a and external radius b under triaxial loading T at the outer surface.

In the region $a < r < b$, the radial and circumferential components of the stress field are

$$\sigma_{rr} = \frac{T}{2} + \frac{Tb^3}{2(b^3 - a^3)}\left[1 + \left(\frac{a}{b}\right)^3 - 2\left(\frac{a}{r}\right)^3\right], \tag{5.16}$$

and

$$\sigma_{\theta\theta} = \sigma_{\phi\phi} = \frac{T}{2} + \frac{Tb^3}{2(b^3 - a^3)}\left[1 + \left(\frac{a}{b}\right)^3 + \left(\frac{a}{r}\right)^3\right]. \tag{5.17}$$

Using Maple, we obtain the expression for the strain energy density as

$$W = \frac{3T^2}{8\mu(1+\nu)(b^3 - a^3)^2}\left[2 - 4\nu + (1+\nu)\frac{a^6}{r^6}\right]. \tag{5.18}$$

The total energy the system under external loading $\boldsymbol{F}$ can be written as

$$\begin{aligned}\mathcal{E}^{tot} &= W^{elastic} - \int_S F_i(u_i + u_i^o)dS \\ &= \int_a^b W 4\pi r^2 dr - T u_r 4\pi b^2 \\ &= -\frac{\pi T^3 b^2}{2\mu(1+\nu)(b^3-a^3)}[a^3(1+\nu) + (2-4\nu)b^3].\end{aligned} \tag{5.19}$$

We can next write, for case of an infinite matrix

$$\lim_{b\to\infty} \frac{\partial \mathcal{E}^{tot}}{\partial a} = -\frac{9\pi a^2(1-\nu)T^2}{2\mu(1+\nu)}. \tag{5.20}$$

By doing symbolic algebraic calculations with Maple as $b \to \infty$, the expression for the M-integral outside of the cavity is

$$M = \frac{9\pi a^3(1-\nu)T^2}{2\mu(1+\nu)}, \tag{5.21}$$

inside the cavity, for $r \leq 0$, the M-integrals is zero. Hence, from this general approach also, for a cavity inside an infinite material under triaxial tension, we obtain

$$\left[M(a^+) - M(a^-)\right] = -d\mathcal{E}^{tot}/dl, \tag{5.22}$$

where l is the scaling parameter, we also used the fact $d\mathcal{E}^{tot}/dl = (\partial \mathcal{E}^{tot}/\partial a)da/dl = (\partial \mathcal{E}^{tot}\partial a)a$.

5.3 Inclusions: Eigenstrains and Inhomogeneities

Simple Inclusion and Eshelby's Solution

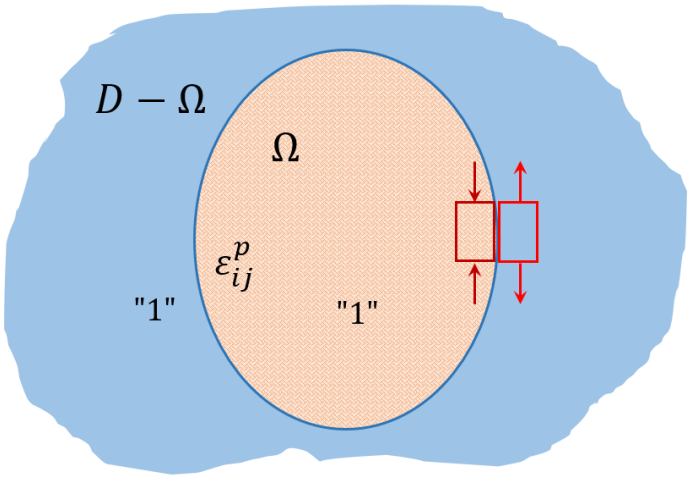

Figure 5.4. Simple ellipsoidal inclusion Ω in an infinity matrix $D-\Omega$.

A simple inclusion is defined as a subdomain Ω in domain D, where eigenstrain ε_{ij}^{p} is prescribed in Ω and is identically equal to zero in $D-\Omega$. The elastic moduli in Ω and $D-\Omega$ are assumed to be the same (material "1"). The remaining domain $D-\Omega$ is called the matrix (Figure 5.4). Note that there will be jump in hoop stresses at the boundary of the inclusion.

Eshelby's Solution: Consider an ellipsoidal inclusion Ω (Figure 5.4) with a constant eigenstrain ε_{ij}^{p} in an isotropic matrix $D-\Omega$. The strain field inside the inclusion is $\varepsilon_{ij}^{c} = S_{ijkl}\varepsilon_{kl}^{p}$, and stress field inside the inclusion is $\sigma_{ij} = C_{ijkl}^{(1)}(\varepsilon_{ij}^{c} - \varepsilon_{ij}^{p})$, where $C_{ijkl}^{(1)}$ are the elastic moduli of material "1", and S_{ijkl} is called Eshelby's tensor (Mura, 1987, chap. 2). Eshelby's tensor S_{ijkl} is constant for ellipsoidal inclusions, depends only on the axes ratio and Poisson's ratio of the material (Eshelby, 1961). Mura (1987, chap. 2) has provided methods to evaluate the elastic field at exterior points.

Ellipsoidal Inhomogeneity and Equivalent Inclusion Method

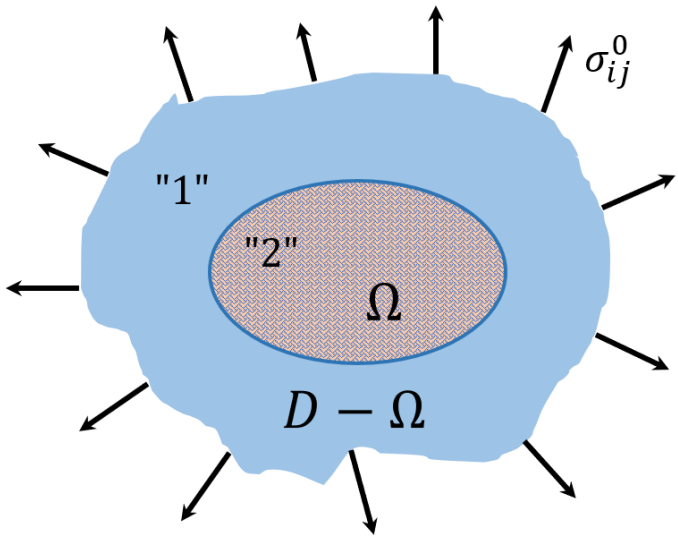

Figure 5.5. Ellipsoidal inhomogeneity Ω in an infinity matrix $D-\Omega$.

When the elastic moduli of an ellipsoidal subdomain Ω of a material (material "2") differs from those of the matrix (material "1"), the subdomain Ω is called an ellipsoidal inhomogeneity (Figure 5.5). A material containing inhomogeneities is free from any stress field unless a load is applied. On the other hand, a material containing inclusions is subjected to an internal stress (eigenstress) field even if it is free from any external loading (Mura, 1987, chap. 4). An uniform applied stress (σ_{ij}^0 in Figure 5.5) at infinity is not uniform in the neighborhood of the inhomogeneity.

Equivalent Inclusion Method: Eshelby (1957) pointed out that the disturbance in an applied stress due to the presence of an inhomogeneity can be simulated by eigenstresses caused by an inclusion when the eigenstrain is chosen properly, this is called equivalent inclusion method. Therefore, we say that an inhomogeneity is same as a simple inclusion with *'equivalent eigenstrain'*, ε_{ij}^*.

Let σ_{ij}^0 be applied stress at infinity, and the corresponding strain is ε_{ij}^0, and σ_{ij} and ε_{ij} are disturbance stress and strain fields, respectively. From Hooke's law the stress field inside the

subdomain Ω is given by

$$\begin{aligned} \sigma^0_{ij} + \sigma_{ij} &= C^{(2)}_{ijkl}(\varepsilon^0_{kl} + \varepsilon_{kl}) = C^{(1)}_{ijkl}(\varepsilon^0_{kl} + \varepsilon_{kl} - \varepsilon^*_{kl}) \\ &\Longrightarrow C^{(2)}_{ijkl}(\varepsilon^0_{kl} + \varepsilon_{kl}) = C^{(1)}_{ijkl}(\varepsilon^0_{kl} + \varepsilon_{kl} - \varepsilon^*_{kl}), \end{aligned} \tag{5.23}$$

where $C^{(1)}_{ijkl}$ and $C^{(2)}_{ijkl}$ are the elastic moduli of material "1" and material "2", respectively. Substituting the disturbance strain field $\varepsilon_{kl} = S_{klmn}\varepsilon^*_{mn}$ in equation (5.23) leads to

$$C^{(2)}_{ijkl}(\varepsilon^0_{kl} + S_{klmn}\varepsilon^*_{mn}) = C^{(1)}_{ijkl}(\varepsilon^0_{kl} + S_{klmn}\varepsilon^*_{mn} - \varepsilon^*_{kl}). \tag{5.24}$$

From the above equation the six unknowns, ε^*_{ij}, are determined.

Inhomogeneous Inclusion

If the inhomogeneity carries its own eigenstrain, then it is called the inhomogeneous inclusion. This means a subdomain Ω, which has different elastic constants (material "2") from those of the matrix (material "1"), also have a given eigenstrain ε^p_{ij}. The inhomogeneous inclusion is simulated by an inclusion in the homogeneous material with eigenstrain ε^p_{ij}, plus equivalent eigenstrain ε^*_{ij} due to the material mismatch in the inclusion and that in the matrix (Mura, 1987, chap. 4). The disturbance strain inside the inclusion is $\varepsilon_{kl} = S_{klmn}\varepsilon^{**}_{mn}$, where $\varepsilon^{**}_{ij} = \varepsilon^p_{ij} + \varepsilon^*_{ij}$, and S_{ijkl} is Eshelby's tensor. Therefore, the inhomogeneous inclusion is same as a simple inclusion with eigenstrain ε^{**}_{ij}.

5.3.1 Spherical Inclusion with Eigenstrain

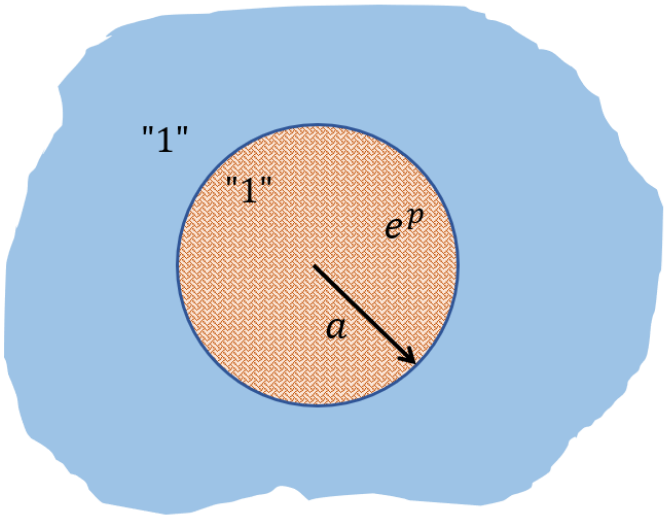

Figure 5.6. Spherical inclusion of radius a in an infinity matrix with an eigenstrain $\varepsilon_{ij}^p = e^p \delta_{ij}$.

Interior Fields

The stress field components inside the inclusion ($r < a$) are (Mura, 1987, chap. 2)

$$\sigma_{rr} = \sigma_{\theta\theta} = \sigma_{\phi\phi} = -\frac{4\mu}{3}\left(\frac{1+\nu_1}{1-\nu_1}\right)e^p, \tag{5.25}$$

and strain field components are

$$\varepsilon_{rr} = \varepsilon_{\theta\theta} = \varepsilon_{\phi\phi} = \frac{1}{3}\left(\frac{1+\nu_1}{1-\nu_1}\right)e^p. \tag{5.26}$$

The radial displacement is

$$u_r = r\varepsilon_{\theta\theta} = \frac{r}{3}\left(\frac{1+\nu_1}{1-\nu_1}\right)e^p. \tag{5.27}$$

The strain density inside the inclusion is

$$W = \frac{3}{2}\sigma_{rr}(\varepsilon_{rr} - e^p) = \frac{4\mu(1+\nu_1)(1-2\nu_1)e^{p2}}{3(1-\nu_1)^2}. \tag{5.28}$$

Now, from equation (5.3), we can evaluate the M-integral inside the inclusion as

$$M(r) = \frac{8\mu\pi(1+\nu_1)e^{p2}r^3}{1-\nu_1}, \tag{5.29}$$

and we can get

$$M(a^-) = \frac{8\mu\pi(1+\nu_1)e^{p2}a^3}{1-\nu_1}. \tag{5.30}$$

Exterior Fields

The stress field components outside the inclusion ($r > a$) are (Mura, 1987, chap. 2)

$$\sigma_{rr} = -\frac{4\mu}{3}\left(\frac{1+\nu_1}{1-\nu_1}\right)\frac{a^3}{r^3}e^p, \quad \text{and} \quad \sigma_{\theta\theta} = \sigma_{\phi\phi} = \frac{2\mu}{3}\left(\frac{1+\nu_1}{1-\nu_1}\right)\frac{a^3}{r^3}e^p. \tag{5.31}$$

The strain field components are

$$\varepsilon_{rr} = -\frac{2}{3}\left(\frac{1+\nu_1}{1-\nu_1}\right)\frac{a^3}{r^3}e^p, \quad \text{and} \quad \varepsilon_{\theta\theta} = \varepsilon_{\phi\phi} = \frac{1}{3}\left(\frac{1+\nu_1}{1-\nu_1}\right)\frac{a^3}{r^3}e^p. \tag{5.32}$$

The radial displacement is

$$u_r = r\varepsilon_{\theta\theta} = \frac{1}{3}\left(\frac{1+\nu_1}{1-\nu_1}\right)\frac{a^3}{r^2}e^p. \tag{5.33}$$

The strain density inside the inclusion is

$$W = \frac{1}{2}\sigma_{rr}\varepsilon_{rr} + \frac{2}{2}\sigma_{\theta\theta}\varepsilon_{\theta\theta} = \frac{2\mu}{3}\left(\frac{1+\nu_1}{1-\nu_1}\right)^2\frac{a^6}{r^6}e^{p2}. \tag{5.34}$$

Now, from equation (5.3), we can evaluate the M-integral inside the inclusion as

$$M(r) = 0. \tag{5.35}$$

Which means

$$M(a^+) = 0. \tag{5.36}$$

Total Energy of the System

For the case of a simple inclusion, the total energy is given by equation (25.19) in Mura (1987) as

$$\mathcal{E}^{tot} = -\frac{1}{2}\int_\Omega \sigma_{ij}\varepsilon^p_{ij} dV = \frac{8\mu\pi(1+\nu_1)e^{p2}a^3}{3(1-\nu_1)}, \tag{5.37}$$

where Ω is region with eigenstrain (inclusion). Now, we differentiate the total energy with respect to the radius of the inclusion a to obtain

$$\frac{\partial \mathcal{E}^{tot}}{\partial a} = \frac{8\mu\pi(1+\nu_1)e^{p2}a^2}{1-\nu_1} \tag{5.38}$$

Since $d\mathcal{E}^{tot}/dl = (\partial\mathcal{E}^{tot}/\partial a)da/dl = (\partial\mathcal{E}^{tot}\partial a)a$, from equation (5.30), (5.36) and (5.38) we obtain

$$\left[M(a^+) - M(a^-)\right] = -d\mathcal{E}^{tot}/dl. \tag{5.39}$$

Therefore, we conclude that, the total energy release rate of the system per unit scaling parameter l is equal to the total M-integral when the inclusion expands self-similarly (Markenscoff and Singh, 2015).

5.3.2 Spherical Inhomogeneity under Loading at infinity

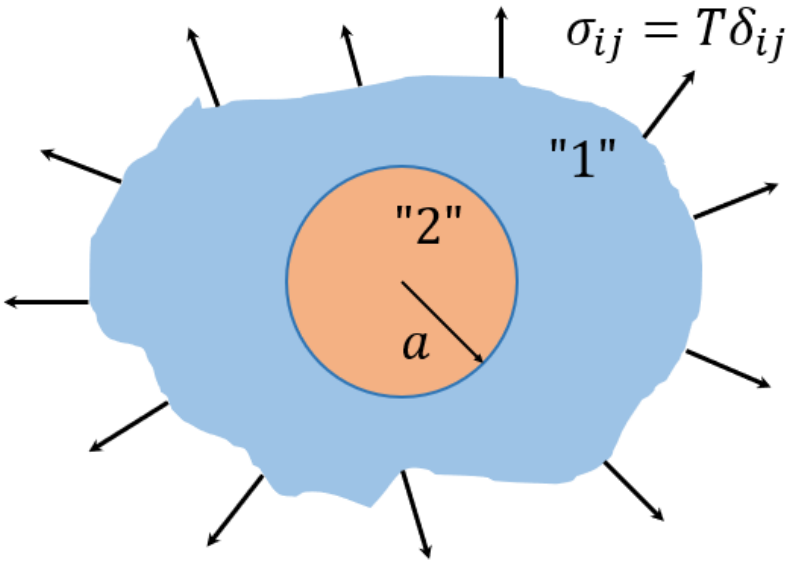

Figure 5.7. Spherical inhomogeneity of radius a with material "2" in an infinite matrix of material "1" under triaxial loading T at infinity.

To solve the stress and strain fields for this problem, we evaluate the equivalent eigenstrain due to the inhomogeneity, and this problem becomes equivalent to an inclusion with an *'equivalent eigenstrain'* inside an infinite matrix of same material. As given by equation (22.25) in Mura (1987), the equivalent eigenstrain would be $\varepsilon^*_{ij} = e^*\delta_{ij}$, where

$$e^* = \frac{T(1-\nu_1)(K_1-K_2)}{(1+\nu_1)K_1K_2 + 2(1-2\nu_1)K_1^2}, \tag{5.40}$$

where K_1 and K_2 are the bulk moduli of the matrix and inhomogeneity, respectively.

Interior Fields

The stress field components inside the inhomogeneity ($r < a$) are (Mura, 1987, chap. 4)

$$\sigma_{rr} = \sigma_{\theta\theta} = \sigma_{\phi\phi} = -\frac{4\mu}{3}\left(\frac{1+\nu_1}{1-\nu_1}\right)e^* + T, \tag{5.41}$$

and the strain field components are

$$\varepsilon_{rr} = \varepsilon_{\theta\theta} = \varepsilon_{\phi\phi} = \frac{1}{3}\left(\frac{1+\nu_1}{1-\nu_1}\right)e^* + \frac{T(1-2\nu_1)}{2\mu_1(1+\nu_1)}. \tag{5.42}$$

The radial displacement is

$$u_r = r\varepsilon_{\theta\theta} = \frac{r}{3}\left(\frac{1+\nu_1}{1-\nu_1}\right)e^* + \frac{T(1-2\nu_1)}{2\mu_1(1+\nu_1)}r, \tag{5.43}$$

The strain density inside the inhomogeneity is

$$W = \frac{3}{2}\sigma_{rr}\varepsilon_{rr} \tag{5.44}$$

Now, from equation (5.3), we can evaluate the M-integral inside the inhomogeneity as

$$M(r) = 0. \tag{5.45}$$

Which means

$$M(a^-) = 0. \tag{5.46}$$

Exterior Fields

The stress field components outside the inhomogeneity ($r > a$) are (Mura, 1987, chap. 4)

$$\sigma_{rr} = -\frac{4\mu}{3}\left(\frac{1+\nu_1}{1-\nu_1}\right)\frac{a^3}{r^3}e^* + T, \quad \text{and} \quad \sigma_{\theta\theta} = \sigma_{\phi\phi} = \frac{2\mu}{3}\left(\frac{1+\nu_1}{1-\nu_1}\right)\frac{a^3}{r^3}e^* + T. \tag{5.47}$$

The strain field components are

$$\varepsilon_{rr} = -\frac{2}{3}\left(\frac{1+\nu_1}{1-\nu_1}\right)\frac{a^3}{r^3}e^* + \frac{T(1-2\nu_1)}{2\mu_1(1+\nu_1)} \tag{5.48}$$

and

$$\varepsilon_{\theta\theta} = \varepsilon_{\phi\phi} = \frac{1}{3}\left(\frac{1+\nu_1}{1-\nu_1}\right)\frac{a^3}{r^3}e^* + \frac{T(1-2\nu_1)}{2\mu_1(1+\nu_1)}. \tag{5.49}$$

The radial displacement is

$$u_r = r\varepsilon_{\theta\theta} = \frac{1}{3}\left(\frac{1+\nu_1}{1-\nu_1}\right)\frac{a^3}{r^2}e^* + \frac{T(1-2\nu_1)}{2\mu_1(1+\nu_1)}r. \tag{5.50}$$

The strain density inside the inhomogeneity is

$$W = \frac{1}{2}\sigma_{rr}\varepsilon_{rr} + \frac{2}{2}\sigma_{\theta\theta}\varepsilon_{\theta\theta}. \tag{5.51}$$

Now, from equation (5.3), we can evaluate the M-integral inside the inhomogeneity

$$M(r) = 6\pi T e^* a^3. \tag{5.52}$$

Which means

$$M(a^+) = 6\pi T e^* a^3. \tag{5.53}$$

Total Energy of the System

For the case of an inhomogeneity in an infinite matrix, the total energy is given by equation (25.19) in Mura (1987) as

$$\mathcal{E}^{tot} = \overline{W} - \frac{1}{2}\int_\Omega \sigma^o_{ij}\varepsilon^*_{ij}dV = \overline{W} - 2T\pi e^* a^3, \tag{5.54}$$

where Ω is region with inhomogeneity, σ^o_{ij} is stress at infinity and $\overline{W}$ is function of homogeneous loading (T) which does not depend on size or magnitude of inhomogeneity. Now, we differentiate

the total energy with respect to the radius of the inclusion a to obtain

$$\frac{\partial \mathcal{E}^{tot}}{\partial a} = -6T\pi e^{*} a^{2}. \tag{5.55}$$

Since $d\mathcal{E}^{tot}/dl = (\partial \mathcal{E}^{tot}/\partial a)da/dl = (\partial \mathcal{E}^{tot}\partial a)a$, from equation (5.46), (5.53) and (5.55), we can obtain

$$\left[M(a^{+}) - M(a^{-})\right] = -d\mathcal{E}^{tot}/dl. \tag{5.56}$$

Therefore, we conclude that, the total energy release rate of the system per unit scaling parameter l is equal to the total M-integral when the inhomogeneity expands self-similarly (Markenscoff and Singh, 2015).

5.3.3 Spherical Inhomogeneous Inclusion under Loading at infinity

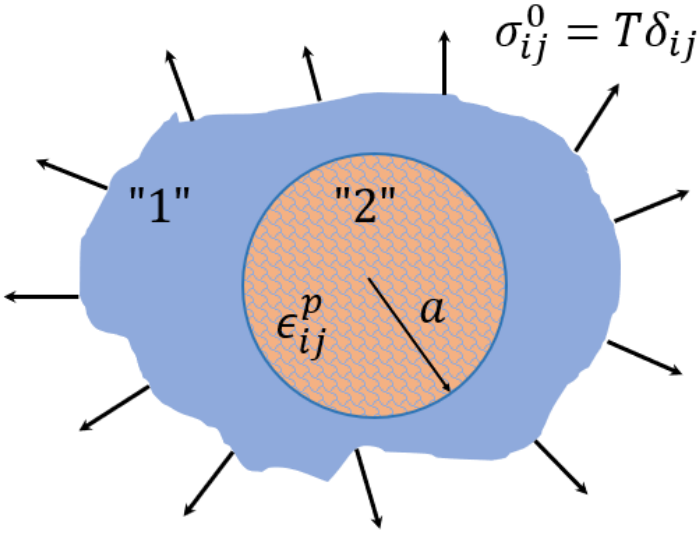

Figure 5.8. Spherical inhomogeneity of radius a with material "2" and also with an eigenstrain $\varepsilon_{ij}^{p} = e^{p}\delta_{ij}$ in an infinite matrix of material "1" under triaxial-loading T at infinity.

To solve the stress and strain filed for this problem, we evaluate the combined equivalent

eigenstrain due to the inhomogeneity and the given eigenstrain. Now this problem becomes equal to an inclusion with *equivalent eigenstrain* inside an infinite matrix of same material. As given by equation (22.25) in Mura (1987), the equivalent eigenstrain is $\varepsilon_{ij}^{**} = e^{**}\delta_{ij}$, and

$$e^{**} = e^{p} + e^{*} = \frac{\{(K_1 - K_2)\varepsilon_{ii}^{0} - 3K_2 e^{p}\}(1-\nu_1)}{(1+\nu_1)K_2 + 2(1-2\nu_1)K_1}, \tag{5.57}$$

where $\varepsilon_{ii}^{0} = 3T(1-2\nu_1)/\{2\mu_1(1+\nu_1)\}$, e^{*} is the eigenstrain due to the inhomogeneity, and K_1 and K_2 are the bulk moduli of the matrix and inhomogeneity, respectively.

Interior Fields

The stress field components inside the inclusion ($r < a$) are (Mura, 1987, chap. 4)

$$\sigma_{rr} = \sigma_{\theta\theta} = \sigma_{\phi\phi} = -\frac{4\mu}{3}\left(\frac{1+\nu_1}{1-\nu_1}\right)e^{**} + T, \tag{5.58}$$

and the strain field components are

$$\varepsilon_{rr} = \varepsilon_{\theta\theta} = \varepsilon_{\phi\phi} = \frac{1}{3}\left(\frac{1+\nu_1}{1-\nu_1}\right)e^{**} + \frac{T(1-2\nu_1)}{2\mu_1(1+\nu_1)}. \tag{5.59}$$

The radial displacement is

$$u_r = r\varepsilon_{\theta\theta} = \frac{r}{3}\left(\frac{1+\nu_1}{1-\nu_1}\right)e^{**} + \frac{T(1-2\nu_1)}{2\mu_1(1+\nu_1)}r, \tag{5.60}$$

The strain density inside the inclusion is

$$W = \frac{3}{2}\sigma_{rr}(\varepsilon_{rr} - e^{p}) \tag{5.61}$$

Now, from equation (5.3), we can evaluate the M-integral inside the inclusion

$$M(r) = \frac{8\mu\pi(1+\nu_1)e^p e^{**} r^3}{1-\nu_1} - 6T\pi r^3 e^p. \tag{5.62}$$

Which means

$$M(a^-) = \frac{8\mu\pi(1+\nu_1)e^p e^{**} a^3}{1-\nu_1} - 6T\pi a^3 e^p. \tag{5.63}$$

Exterior Fields

The stress field components outside the inclusion ($r > a$) are (Mura, 1987, chap. 4)

$$\sigma_{rr} = -\frac{4\mu}{3}\left(\frac{1+\nu_1}{1-\nu_1}\right)\frac{a^3}{r^3}e^{**} + T, \quad \text{and} \quad \sigma_{\theta\theta} = \sigma_{\phi\phi} = \frac{2\mu}{3}\left(\frac{1+\nu_1}{1-\nu_1}\right)\frac{a^3}{r^3}e^{**} + T. \tag{5.64}$$

The strain field components are

$$\varepsilon_{rr} = -\frac{2}{3}\left(\frac{1+\nu_1}{1-\nu_1}\right)\frac{a^3}{r^3}e^{**} + \frac{T(1-2\nu_1)}{2\mu_1(1+\nu_1)} \tag{5.65}$$

and

$$\varepsilon_{\theta\theta} = \varepsilon_{\phi\phi} = \frac{1}{3}\left(\frac{1+\nu_1}{1-\nu_1}\right)\frac{a^3}{r^3}e^{**} + \frac{T(1-2\nu_1)}{2\mu_1(1+\nu_1)}. \tag{5.66}$$

The radial displacement is

$$u_r = r\varepsilon_{\theta\theta} = \frac{1}{3}\left(\frac{1+\nu_1}{1-\nu_1}\right)\frac{a^3}{r^2}e^{**} + \frac{T(1-2\nu_1)}{2\mu_1(1+\nu_1)}r. \tag{5.67}$$

The strain density inside the inclusion is

$$W = \frac{1}{2}\sigma_{rr}\varepsilon_{rr} + \frac{2}{2}\sigma_{\theta\theta}\varepsilon_{\theta\theta}. \tag{5.68}$$

Now, from equation (5.3), we can evaluate the M-integral inside the inclusion

$$M(r) = 6\pi T e^{**} a^3. \tag{5.69}$$

Which means

$$M(a^+) = 6\pi T e^{**} a^3. \tag{5.70}$$

Total Energy of the System

For the case of an inhomogeneity in an infinite matrix, the total energy is given by equation (25.19) in Mura (1987) as

$$\begin{aligned}\mathcal{E}^{tot} &= \overline{W} - \frac{1}{2}\int_\Omega \sigma_{ij}^o \varepsilon_{ij}^* dV - \frac{1}{2}\int_\Omega \sigma_{ij}\varepsilon_{ij}^p dV - \int_\Omega \sigma_{ij}^o \varepsilon_{ij}^p dV \\ &= \overline{W} - 2T\pi e^* a^3 - 4T\pi e^p a^3 + \frac{8\mu\pi(1+\nu_1)e^{**}e^p a^3}{3(1-\nu_1)},\end{aligned} \tag{5.71}$$

where Ω is region with inhomogeneity, σ_{ij}^o is stress at infinity and $\overline{W}$ is function of homogeneous loading (T) which does not depend on size or magnitude of inhomogeneity. Now, we differentiate the total energy with respect to the radius of the inclusion a to obtain

$$\begin{aligned}\frac{\partial \mathcal{E}^{tot}}{\partial a} &= -6T\pi e^* a^2 - 12T\pi e^p a^2 + \frac{8\mu\pi(1+\nu_1)e^{**}e^p a^2}{1-\nu_1} \\ &= -6T\pi e^{**} a^2 - 6T\pi e^p a^2 + \frac{8\mu\pi(1+\nu_1)e^{**}e^p a^2}{1-\nu_1}\end{aligned} \tag{5.72}$$

Since $d\mathcal{E}^{tot}/dl = (\partial\mathcal{E}^{tot}/\partial a)da/dl = (\partial\mathcal{E}^{tot}\partial a)a$, from equation (5.63), (5.70) and (5.72), we can state that

$$\left[M(a^+) - M(a^-)\right] = -d\mathcal{E}^{tot}/dl. \tag{5.73}$$

Therefore, we conclude that the total energy release rate of the system per unit scaling parameter l is equal to the total M-integral when the inhomogeneous inclusion expands self-similarly (Markenscoff and Singh, 2015).

5.4 Conclusion

We conclude that the total energy release rate of the system per unit scaling parameter l is equal to the total M-integral when cavities, inclusions, or inhomogeneities expand self-similarly (Markenscoff and Singh, 2015). These calculations are useful to understand the mechanism of nucleation in a material by knowing the critical value of the M- integral required for the nucleation to start.

The work of Chapter 5 has been done with Professor X. Markenscoff. The dissertation author was the primary investigator of this research work. The work is being prepared for a publication.

Appendix A

Dynamic M-integral in Terms of Jumps for Expanding Plane Boundary

Here we derive the expression for the dynamic M-integral in terms of the *'jumps'*, which can be applied to calculate the M-integral for expanding inhomogeneities. We start with expression (4.63) from Chapter 4 for the dynamic M-integrals (Markenscoff and Singh, 2015)

$$M^{\text{dyn}} = \int_{\Omega} \left[\frac{\partial}{\partial x_i} \left\{ (T-W)x_i + \frac{n-1}{2}\sigma_{ij}u_j + \sigma_{ij}u_{j,k}x_k + t\sigma_{ij}\dot{u}_j \right\} + \frac{\partial}{\partial t} \left\{ t(T-W) - \frac{n-1}{2}\rho\dot{u}_j u_j - \rho\dot{u}_j u_{j,k}x_k - t\rho\dot{u}_j\dot{u}_j \right\} \right] dV, \tag{A.1}$$

where the strain energy density is $W = \frac{1}{2}C_{ijkl}\varepsilon_{ij}\varepsilon_{kl} = \frac{1}{2}C_{ijkl}\,u_{i,j}u_{k,l}$, and the specific kinetic energy is $T = \frac{1}{2}\rho\dot{u}_i\dot{u}_i$. We can further write the above expression as

$$M^{\text{dyn}} = \int_{\Omega} \frac{\partial}{\partial x_i} \left\{ (T-W)x_i + \frac{n-1}{2}\sigma_{ij}u_j + \sigma_{ij}u_{j,k}x_k + t\sigma_{ij}\dot{u}_j \right\} dV - \int_{\Omega} \frac{\partial}{\partial t} \left\{ t(T+W) + \frac{n-1}{2}\rho\dot{u}_j u_j + \rho\dot{u}_j u_{j,k}x_k \right\} dV. \tag{A.2}$$

Now using the *'rigid transport'* assumption Eshelby (1970), we can write

$$M^{\text{dyn}} = \int_{\Omega} \frac{d}{dx_i}\left\{(T-W)x_i + \frac{n-1}{2}\sigma_{ij}u_j + \sigma_{ij}u_{j,k}x_k + t\sigma_{ij}\dot{u}_j\right\} dV$$
$$+ v_i \int_{\partial\Omega}\left\{t(T+W) + \frac{n-1}{2}\rho\dot{u}_j u_j + \rho\dot{u}_j u_{j,k}x_k\right\} n_i\, dS, \tag{A.3}$$

where v_i is the rate of self-similar expansion of the inhomogeneity. Using the divergence theorem we convert the remaining volume integral to the surface integrals to obtain

$$M^{\text{dyn}} = \int_{\partial\Omega}\left\{(T-W)n_i x_i + \frac{n-1}{2}\sigma_{ij}u_j n_i + \sigma_{ij}u_{j,k}x_k n_i + t\sigma_{ij}\dot{u}_j n_i\right.$$
$$\left. + v_i t(T+W)n_i + \frac{n-1}{2}v_i\rho\dot{u}_j u_j n_i + v_i\rho\dot{u}_j u_{j,k}x_k n_i\right\} dS, \tag{A.4}$$

or it can be written as

$$M^{\text{dyn}} = \int_{\partial\Omega}\left\{(T-W)n_i x_i + \frac{n-1}{2}\sigma_{ij}u_j n_i + \sigma_{ij}u_{j,k}x_k n_i + t\sigma_{ij}\dot{u}_j n_i\right.$$
$$\left. + v_n t(T+W) + \frac{n-1}{2}v_n\rho\dot{u}_j u_j + v_n\rho\dot{u}_j u_{j,k}x_k\right\} dS. \tag{A.5}$$

For the moving plane boundary $\{(x_1, x_2, x_3)|x_1 = R_0 + l(t)\}$, the integral surface $\partial\Omega \equiv S_\epsilon$ enclosing the boundary consists of the planes $\{(x_1, x_2, x_3)|x_1 = R_0 + l(t) \pm \varepsilon\}$ on either side of the moving boundary for an infinitesimal number $\varepsilon > 0$ (plus the areas at lateral boundaries at infinity, which

give negligible contribution), so we can write

$$
\begin{aligned}
M^{\mathrm{dyn}} &= \lim_{\varepsilon\to 0}\int\limits_{S_\varepsilon}\Big\{(T-W)n_i x_i + \frac{n-1}{2}\sigma_{ij}u_j n_i + \sigma_{ij}u_{j,k}x_k n_i + t\sigma_{ij}\dot{u}_j n_i \\
&\quad + v_n t(T+W) + \frac{n-1}{2}v_n\rho\dot{u}_j u_j + v_n\rho\dot{u}_j u_{j,k}x_k\Big\}\,dS \\
&= \int\limits_{-\infty}^{\infty}\int\limits_{-\infty}^{\infty}\Big\{x_i n_i[\![T-W]\!] + \frac{n-1}{2}n_i[\![\sigma_{ij}u_j]\!] + x_k n_i[\![\sigma_{ij}u_{j,k}]\!] + t n_i[\![\sigma_{ij}\dot{u}_j]\!] \\
&\quad + \dot{l}_n t[\![T+W]\!] + \frac{n-1}{2}\dot{l}_n[\![\rho\dot{u}_j u_j]\!] + \dot{l}_n x_k[\![\rho\dot{u}_j u_{j,k}]\!]\Big\}\,dx_2\,dx_3,
\end{aligned}
\tag{A.6}
$$

note that in this case v_n becomes equal to $\dot{l}_n$. Next, we use well-known Hadamard jump conditions

$$
n_j[\![\sigma_{ij}]\!] = -\dot{l}_n\rho[\![\dot{u}_i]\!] \tag{A.7}
$$

and

$$
[\![\dot{u}_i]\!] = -\dot{l}_n[\![\partial u_i/\partial n]\!] \tag{A.8}
$$

across the interface, and also the relation $[\![\partial u_i/\partial n]\!]n_j = [\![\partial u_i/\partial x_j]\!]$. We furthere employ the fact $n_i[\![\sigma_{ij}u_j]\!] = n_i\langle\sigma_{ij}\rangle[\![u_j]\!] + n_i[\![\sigma_{ij}]\!]\langle u_j\rangle = n_i\langle\sigma_{ij}\rangle[\![u_j]\!] - \dot{l}_n\rho[\![\dot{u}_j]\!]\langle u_j\rangle$ and $\dot{l}_n[\![\rho\dot{u}_j u_j]\!] = \dot{l}_n\rho\langle\dot{u}_j\rangle[\![u_j]\!] + \dot{l}_n\rho[\![\dot{u}_j]\!]\langle u_j\rangle$. Also $[\![u_j]\!] = 0$, we get $n_i[\![\sigma_{ij}u_j]\!] + \dot{l}_n[\![\rho\dot{u}_j u_j]\!] = 0$. Now equation (A.6) can be written as

$$
\begin{aligned}
M^{\mathrm{dyn}} &= \int\limits_{-\infty}^{\infty}\int\limits_{-\infty}^{\infty}\big\{x_i n_i[\![T-W]\!] + x_k n_i[\![\sigma_{ij}u_{j,k}]\!] + t n_i[\![\sigma_{ij}\dot{u}_j]\!] \\
&\quad + \dot{l}_n t[\![T+W]\!] + \dot{l}_n x_k[\![\rho\dot{u}_j u_{j,k}]\!]\big\}\,dx_2\,dx_3.
\end{aligned}
\tag{A.9}
$$

Since $x_i n_i[\![T]\!] = x_i n_i\rho\langle\dot{u}_j\rangle[\![\dot{u}_j]\!] = -\dot{l}_n x_i n_i\rho\langle\dot{u}_j\rangle[\![\partial u_j/\partial n]\!] = -\dot{l}_n x_i\rho\langle\dot{u}_j\rangle[\![u_{j,i}]\!]$ and $\dot{l}_n x_k[\![\rho\dot{u}_j u_{j,k}]\!] = \dot{l}_n x_k\rho\langle\dot{u}_j\rangle[\![u_{j,k}]\!] + \dot{l}_n x_k\rho[\![\dot{u}_j]\!]\langle u_{j,k}\rangle$, we get $\dot{l}_n x_k[\![\rho\dot{u}_j u_{j,k}]\!] + x_i n_i[\![T]\!] = \dot{l}_n x_k\rho[\![\dot{u}_j]\!]\langle u_{j,k}\rangle$. So the above

equation can be written as

$$M^{\text{dyn}} = \int_{-\infty}^{\infty}\int_{-\infty}^{\infty} \Big\{ -x_i n_i [\![W]\!] + \dot{l}_n x_k \rho [\![\dot{u}_j]\!] \langle u_{j,k} \rangle + x_k n_i [\![\sigma_{ij} u_{j,k}]\!] \\ + t n_i [\![\sigma_{ij} \dot{u}_j]\!] + \dot{l}_n t [\![T + W]\!] \Big\} \, dx_2 \, dx_3. \tag{A.10}$$

Since $x_k n_i [\![\sigma_{ij} u_{j,k}]\!] = x_k n_i [\![\sigma_{ij}]\!] \langle u_{j,k} \rangle + x_k n_i \langle \sigma_{ij} \rangle [\![u_{j,k}]\!] = -x_k \dot{l}_n \rho [\![\dot{u}_j]\!] \langle u_{j,k} \rangle + x_k n_i \langle \sigma_{ij} \rangle [\![u_{j,k}]\!]$, now substituting it back into the above equation and simplifying provides

$$M^{\text{dyn}} = \int_{-\infty}^{\infty}\int_{-\infty}^{\infty} \Big\{ -x_i n_i [\![W]\!] + x_k n_i \langle \sigma_{ij} \rangle [\![u_{j,k}]\!] + t n_i [\![\sigma_{ij} \dot{u}_j]\!] + \dot{l}_n t [\![T + W]\!] \Big\} \, dx_2 \, dx_3. \tag{A.11}$$

We know that $t\, n_i [\![\sigma_{ij} \dot{u}_j]\!] = t\, n_i \langle \sigma_{ij} \rangle [\![\dot{u}_j]\!] + t\, n_i [\![\sigma_{ij}]\!] \langle \dot{u}_j \rangle = -\dot{l}_n t\, n_i \langle \sigma_{ij} \rangle [\![\partial u_j / \partial n]\!] - t \rho \dot{l}_n [\![\dot{u}_j]\!] \langle \dot{u}_j \rangle = -\dot{l}_n t \langle \sigma_{ij} \rangle [\![u_{j,i}]\!] - \dot{l}_n t [\![T]\!]$. Substituting it back into the above equation and simplifying provides

$$M^{\text{dyn}} = \int_{-\infty}^{\infty}\int_{-\infty}^{\infty} \Big\{ -x_i n_i [\![W]\!] + x_k n_i \langle \sigma_{ij} \rangle [\![u_{j,k}]\!] + \dot{l}_n t [\![W]\!] - \dot{l}_n t \langle \sigma_{ij} \rangle [\![u_{j,i}]\!] \Big\} \, dx_2 \, dx_3. \tag{A.12}$$

In view of relation $[\![\partial u_i / \partial x_j]\!] = [\![\partial u_i / \partial n]\!] n_j$, we can rewrite the above equations as

$$M^{\text{dyn}} = \int_{-\infty}^{\infty}\int_{-\infty}^{\infty} \Big\{ -x_i n_i [\![W]\!] + x_k n_i n_k \langle \sigma_{ij} \rangle [\![\partial u_j / \partial n]\!] + \dot{l}_n t [\![W]\!] - \dot{l}_n t \langle \sigma_{ij} \rangle [\![u_{j,i}]\!] \Big\} \, dx_2 \, dx_3. \tag{A.13}$$

Or

$$M^{\text{dyn}} = \int_{-\infty}^{\infty}\int_{-\infty}^{\infty} \Big\{ -x_i n_i [\![W]\!] + x_k n_k \langle \sigma_{ij} \rangle [\![u_{j,i}]\!] + \dot{l}_n t [\![W]\!] - \dot{l}_n t \langle \sigma_{ij} \rangle [\![u_{j,i}]\!] \Big\} \, dx_2 \, dx_3. \tag{A.14}$$

Since $\sigma_{ij} = \sigma_{ji}$, we can write

$$M^{\text{dyn}} = \int_{-\infty}^{\infty}\int_{-\infty}^{\infty} \left\{-x_k n_k [\![W]\!] + x_k n_k \langle\sigma_{ij}\rangle [\![u_{i,j}]\!] + \dot{l}_n t [\![W]\!] - \dot{l}_n t \langle\sigma_{ij}\rangle [\![u_{i,j}]\!]\right\} dx_2\, dx_3. \tag{A.15}$$

A further simplification provides a compact form of expression for the dynamic M-integral for expanding plane inhomogeneities

$$M^{\text{dyn}} = -\int_{-\infty}^{\infty}\int_{-\infty}^{\infty} (x_k n_k - \dot{l}_n t)\Big([\![W]\!] - \langle\sigma_{ij}\rangle [\![u_{i,j}]\!]\Big) dx_2\, dx_3. \tag{A.16}$$

The mathematical derivations in Appendix have been done with Professor X. Markenscoff. The dissertation author was the primary investigator of this research work. The work is being prepared for a publication.

Bibliography

Atkinson, C. and Eshelby, J. (1968). The flow of energy into the tip of a moving crack. International Journal of Fracture Mechanics, 4(1):3–8.

Brillouin, L. (1948). Wave guides for slow waves. Journal of Applied Physics, 19(11):1023–1041.

Budiansky, B. and Rice, J. R. (1973). Conservation laws and energy-release rates. Journal of applied mechanics, 40(1):201–203.

Bui, H. (1977). Stress and crack-displacement intensity factors in elastodynamics. In ICF4, Waterloo (Canada) 1977.

Callias, C. and Markenscoff, X. (1988). Singular asymptotics of integrals and the near-field radiated from nonuniformly moving dislocations. Archive for Rational Mechanics and Analysis, 102(3):273–285.

Clifton, R. and Markenscoff, X. (1981). Elastic precursor decay and radiation from nonuniformly moving dislocations. Journal of the Mechanics and Physics of Solids, 29(3):227–251.

Croënne, C., Manga, E., Morvan, B., Tinel, A., Dubus, B., Vasseur, J., and Hladky-Hennion, A.-C. (2011). Negative refraction of longitudinal waves in a two-dimensional solid-solid phononic crystal. Physical Review B, 83(5):054301.

Eischen, J. and Herrmann, G. (1987). Energy release rates and related balance laws in linear elastic defect mechanics. Journal of Applied Mechanics, 54:388.

Eshelby, J. (1959). Scope and limitations of the continuum approach. In Rassweiler, G.N., G.-W., editor, Internal stresses and fatigue in metals, pages 41–58. Elservier, Amsterdam. (Also see Markenscoff, X., Gupta, A. (Eds.), Collected Works of J.D. Eshelby: The Mechanics of Defects and Inhomogeneities, Springer, Netherlands, 2006, pages 269–286).

Eshelby, J. (1961). Elastic inclusion and inhomogeneities. Progress in solid mechanics, 2:89–140.

Eshelby, J. D. (1951). The force on an elastic singularity. Philosophical Transactions of the Royal Society of London. Series A, Mathematical and Physical Sciences, 244(877):87–112.

Eshelby, J. D. (1956). The continuum theory of lattice defects. Solid State Physics, 3:79–144.

Eshelby, J. D. (1957). The determination of the elastic field of an ellipsoidal inclusion, and related problems. Proc. R. Soc. Lond. A, 241(1226):376–396.

Eshelby, J. D. (1970). Energy relations and the energy-momentum tensor in continuum mechanics. In Kanninen, M., Adler, W., Rosenfeld, A., and Jaffe, R., editors, Inelastic Behavior of Solids, pages 77–155. McGraw-Hill, New York.

Eshelby, J. D. (1975). The elastic energy-momentum tensor. Journal of Elasticity, 5(3-4):321–335.

Fletcher, D. C. (1976). Conservation laws in linear elastodynamics. Archive for Rational Mechanics and Analysis, 60(4):329–353.

Freund, L. (1972). Energy flux into the tip of an extending crack in an elastic solid. Journal of Elasticity, 2(4):341–349.

Freund, L. (1990). Dynamic Fracture Mechanics. Cambridge Monographs on Mechanics. Cambridge University Press.

García-Chocano, V. M., Christensen, J., and Sánchez-Dehesa, J. (2014). Negative refraction and energy funneling by hyperbolic materials: An experimental demonstration in acoustics. Physical review letters, 112(14):144301.

Gelfand, I., Fomin, S., and Silverman, R. (2000). Calculus of Variations. Dover Publications.

Günther, W. (1962). Über einige randintegrale der elastomechanik. Abh. Brauchschw. Wiss. Ges, 14:53–72.

Gupta, A. and Markenscoff, X. (2008). Configurational forces as dissipative mechanisms: a revisit. Comptes Rendus Mecanique, 336(1):126–131.

Gupta, A. and Markenscoff, X. (2012). A new interpretation of configurational forces. Journal of Elasticity, 108(2):225–228.

Herrmann, A. G. (1981). On conservation laws of continuum mechanics. International Journal of Solids and Structures, 17(1):1–9.

Herrmann, A. G. (1982). Material momentum tensor and path-independent integrals of fracture mechanics. International Journal of Solids and Structures, 18(4):319–326.

Herrmann, G. and Kienzler, R. (1999). On the representation of basic laws of continuum mechanics by 4× 4 tensors. Mechanics research communications, 26(2):145–150.

Kaina, N., Lemoult, F., Fink, M., and Lerosey, G. (2015). Negative refractive index and acoustic superlens from multiple scattering in single negative metamaterials. Nature, 525(7567):77.

Kienzler, R. and Herrmann, G. (2000). Mechanics in material space: with applications in defect and fracture mechanics. Springer.

Knowles, J. K. and Sternberg, E. (1972). On a class of conservation laws in linearized and finite elastostatics. Archive for Rational Mechanics and Analysis, 44(3):187–211.

Kushwaha, M. S., Halevi, P., Dobrzynski, L., and Djafari-Rouhani, B. (1993). Acoustic band structure of periodic elastic composites. Physical review letters, 71(13):2022.

Lee, M. K., Ma, P. S., Lee, I. K., Kim, H. W., and Kim, Y. Y. (2011). Negative refraction experiments with guided shear-horizontal waves in thin phononic crystal plates. Applied Physics Letters, 98(1):011909.

Lee, S. H., Park, C. M., Seo, Y. M., Wang, Z. G., and Kim, C. K. (2010). Composite acoustic medium with simultaneously negative density and modulus. Physical review letters, 104(5):054301.

Li, J. and Chan, C. (2004). Double-negative acoustic metamaterial. Physical Review E, 70(5):055602.

Liu, Z., Zhang, X., Mao, Y., Zhu, Y., Yang, Z., Chan, C. T., and Sheng, P. (2000). Locally resonant sonic materials. Science, 289(5485):1734–1736.

Lubarda, V. and Markenscoff, X. (2007). Dual conservation integrals and energy release rates. International journal of solids and structures, 44(11):4079–4091.

Lubliner, J. (2008). Plasticity theory. Courier Dover Publications.

Markenscoff, X. (2006). Eshelby generalization for the dynamic j, l, m integrals. Comptes Rendus Mecanique, 334(12):701–706.

Markenscoff, X. and Ni, L. (2010). The energy-release rate and âĂIJself-forceâĂİ of dynamically expanding spherical and plane inclusion boundaries with dilatational eigenstrain. Journal of the Mechanics and Physics of Solids, 58(1):1–11.

Markenscoff, X. and Singh, S. (2015). Dynamic conservation integrals as dissipative mechanisms in the evolution of inhomogeneities. Journal of Mechanics of Materials and Structures, 10(3):331–353.

Maugin, G. (1993). Material Inhomogeneities in Elasticity. Applied Mathematics. Taylor & Francis.

Minagawa, S. and Nemat-Nasser, S. (1976). Harmonic waves in three-dimensional elastic composites. International Journal of Solids and Structures, 12(11):769–777.

Morvan, B., Tinel, A., Hladky-Hennion, A.-C., Vasseur, J., and Dubus, B. (2010). Experimental demonstration of the negative refraction of a transverse elastic wave in a two-dimensional solid phononic crystal. Applied Physics Letters, 96(10):101905.

Mura, T. (1987). Micromechanics of defects in solids. Martinus Nijhoff.

Nemat-Nasser, S. (1972a). General variational methods for waves in elastic composites. Journal of Elasticity, 2(2):73–90.

Nemat-Nasser, S. (1972b). Harmonic waves in layered composites. J. Appl. Mech, 39(3):850–852.

Nemat-Nasser, S. (2015). Refraction characteristics of phononic crystals. Acta Mechanica Sinica, 31(4):481–493.

Nemat-Nasser, S. (2017a). Inherent negative refraction on acoustic branch of two dimensional phononic crystals. arXiv preprint arXiv:1709.07768.

Nemat-Nasser, S. (2017b). Unified homogenization of photonic/phononic crystals with first-band negative refraction. Mechanics of Materials, 105:29–41.

Nemat-Nasser, S., Fu, F., and Minagawa, S. (1975). Harmonic waves in one-, two-and three-dimensional composites: Bounds for eigenfrequencies. International Journal of Solids and Structures, 11(5):617–642.

Nemat-Nasser, S., Willis, J. R., Srivastava, A., and Amirkhizi, A. V. (2011). Homogenization of periodic elastic composites and locally resonant sonic materials. Physical Review B, 83(10):104103.

Ni, L. and Markenscoff, X. (2009). The logarithmic singularity of a generally accelerating dislocation from the dynamic energyâĂŤmomentum tensor. Mathematics and Mechanics of Solids, 14(1-2):38–51.

Ni, L. and Markenscoff, X. (2015). On self-similarly expanding eshelby inclusions: Spherical inclusion with dilatational eigenstrain. Mechanics of Materials, 90:30–36.

Noether, E. (1918). Invariante variationsprobleme. Nachrichten von der Gesellschaft der Wissenschaften zu Göttingen, mathematisch-physikalische Klasse, 1918:235–257.

Olympus (2016). Panametrics Ultrasonic Transducers. Olympus.

Rice, J. and Drucker, D. C. (1967). Energy changes in stressed bodies due to void and crack

growth. International Journal of Fracture Mechanics, 3(1):19–27.

Rice, J. R. (1968). A path independent integral and the approximate analysis of strain concentration by notches and cracks. Journal of Applied Mechanics, 35(2):379–386.

Rice, J. R. (1985). Conserved integrals and energetic forces. In Bilby, B. A., Miller, K. J., and Willis, J. R., editors, Fundamentals of deformation and fracture, pages 33–56. Cambridge: Cambridge University Press.

Sadeghi, H. (2016). Microstructurally Controlled Composites with Optimal Elastodynamic Properties. PhD thesis, UC San Diego.

Srivastava, A. (2015). Elastic metamaterials and dynamic homogenization: a review. International Journal of Smart and Nano Materials, 6(1):41–60.

Srivastava, A. and Nemat-Nasser, S. (2014). Mixed-variational formulation for phononic band-structure calculation of arbitrary unit cells. Mechanics of Materials, 74:67–75.

Wei, P., Liu, F., Liang, Z., Xu, Y., Chu, S. T., and Li, J. (2015). An acoustic beam shifter with enhanced transmission using perforated metamaterials. EPL (Europhysics Letters), 109(1):14004.

Willis, J. (2016). Negative refraction in a laminate. Journal of the Mechanics and Physics of Solids, 97:10–18.

Yang, S., Page, J. H., Liu, Z., Cowan, M. L., Chan, C. T., and Sheng, P. (2004). Focusing of sound in a 3d phononic crystal. Physical review letters, 93(2):024301.

Zhang, S., Yin, L., and Fang, N. (2009). Focusing ultrasound with an acoustic metamaterial network. Physical review letters, 102(19):194301.

Zhu, R., Liu, X., Hu, G., Sun, C., and Huang, G. (2014). Negative refraction of elastic waves at the deep-subwavelength scale in a single-phase metamaterial. Nature communications, 5:ncomms6510.